NASA CR-134683

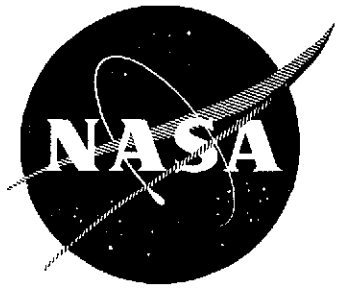

(NASA-CR-134683) FLOW STUDIES IN A WET STEAM TURBINE Contractor Report, 30 Jun. 1969 - 31 Mar. 1974 (Westinghouse Astronuclear Lab., Pittsburgh) 156 p HC $5.00 CSCL 20D G3/12 48536 Unclas N74-32748

FLOW STUDIES IN A WET STEAM TURBINE

BY

D. H. EVANS AND W. D. POUCHOT

PREPARED FOR

NATIONAL AERONAUTICS AND SPACE ADMINISTRATION
NASA LEWIS RESEARCH CENTER
CONTRACT NAS 3-13230

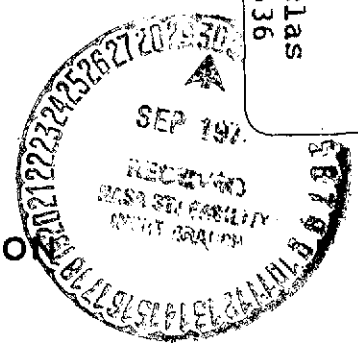

WESTINGHOUSE ELECTRIC CORPORATION
ASTRONUCLEAR LABORATORY
PITTSBURGH, PENNSYLVANIA, 15236

1. Report No.	2. Government Accession No.	3. Recipient's Catalog No.
NASA CR-134683		

4. Title and Subtitle	5. Report Date
FLOW STUDIES IN A WET STEAM TURBINE	August 13, 1974
	6. Performing Organization Code

7. Author(s)	8. Performing Organization Report No.
D.H. Evans and W.D. Pouchot	WANL-13230F
	10. Work Unit No.

9. Performing Organization Name and Address	11. Contract or Grant No.
Westinghouse Electric Corporation P.O. Box 10864 Pittsburgh, Pennsylvania 15236	NAS 3-13230
	13. Type of Report and Period Covered
12. Sponsoring Agency Name and Address	Contractor-6/30/69-3/31/74
National Aeronautics and Space Administration Washington, D.C. 20546	14. Sponsoring Agency Code

15. Supplementary Notes

Project Manager, Gerald J. Barna, Power Systems Division, NASA Lewis Research Center, Cleveland, Ohio

16. Abstract

The design and test results of a four stage wet vapor turbine operating with slightly superheated inlet steam and expanding to 10% exit moisture are presented. High speed movies at 3000 frames per second of liquid movement on the pressure side and along the trailing edge of the last stator blade are discussed along with back lighted photographs of moisture drops as they were torn from the stator blade trailing edge. Movies at lower framing rates were also taken of the exit of the last rotating blade and the casing moisture removal slot located in line with the rotor blade shroud. Also moisture removal data are presented of casing slot removal at the exit of the third and fourth rotor blades and for slots located in the trailing edge of the last stator blade. Finally, the degradation of turbine thermodynamic performance due to condensation formation and movement is discussed.

17. Key Words (Suggested by Author(s))	18. Distribution Statement
Steam turbine, moisture, photography, removal device,	Unclassified-unlimited

19. Security Classif. (of this report)	20. Security Classif. (of this page)	21. No. of Pages	22. Price*
Unclassified	Unclassified	152	~~$3.00~~

* For sale by the National Technical Information Service, Springfield, Virginia 22151

TABLE OF CONTENTS

LIST OF FIGURES

LIST OF FIGURES

LIST OF FIGURES

LIST OF FIGURES

LIST OF TABLES

1.0 SUMMARY

Condensate in vapor turbines that operate in the "wet" region of the Molliere diagram reduces turbine efficiency and can cause erosion damage to rotor blades and shrouds. The objectives of this program were to make visual and photographic observations inside a wet steam turbine and to evaluate the performance of internal moisture removal devices. A four stage turbine, capable of expanding from an initially superheated state to a sufficiently high level of moisture to make meaningful observations, was designed to fit an existing test facility. Standard steam turbine blading was utilized in the first three stages and served primarily as a slave turbine to provide the desired moisture level. The last stage was especially designed to accept the necessary optical systems. All photographic testing was performed on the fourth turbine stage. Boroscopes and fiber optic light tubes were selected as the general optical instrumentation approach. High speed motion picture photographs using stroboscopic lighting were made as well as motion pictures at normal framing rates using incadescent lighting. Movie films were taken of the fourth rotor casing slot and stator trailing edge slots while moisture was being removed and with the removal systems inactive. Other films were taken to record liquid movement across the blade pressure surface. High speed movies were also taken of drops being shed from the fourth stator blade utilizing a backlighted technique that enabled some drop size measurements to be made on a film analyzer.

Because of the intense fog and the collection of liquid and gradual formation of a hazy film on the optical systems, photographs and visual observations were difficult to make. Careful study of the successful films, however, led to some interesting deductions about the condensate flow.

No appreciable moisture was observed on the blade pressure surface. The films clearly showed that no moisture existed in rivulet form although the possibility of a thin film over the surface cannot be dismissed. The liquid on the stator blades appears to collect primarily at the junction of the blade and casing due to secondary flow. Large drops then are torn from the trailing edge in the vicinity of the casing or move radially inward along the trailing edge until they

are swept off by the main vapor flow. In either case, strong radial velocities are observed due to secondary flow.

Backlighted photography at the stator exit gave good resolution of large drops detaching from the trailing edge. Drop diameters as small as 60 micrometers were determined on a film analyzer. Maximum drop sizes agreed fairly well with present day theory, although some exceptions were noted.

A fairly uniform fog distribution was observed at the exit of the fourth rotor blade. No concentrated moisture could be observed departing the shroud and entering the casing removal slot. Liquid photographed on the face of the casing slot was moving tangentially in the direction of the blade shroud. No significant difference was observed in this view when the moisture removal system was activated.

Movies of the stator trailing edge slots demonstrated convincingly that the slot removal system did not remove all liquid at the blade trailing edge. This was especially significant since moisture removal effectiveness measurements were encouraging and may have been interpreted incorrectly as to the effectiveness of the slots in removing potentially damaging liquid.

The effectiveness of the moisture removal devices was determined by external separation and measurement of the liquid and vapor extracted from the casing and trailing edge slots. The third rotor blade slot removed nearly 70% of the liquid predicted analytically to have collected on the turbine surfaces. The fourth rotor blade slot performance was significantly poorer than this. The trailing edge slots in the fourth stator blades removed around 70% of the predicted moisture collected on the blade surface. The high speed movies indicated that large drop detachment from the trailing edge persisted when the trailing edge slots were operating, however.

Testing also included thermodynamic performance measurements of the turbine over a range of moisture levels. The purpose of these tests was to investigate the thermodynamic degradation that occurs due to condensate formation and movement in the turbine. Test results indicate a non-linear relationship between moisture level and performance degradation.

2.0 INTRODUCTION

In wet vapor turbines, such as those used in central station steam power plants and potentially in advanced space power systems, the moisture which forms and collects on blade and casing surfaces reduces turbine efficiency and can cause serious damage to turbine blades and shrouds. These effects have been of interest and subjected to observation for many years[1]. However, during the decade just past, substantial programs investigating the flow phenomena in wet vapor turbines were undertaken in both the United States and abroad. In the United States, NASA conducted such programs, primarily as a part of its interest in Rankine-cycle power plants for space. Others[2,3] conducted programs because of the increased moisture levels utilized by nuclear steam plants relative to fossil plants and the increases in turbine tip speeds available through improved materials. NASA has conducted both experimental[4] and analytical[5] erosion related programs as well as testing two-[6] and three-stage[7] potassium turbines as a part of its work on technology for advanced Rankine-cycle power plants.

The NASA program reported here was aimed at improving understanding of the moisture flow in wet-vapor turbines. A four-stage steam turbine was used as the test vehicle. The first three stages of the turbine are primarily for the purpose of producing naturally formed turbine moisture to be observed in the fourth (last) stage. Numerical data and/or observations were made on: 1) moisture flow in the fourth stage by high speed photography and by visual observation; 2) measurement of the effectiveness of casing removal slots at the third and fourth rotors and stator trailing edge removal slots in the fourth stator; and 3) measurement of the effects of moisture on turbine efficiency. This report describes the test apparatus used, outlines the test procedures, and discusses the test results obtained and some conclusions formed.

3.0 CONDENSATE FLOW PHENOMENA

A widely held model of the qualitative aspects of condensate flow in wet vapor turbines is given in NASA CR-1830[5]. This qualitative model has not been totally confirmed in all details by the observations of this program, but the discussion of this Section 3.0 is mainly along the lines given in NASA CR-1830.

If a superheated vapor expands in a nozzle or turbine until the temperature of the vapor is reduced to that of equilibrium saturation, the vapor does not condense in any appreciable quantity immediately. Rather, the vapor must be cooled to produce sufficient supersaturation to cause rapid condensation. The condition at initiation of rapid spontaneous condensation is called the Wilson point or line. At the Wilson line, condensation takes place rapidly and the moisture content quickly approaches equilibrium. Thereafter, the expansion process follows with but slight lag an equilibrium expansion because the original spontaneous nucleation creates sufficient surface area to allow further condensation to occur with minimal supersaturation.

As originally formed, the condensation nuclei are extremely small and are of relatively uniform size because of the short period of time involved. The nuclei grow quite rapidly to about 0.2 micrometer (7.9 microinches) diameter as the supersaturation potential created by the expansion in advance of spontaneous condensation is exhausted. Thereafter, a slower growth takes place as the droplets progress through the turbine. The calculated supersaturation in equivalent moisture to initiate spontaneous condensation in steam turbines is about 2.5%.

Because of their small size, most of the condensate particles remain in the vapor flow. Only a small percentage of the condensate fog collects on surfaces. It is often hypothesized that the major mechanism in collection of these particles is by inertial impaction on the nose and concave surfaces of the turbine blades. The calculated values of moisture collection reported in Section 4.0 are based on this assumption.

The small percentage of fog particles collected form rivulets, films, and drops on the blading surfaces. On the rotating blading, the predominant force over most of the blading surface is that of the centrifugal field of the blades. Under this force, the liquid collected on the rotors flows nearly radially outwards and is thrown from the tips of the blades or shroud if one is present according to the model. The photos of this program suggest, however, that a substantial amount of liquid leaves the back of the fourth rotor blades below the blade tips and shroud. Because of the high peripheral velocity of the rotor blades and shrouds, the liquid flung from them is very well atomized and rarely causes any erosion damage of consequence to either the turbine casing or a succeeding row of stator blades where present. The liquid flung from the rotors mostly collects on the turbine casing. It runs along this casing towards the turbine exit, if not removed, under the drag of the vapor.

According to the model, on the stator blades the primary force acting on the collected liquid is the drag force of the mainstream flow. Under this force, the liquid flows to the rear of the stator where it collects until torn from the stator as rather large particles. This implies that the collected liquid follows the bulk flow streamlines and on a time average basis is uniformly distributed from hub to tip of the stators.

Liquid is torn from the back edges of the stator vanes as relatively large globs. These globs undergo a breakup process into small drops in the wake just downstream of the stators. These smaller drops accelerate rapidly in the space between stator and rotor. However, in the space available between stator and rotor, the drops do not attain vapor stream velocity and because of the velocity vector difference can strike the nose and convex surfaces of the rotating blades with rather large normal velocity components. In turbines with high velocities of these drops relative to the rotor blades, some of the larger drops strike with sufficient force to produce erosion of the blade leading edges, particularly at the rotor blade tips.

4.0 TEST TURBINE AND FACILITY DESCRIPTION

4.1 FACILITY DESCRIPTION

The test facility used was originally designed to determine multi-stage thermodynamic and mechanical performance of high and intermediate pressure steam turbine blading. Figure 1 shows the steam and cooling water services to the laboratory where the facility is located. Two boilers supply steam to a reducing station where the pressure is decreased to a suitable level for the various laboratory test facilities. Two condensers, separate from each other, receive exhaust steam from the various test facilities and condensate is then measured and returned to the power house. Condenser cooling water is pumped from the Delaware River.

Figure 2 shows in greater detail the steam and water piping for the test facility. The turbine operator adjusts the steam inlet pressure and temperature by air operated pressure and desuperheating control valves. Turbine exit pressure is adjusted by a remote controlled butterfly valve between the turbine and condenser. Prior to turbine start, steam is supplied to sealing which surround the turbine shaft to isolate the turbine and condenser from atmospheric pressure.

The turbine output is absorbed by a water disc brake with a maximum speed rating of 225 Hz (13,500 rpm) and a maximum power absorption of 6000 kw (8000 HP). The operator sets the desired turbine speed and the controller maintains this speed by adjusting the water flow to the brake.

The turbine exhaust steam is condensed and then pumped to the weighing tanks. The level of condensate in the condenser is automatically controlled and monitored during testing to assure that a constant mass of condensate remains in the condenser during the weighing process.

A thrust balancing system was required for this test vehicle to maintain allowable thrust bearing loads by reducing the steam pressure at the inlet face of the rotor body. A portion of the inlet steam leaks past a series of rotor seals into the housing and then to a condenser. Since the

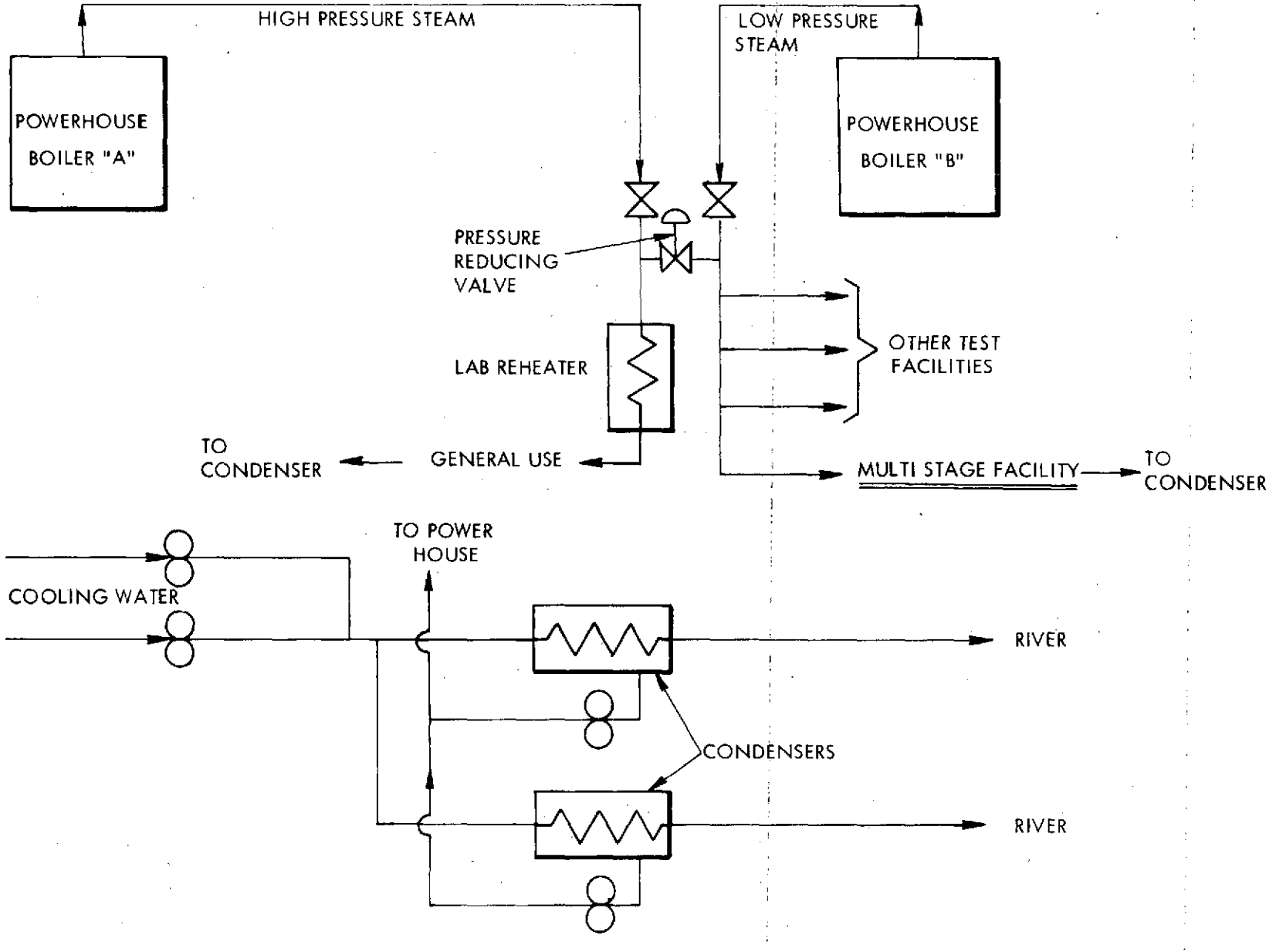

Figure 1. Steam and Cooling Water Services to Laboratory

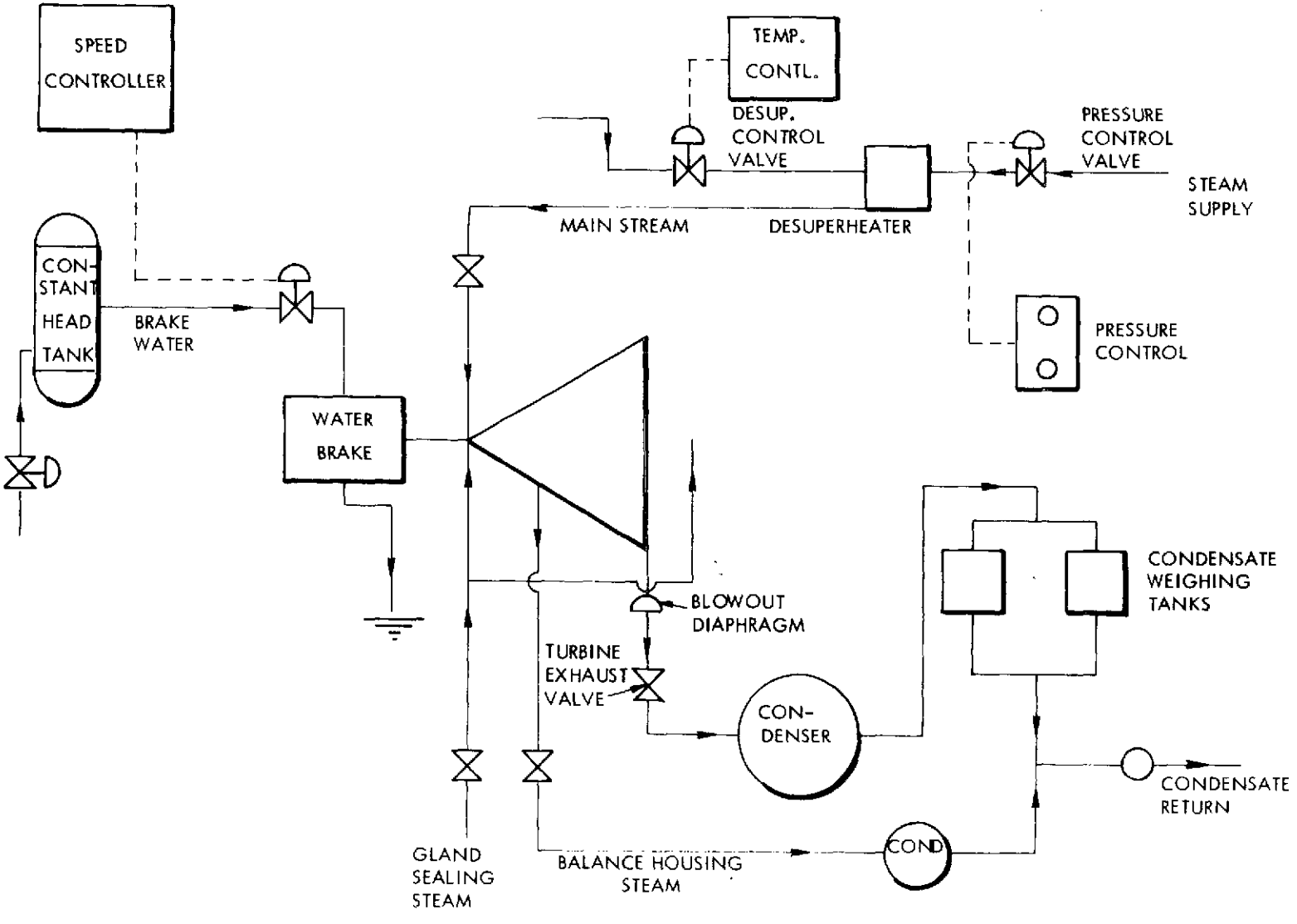

Figure 2. Multistage Steam and Water Flow

balance steam does not pass through the blading, it must be kept isolated from the turbine exhaust flow. The balance housing steam is vented to a separate condenser and the condensate is combined with the main flow downstream of the condensate weigh tanks. The thrust balance housing pressure is controlled by a hand valve.

4.2 TEST TURBINE DESCRIPTION

4.2.1 Physical Description

Turbine Blading and Overall Design

A longitudinal section of the four stage test turbine is shown in Figure 3. A double-casing design is employed with the inner and outer casing separated by an annulus which is, essentially, at turbine inlet pressure. The turbine has a constant mean diameter flow path of 0.642 m (25.3 inches) with blade heights from 1.07 cm (0.42 inch) to 6.9 cm (2.72 inches). The first three stages performed as a "slave turbine" to provide a two phase mixture typical of that formed by the expansion process through turbine blading. Standard steam turbine blading of constant cross-section were used for these stages. The fourth stage blades were designed specifically for this test and special features were incorporated such as moisture removal slots in the trailing edge of the stator blade and a 2.54 cm (1.0 inch) axial space between the stator and rotor blades to allow sufficient space for the insertion of the photographic instruments. All photographic testing was performed on the fourth stage.

The "slave" turbine blading is shown in Figure 4. This standardized blading is extensively used in commercial turbines for power generation. The blading of the slave turbine is a blunt leading edge reaction blade. The blade is of uniform cross-section and untwisted. Small groups of blades are fastened together at their tips by a shroud segment spanning the group of four or five blades but with no interconnection between groups. The inside surface of the shroud forms a conical boundary for the steam. The outer surface of the shroud is machined to a fine tolerance following installation on the blades to form a sealing surface between the rotating shroud and the cylinder seal strips. The shroud is secured to the blade by a round

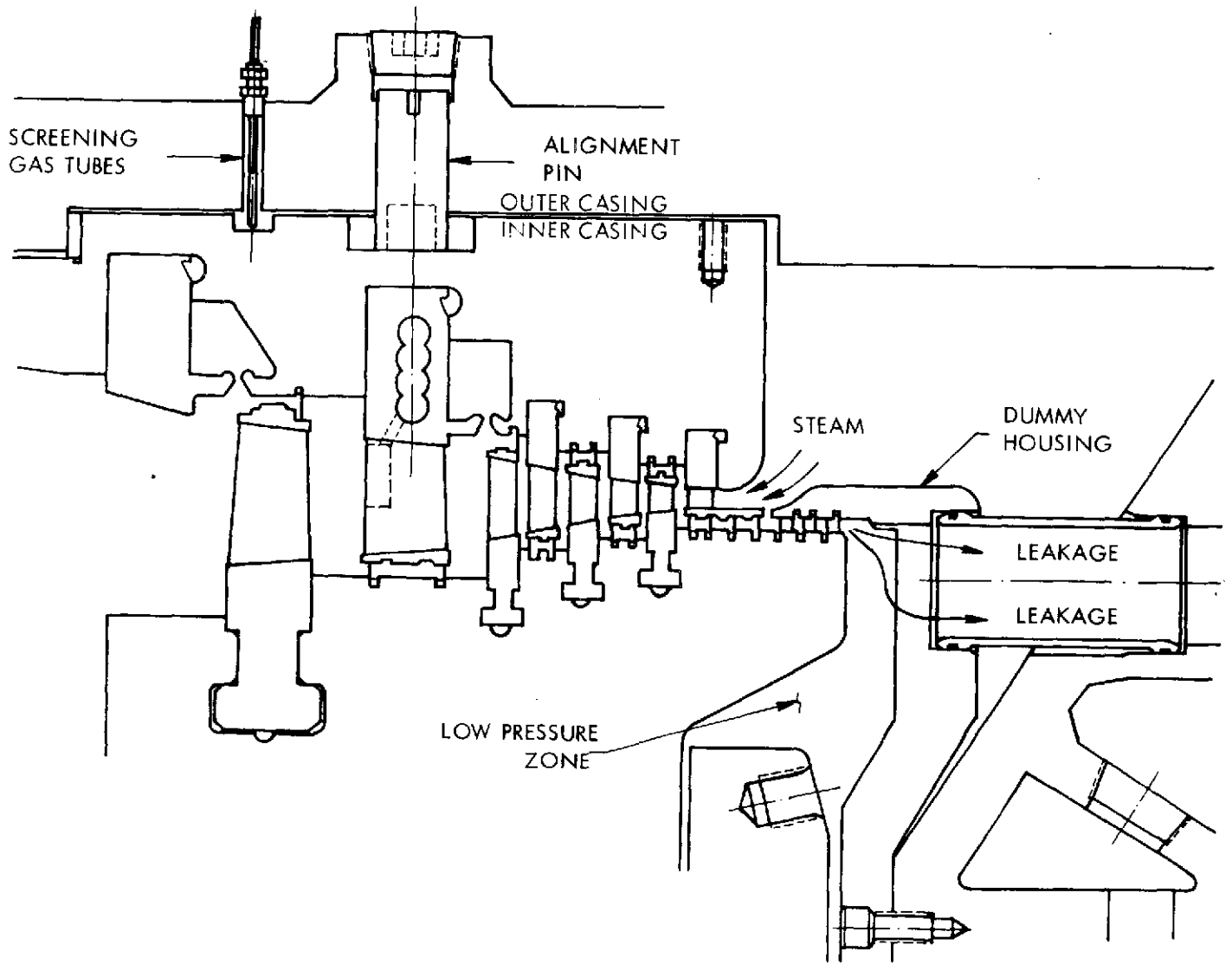

Figure 3. Wet Vapor Turbine Longitudinal

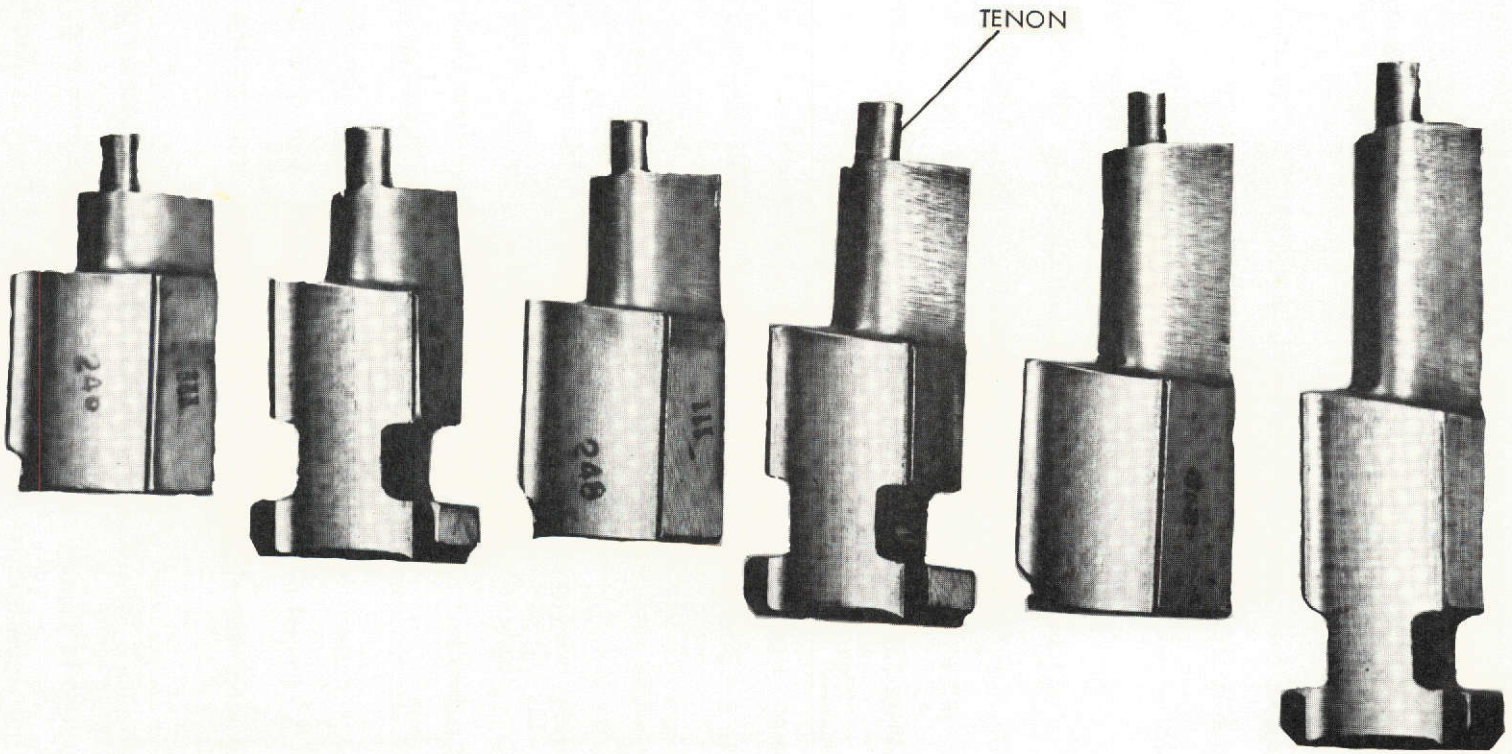

Figure 4. Slave Turbine Blading

projection of the blade tip called a tenon. The tenon passes through a hole in the shroud and is riveted over. The shrouds are machined to close tolerance to provide a sealing surface. Radial seal strips, held in grooves by caulking in the rotor and inner casing, are machined to provide a nominal clearance of 0.025 cm (0.01 inch) between the shrouds and seal strips.

At the inner diameter of the blade, the platforms form a second conical surface that constrains the steam. The blade section, platform and root are machined from a single piece of material. The roots on the rotating blades are of a T profile when viewed in the tangential direction. This T fits into a mating circumferential groove machined in the rotor body. The blades are assembled into the rotor through a radial entry slot in each row and moved circumferentially to their final position. A small piece of soft metal is inserted under the blade and driven in so as to swell it up, thereby forcing the blade outward against the contact surface. This holds the blade in normal position for subsequent shrouding and machining operations.

The stationary blading is generally the same as the rotating blades except the roots are simple rectangles in profile set into a matching groove in the cylinder and held in place by the same sort of soft metal pieces driven along the side of the root.

The fourth stage blades are shown in Figure 5. The stator blade cross-section is constant with height while the rotor blade is a twisted, tapered blade. Considerable thermodynamic design effort was devoted to the test blading to assure a well defined flow field in the passages to be photographed. The steam flow path boundaries are formed in the same manner as for the "slave" turbine. Attachment to the rotor body and the casing is also the same. A single solid rotor body with circumferentially machined grooves was used for the entire turbine. A view of the turbine rotor assembled in the lower half of the inner casing is shown in Figure 6.

Referring back to Figure 3, the slave turbine annulus flare increased from inlet to exit in gradual steps from zero to 12 degrees. The flare is symmetric with respect to the constant mean diameter in the slave turbine and in the test stage. There is also a gradual transition in flare with respect to the slave turbine and the test stage.

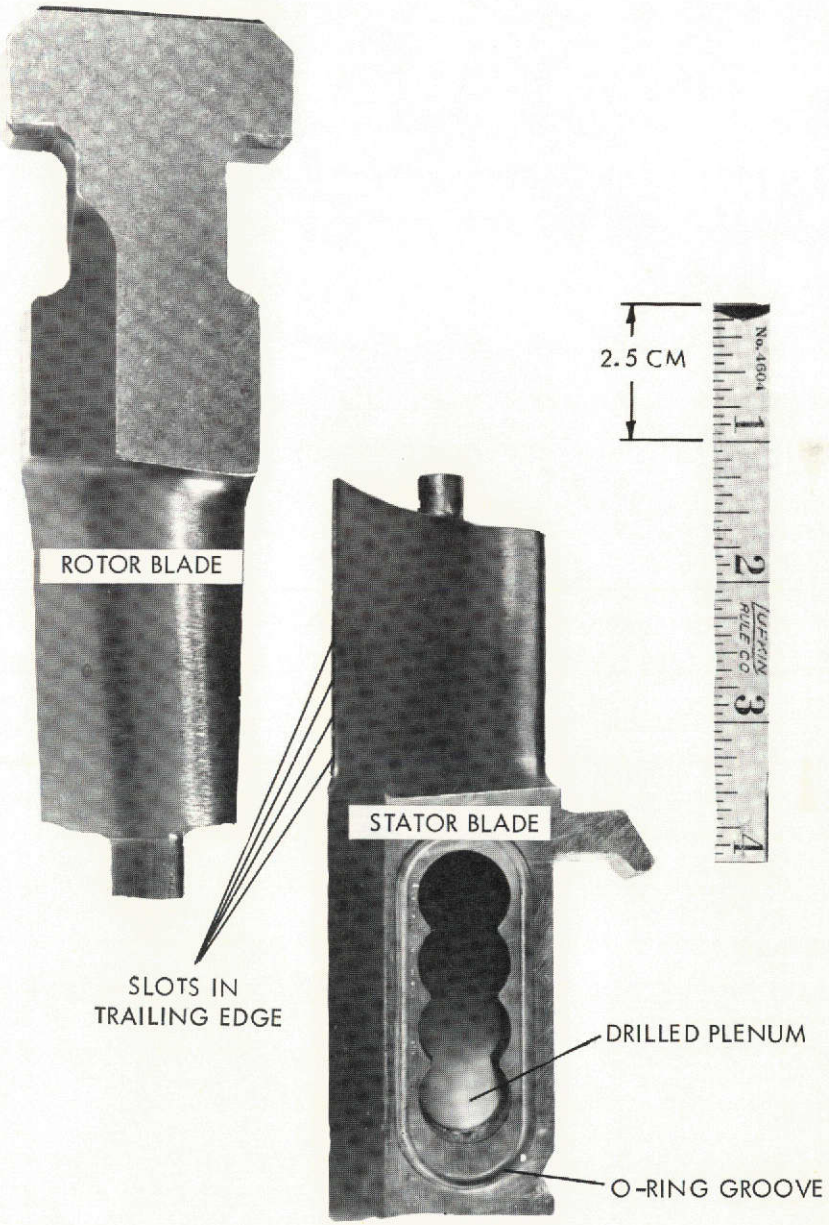

Figure 5. Test Stage Blades

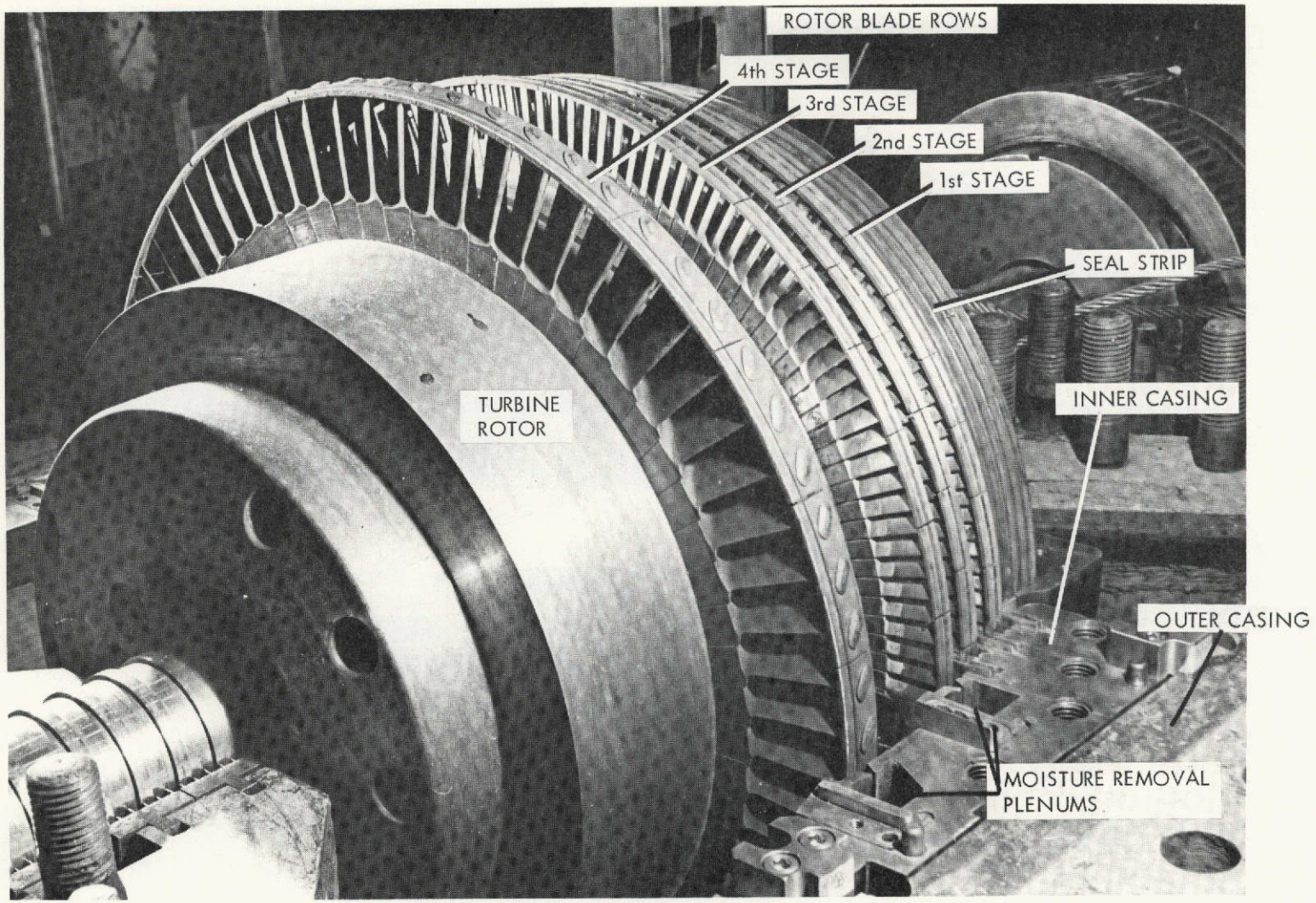

Figure 6. Turbine Rotor Installation

Due to the gradual transition, without abrupt change in the annulus contour, it is not felt that the 12 degree flare has an adverse effect on the turbine performance. As the meridional stream tubes are in general, straight, conical lines, there is no significant effect on the radial equilibrium, due to stream tube curvature, or on the flow in the blade path. This is borne out by the use of the same standard blades as Westinghouse turbines with flare angles in the range of 3 to 12 degrees. There is no detectable difference in the turbine performance associated with the amount of the flare. While the hub to tip diameter ratios are somewhat lower in the regions of the 12 degree flare, possibly in the order of 0.76 to 0.80 diameter ratio, it is improbable that the 12 degree flare would have a notable effect at diameter ratios in the order of 0.88 to 0.90 as in the "slave" turbine. At the higher diameter ratio, there is less disturbance of the meridional stream tubes due to a change in density along the blade height.

Seals and Thrust Balance

Due to the high diameter ratio, leakage control is an important factor particularly at the inlet end of the turbine. A multiple seal arrangement is used on the first stator blade row with two seals used on all other blade rows exclusive of the third and fourth rotor blades. Here, only one seal is used to allow for the moisture extraction groove in the casing.

Additional sealing at the inlet to the turbine was provided in order to control the axial thrust. The maximum allowable rating for the facility thrust bearing is 5440 kg (12,000 lbs). Due to the high stage loading and reaction blading used in the test turbine, the net rotor thrust would exceed this limit. By providing a balance housing at the turbine inlet, the pressure acting on a major portion of the inlet face of the rotor is reduced with a corresponding reduction in rotor thrust. Although testing was performed at essentially two inlet pressures 2.2×10^5 N/m^2 (31.8 psia) and 4.7×10^5 N/m^2 (68.5 psia), the turbine was designed to also accommodate testing at a higher inlet pressure of 9.8×10^5 N/m^2 (142.8 psia). These inlet pressure conditions are referred to as low, medium and high density operation, respectively.

The sealing arrangement as shown in Figure 3 consists of six seals. Seal design clearance is 0.025 cm (0.01 inch). For the high density inlet conditions of $9.8 \times 10^5 N/m^2$ (142.8 psia) which results in the highest thrust loads, the pressure at the seal exit can be maintained at 1.7×10^5 (24.3 psia). For a design turbine exit pressure of 0.7×10^5 (9.8 psia), the net rotor thrust is then within allowable limits. The steam flow through the seals is 0.304 kg/sec (0.686 lb/sec). This flow is removed from the balancing housing by two 5.4 cm (2.1 inch) vent tubes which pass through the turbine casing and piped to a condenser. The turbine casing was modified to accept the two vent tubes.

4.2.2 Thermodynamic and Flow Design Parameters

The function of the three stage slave turbine was to provide steam, at 8% equilibrium moisture, to the test stage. The design conditions for the slave turbine at the low and medium density test conditions are given in the table below:

	Medium Density	Low Density
Inlet Pressure	$4.7 \times 10^5 N/m^2$ (68.5 psia)	$2.2 \times 10^5 N/m^2$ (31.8 psia)
Inlet Temperature	$431^\circ K$ ($316.2^\circ F$)	$402^\circ K$ ($265.0^\circ F$)
Exit Static Pressure	$5.8 \times 10^4 N/m^2$ (8.4 psia)	$2.7 \times 10^4 N/m^2$ (3.9 psia)
Exit Moisture	8%	8%
Total Efficiency	80%	80%

Turbine exit pressure for the medium and low density conditions are 2.6×10^4 N/m^2 (3.8 psia) and $1.1 \times 10^4 N/m^2$ (1.6 psia) respectively, with exit qualities of 10.1% and 9.9%. The actual expansion lines for the turbine, including the test stage, are shown in Figure 7.

In order to satisfy the desired moisture level of 8% into the test stage for the high density conditions, a slave turbine efficiency of 80% was necessary. Although increasing the inlet pressure or decreasing the inlet superheat also aids in maintaining an acceptable moisture level, these

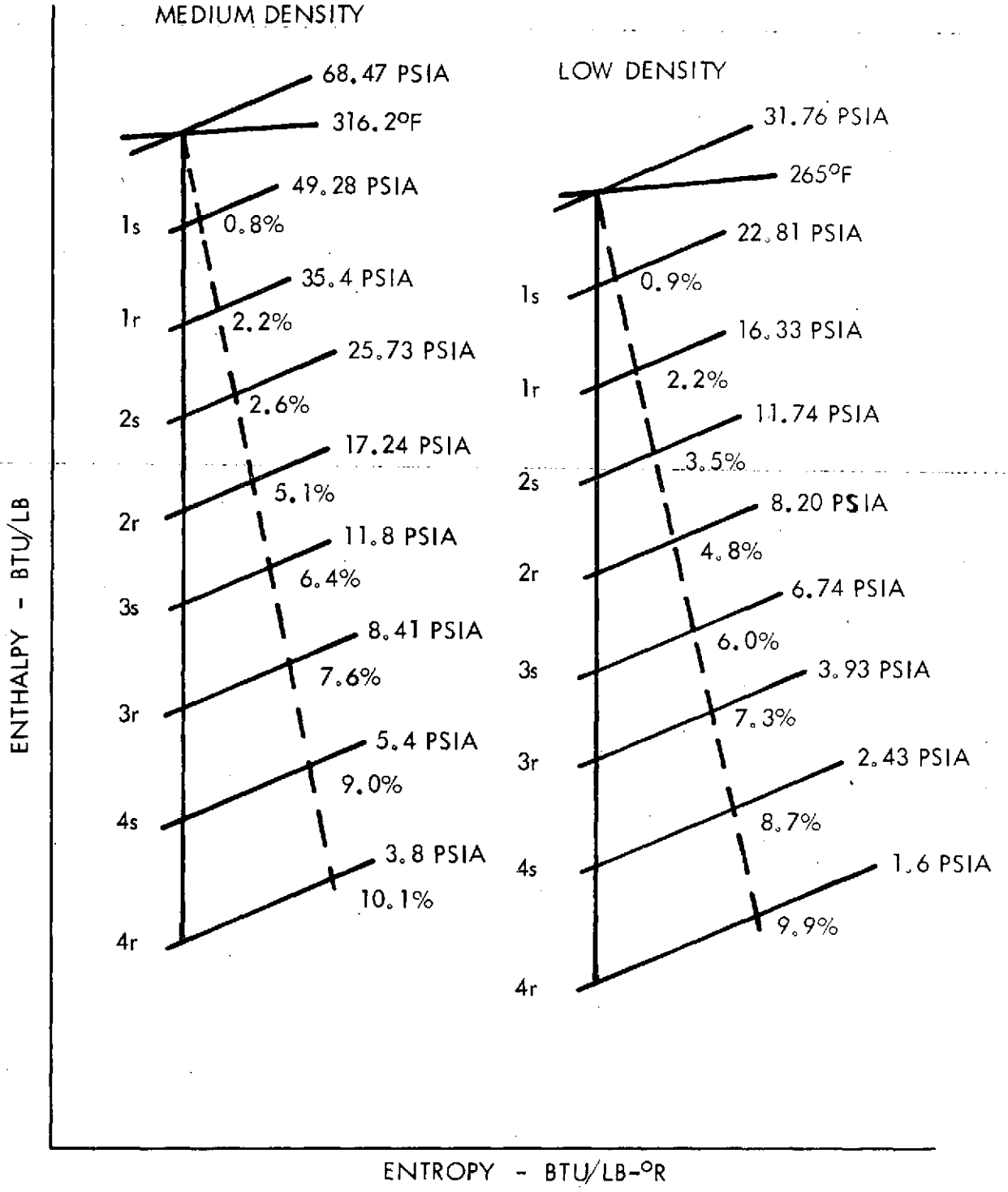

Figure 7a. Expansion Lines - Medium and Low Density

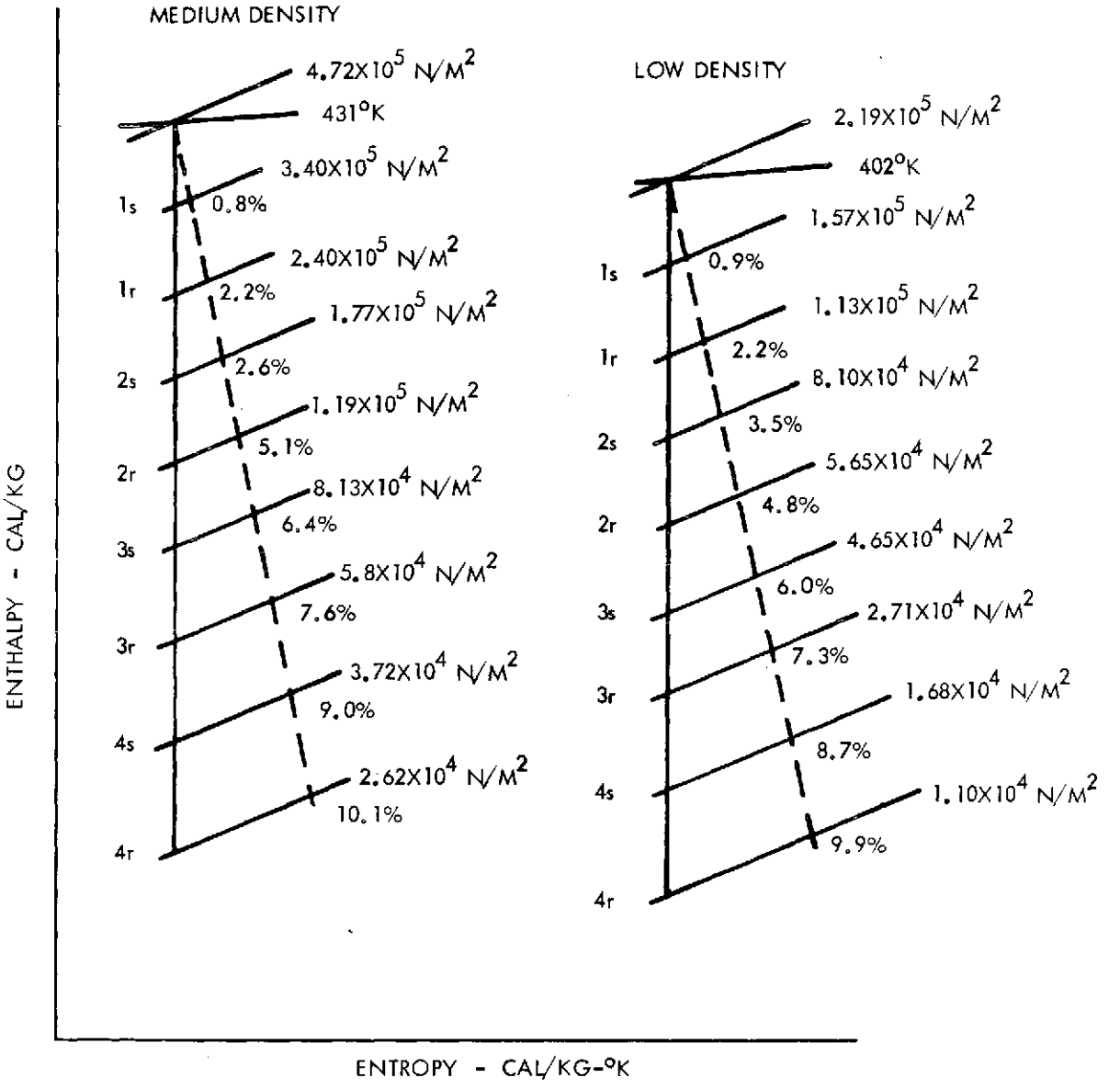

Figure 7b. Expansion Lines - Medium and Low Density

options were not available due to maximum allowable inlet pressures limited by the casing construction and the likelihood that less superheat would result in moisture carryover from the desuperheater section. Turbine inlet temperature was maintained at approximately 8°K (14°F) superheat, as a minimum, in attempting to assure dry steam at the turbine inlet. Appendix A2 gives further details on the thermodynamic design.

4.2.3 Moisture Predictions

Prior to the design of the test hardware, calculations were carried out using available theory to predict the moisture conditions at the fourth stage observation points. The purposes of the calculations were twofold: to provide design criteria for the test hardware and to provide information for a comparison between a theoretical analysis and actual observations.

Fog Particle Radii

As previously outlined in Section 3.0, the entire stream of moisture events starts with the condensation from the bulk flow of small fog particles. Estimates of these fog particle radii were made using empirical data from Gyarmathy and Meyer[8]. This information, for wet steam flow in nozzles, was used to estimate the average particle radius at the Wilson condensation point. The fog particle radii at downstream locations were then estimated assuming uniform condensation takes place on each assumed uniform fog particle, allowing for the fog particles lost by collection on turbine surfaces.

Numbers were generated for a "high" turbine inlet pressure condition, $9.8 \times 10^5 N/m^2$ (142.8 psia) and a "low" turbine inlet condition $2.2 \times 10^5 N/m^2$ (31.8 psia). In both cases, the design quality of the steam exiting the fourth stage of the turbine is 90%, or 10% of the steam has condensed from inlet to exit.

Under both the high and low pressure conditions, the steam remains supersaturated until near the exit of the second stator row. The predicted values of fog particle radii at the fourth stage are given in the following table.

Test Condition	Fourth Stage Location	Average Fog Particle Radius (Micrometers)	(Microinches)
Turbine Inlet $9.8 \times 10^5 N/m^2$ (142.8 psia)	Stage Inlet	0.31	(12.2)
	Stator Exit	0.32	(12.6)
	Stage Outlet	0.33	(13.0)
Turbine Inlet $2.2 \times 10^5 N/m^2$ (31.8 psia)	Stage Inlet	0.19	(7.5)
	Stator Exit	0.20	(7.9)
	Stage Outlet	0.21	(8.3)

Amounts of Moisture Collected

The estimates of the fog particle radii were used to calculate the fraction of condensed moisture collected using a procedure after Fentress[5]. Calculations by Fentress gave the result that most of the moisture is collected by the concave surfaces of the turbine blades. Therefore, only concave surface collection was considered in preparing the estimates of collected moisture fractions at the fourth stage of the test turbine that follow:

	Fourth Stage Location	Cumulative Collected Fraction of Total Moisture - %
Turbine Inlet $9.8 \times 10^5 N/m^2$ (142.8 psia)	Stage Inlet	6.6
	Stator Exit	8.8
	Stage Outlet	11.4
Turbine Inlet $2.2 \times 10^5 N/m^2$ (31.8 psia)	Stage Inlet	4.8
	Stator Exit	7.0
	Stage Outlet	10.0

The foregoing numbers indicate that only about 1% of the total turbine flow collects on the turbine surfaces even though 10% of the total flow condenses. Most of the condensate remains vapor-bourne.

Atomized Drops

By the moisture model used, the moisture collected on surfaces ends up at the trailing edges of the stator blades. This moisture is torn from the stators in relatively large globs by the vapor flowing past. It is further atomized into small drops in the wake of the stator blades by a secondary process. These drops accelerate rapidly downstream of the stators. While the secondary atomized drops are small in an absolute sense and accelerate rapidly, they are much larger than the fog particles and do not reach vapor velocity before they impact the leading edges of the rotor blades.

The atomized drop calculations were carried out using computer programs. First, the blade surface velocities are established through the use of a computer code by Katsanis[9]. These surface velocities are then a part of the input to an atomized drop code[10]. The latter code then calculates atomized drop diameters and drop velocities downstream of the stator blades.

The maximum secondary atomized drops from the fourth stators were calculated to be about 155 micrometers (6102 micro-inches) diameter for the low $2.2 \times 10^5 N/m^2$ (31.8 psia) turbine inlet pressure condition and about 40 micrometers (1575 micro-inches) diameter for the high $9.8 \times 10^5 N/m^2$ turbine inlet pressure condition. The distance downstream of the fourth stator at which secondary atomization is completed was calculated to be about 0.5 cm (0.2 inch). The velocity of 155 micrometers (6102 micro-inches) drop 1 cm (0.4 inch) downstream of the fourth stator at low inlet pressure conditions was found to be about 13 meter/sec (43 ft/sec). The velocity at the inlet plane of the fourth rotor blades for the same drop and inlet pressure is about 66 m/sec (216 ft/sec).

4.2.4 Moisture Removal Features

Trailing edge moisture removal slots were installed in the fourth stage test stator blades. Only the outer half of the blades had slots. This was partly because only the outer half of the blades could be observed optically. It also limited the pressure difference in the radial direction that had to be accommodated, as discussed hereafter.

A consideration in the design of the slot was the centrifugal pressure gradient downstream of the stator blade row. This gradient for the low density condition is approximately 1034 N/m^2 (0.15 psi) with respect to the outer diameter and mean blade height positions. This tends to promote a radial inflow which would carry moisture into the slot in the tip region and out into the flow in the vicinity of the slot inner radius position. In order to overcome this, the extraction slot velocity head must be of the same order of magnitude as the radial pressure gradient at the slot mouth.

Due to the extremely small amount of moisture collected on the stator blades, it is necessary to extract a quantity of steam along with the moisture to induce a sufficiently large velocity in the slot. The required amount of extraction flow can be reduced by compartmenting the slot in the heightwise direction, as shown in Figure 8. As there is less radial pressure gradient along each of the compartments, less velocity and extraction flow is required to overcome the pressure gradient. With four compartments, the estimated required extraction flow is approximately 62% of the estimated required flow with a continuous slot at the low density condition. For a 0.025 cm (0.01 inch) slot width, and four slots extending from the outer to mean position along the blade height, the steam extraction flow is in the order of 0.28% of the stage flow. This is approximately equal to the mass flow of estimated extracted moisture.

The predicted performance at the low density condition using four trailing edge slots is as follows:

$\frac{\text{Steam Flow}}{\text{Stage Flow}}$	$\frac{\text{Moisture Flow}}{\text{Stage Flow}}$	$\frac{\text{Mixture Flow}}{\text{Stage Flow}}$
0.00276	0.00277	0.00553

These data are based on the following design assumptions:

- Collection of 3.2% of the equilibrium moisture available in the vapor.
- 8.65% average equilibrium moisture content based on conditions at inlet and exit of blade.
- Extraction flow velocity head, in slot, equal to 1-1/2 times the radial pressure gradient at the mouth of the slot.
- 0.025 cm (0.01 inch) slot width.
- Slots extend from the outer position to the mean position along the stator blade height.

As the steam extraction flow is roughly directly proportional to the width of the slot, the flow is reduced by minimizing the slot width. Both minimum width and the number of compartments were limited by manufacturing considerations and the danger of clogging the slot. The 0.025 cm (0.01 inch) width appeared to be a reasonable choice.

Refinements to the above analysis were investigated. Using Martinneli-Lockhart data to account for the effect of the two phase flow on the friction factors, the calculated extraction flow is approximately 5% less than reported above. Also, the condensation on the external surface of the stator blade, associated with the temperature drop in the extraction slot, was investigated. Since the extraction flow is a two phase mixture, the pressure drop in the slot is accompanied by a drop in the saturation temperature. This cools the surface of the blade in the vicinity of the slot and promotes condensation. By this calculation, the condensation is in the amount of 0.004 gm/sec (0.034 lb/hr) per blade. This represents an approximate 5% increase in the estimated amount of the collected moisture.

Figure 8 shows the relationship of the extraction slots to the physical arrangement of the collection system internal to the blade. The following discussion traces the extraction flow from the slots to the external collection system.

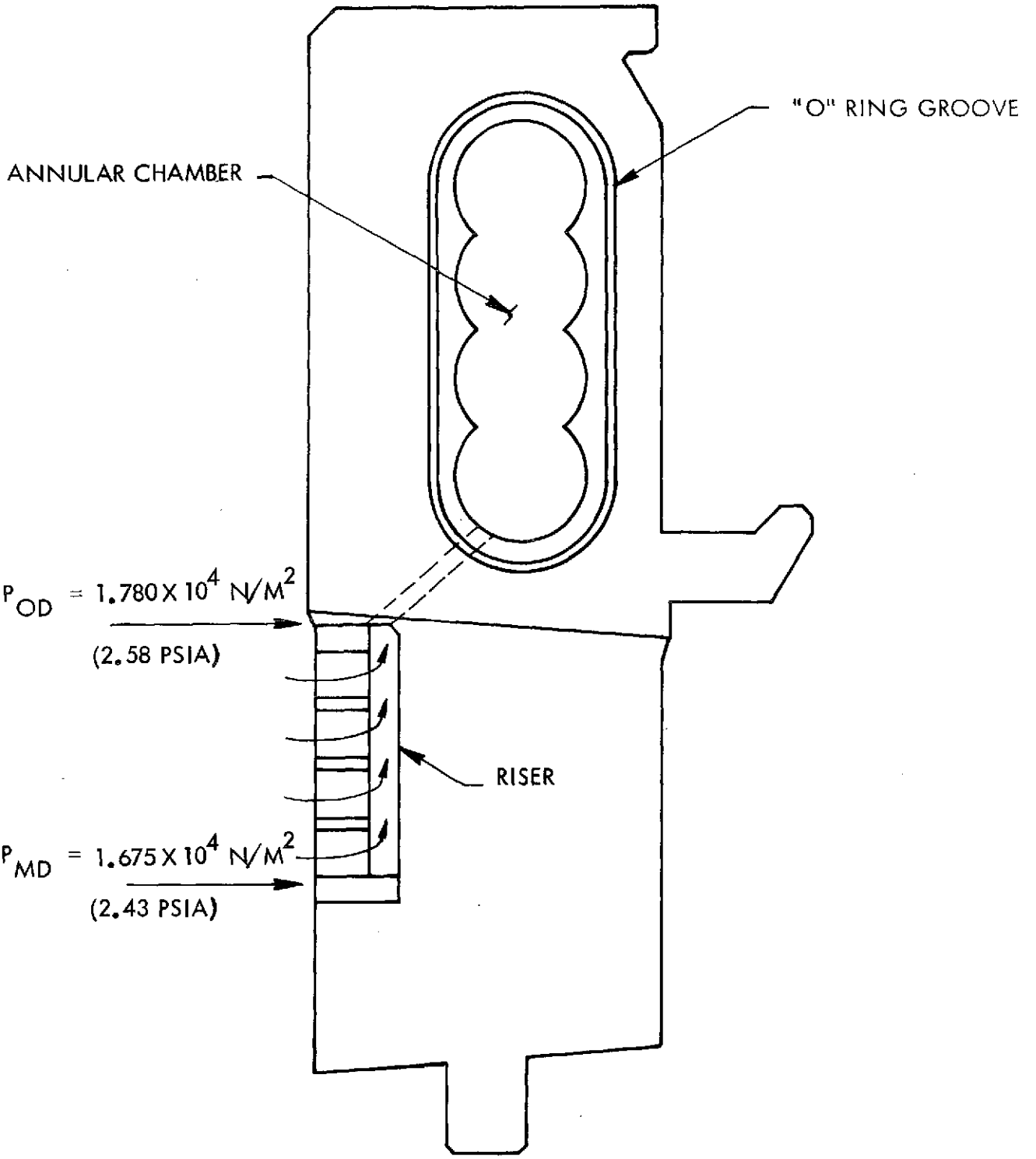

Figure 8. Moisture Removal Slots - Stator Blade

Downstream of the slot, the extraction flow moves radially outward, through the riser, to the annular chamber in the root of the stator blade. The annular chamber was formed by drilling four adjacent holes to form an elongated hole in the blade root. An "O" ring groove is machined on one side of the root around the periphery of the elongated hole. As the blades are assembled in the turbine, the holes in the root of the blades form a continuous annular chamber for the extraction flow. The "O" ring between each blade prevents leakage. Pipes passing through the turbine casing, into the annular chamber at different circumferential locations, carry the extraction mixture to the collection system.

Due to the complexity of the flow path through the stator blade and hence the uncertainties involved in predicting the pressure loss across the blade, pressure drop tests were run at the NASA Lewis Research Center on an actual blade with compressed air. The facility, designed to test cooled gas turbine blades, was particularly suited for this test. Figure 9 shows the measured pressure drop as a function of flow. The data are presented on a referred flow basis to more readily apply the data to the actual steam conditions in the test turbine. The measured losses were higher than originally assumed and this information proved valuable in the design of the removal piping.

Figure 10 shows the removal piping for the stator blades. Six pipes carry the liquid-vapor mixture from the annular pocket in the stator blade roots to a manifold. The circumferential locations of the pipes were influenced by the locations of the light tubes and borescopes inserted in the stationary blades. Due to these insertions, a continuous annular ring could not be maintained. Three separate segments are formed by periodic blocking of the annular ring. One segment consists of two active removal blades while a second segment consists of eight active removal blades. Each of the segments is drained by 0.95 cm (0.37 inch) pipe while the third segment, covering 30 blades, is drained by four 0.95 cm (0.37 inch) pipes. The six pipes enter a common manifold. The flow passes through large piping with low loss to the moisture removal-measurement tanks. The control valve permits varying the extraction steam

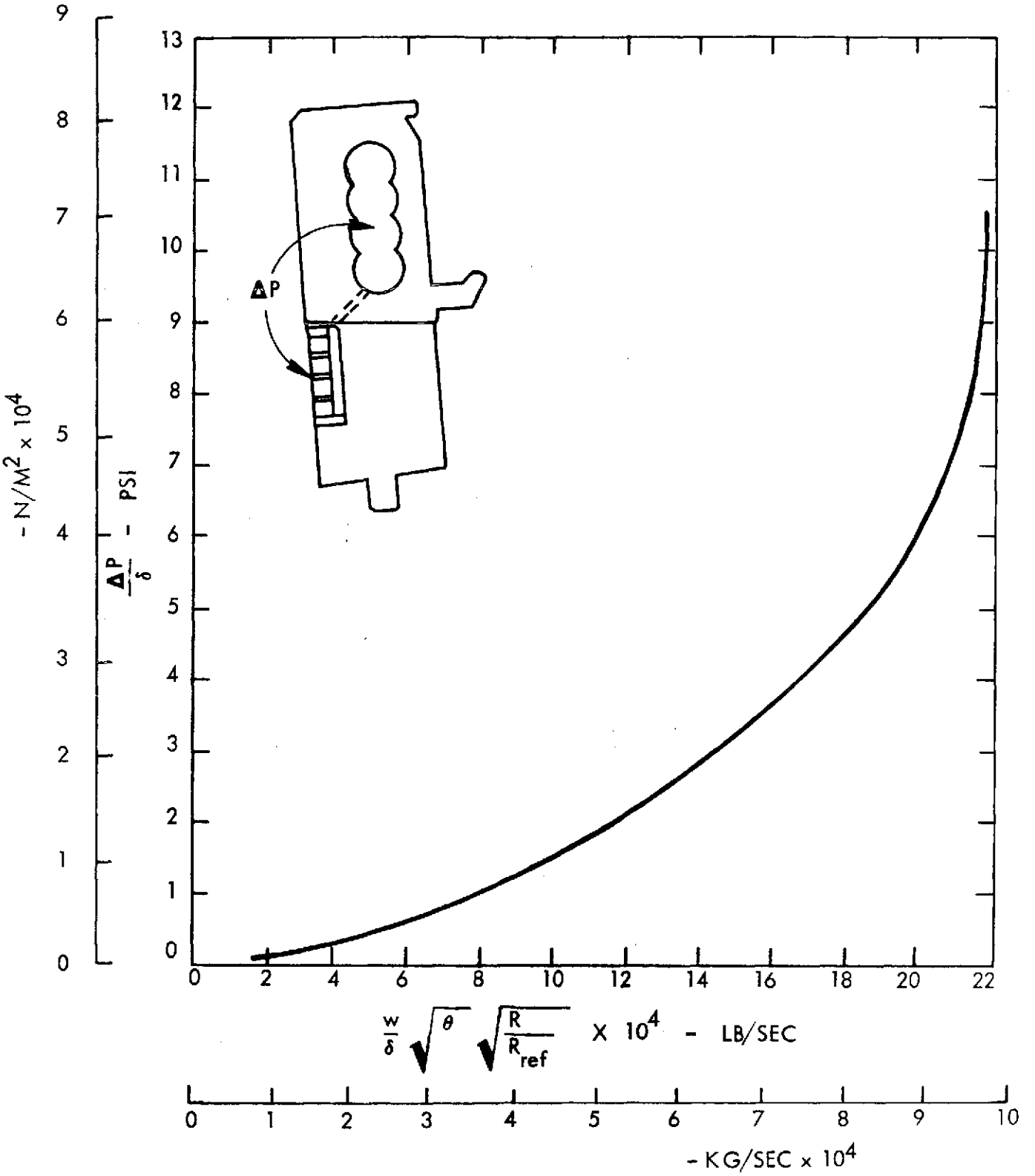

Figure 9. Measured Pressure Loss of Stator Blade

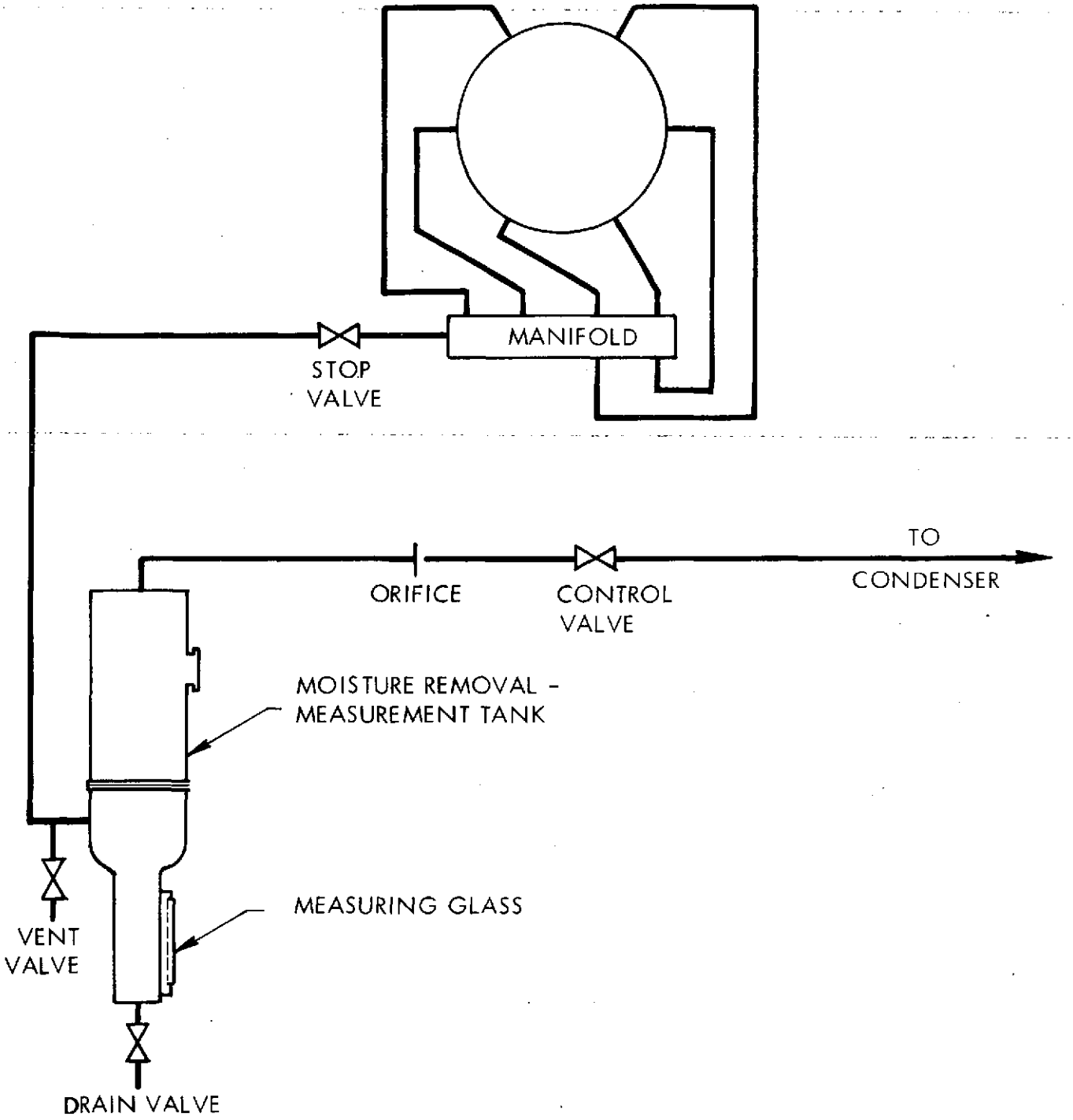

Figure 10. Stator Blade Moisture Removal Piping and Measurement System

rate. The orifice measurement determines the vapor flow rate and the tank serves a dual purpose of separating the liquid from the vapor and determining the liquid rate by measuring the change in liquid level in the base of the tanks. The control valve and stop valve also serve as isolation valves. After completion of a test point, these valves are closed, the vent valve is opened to raise the tank pressure to atmosphere and the tank is then emptied through the drain valve.

Referring to the photograph of one of the separator tanks (Figure 11), the separation of condensate from the extracted flow is achieved by a wire mesh mounted near the top of the tank. The tank diameter of approximately 41 cm (16 inches) was influenced by the necessity of keeping the vapor velocity through the wire mesh sufficiently low to assure 100% liquid removal. The window near the top of the tank permits observation of the condensate in the mesh. Visual observations confirmed the mesh was not flooded assuring a near 100% liquid separation.

The removal slots in the casing at the trailing edge of the third and fourth stage rotor blade rows are a rather conventional design. The center of each slot was placed in the same plane as the downstream edge of the corresponding rotor blade shroud. The performance of these removal slots is dependent on proper sizing of the slot area, the removal plenum geometry, and the number of extraction pipes taking the moisture and vapor flow out to the rest of the collection system. A large number of small pipes is desirable for uniform removal. Due to the double wall construction of the test turbine and the number of penetrations required for the borescopes and light tubes, the number of extraction pipes was limited. A schematic diagram for the rotor casing slot removal and measurement system is shown in Figure 12. The system is similar to that used for the stator blade collection system. Six pipes are used for the third stage and five for the fourth stage. The manifold and valving was arranged such that either system could be operated separately or simultaneously.

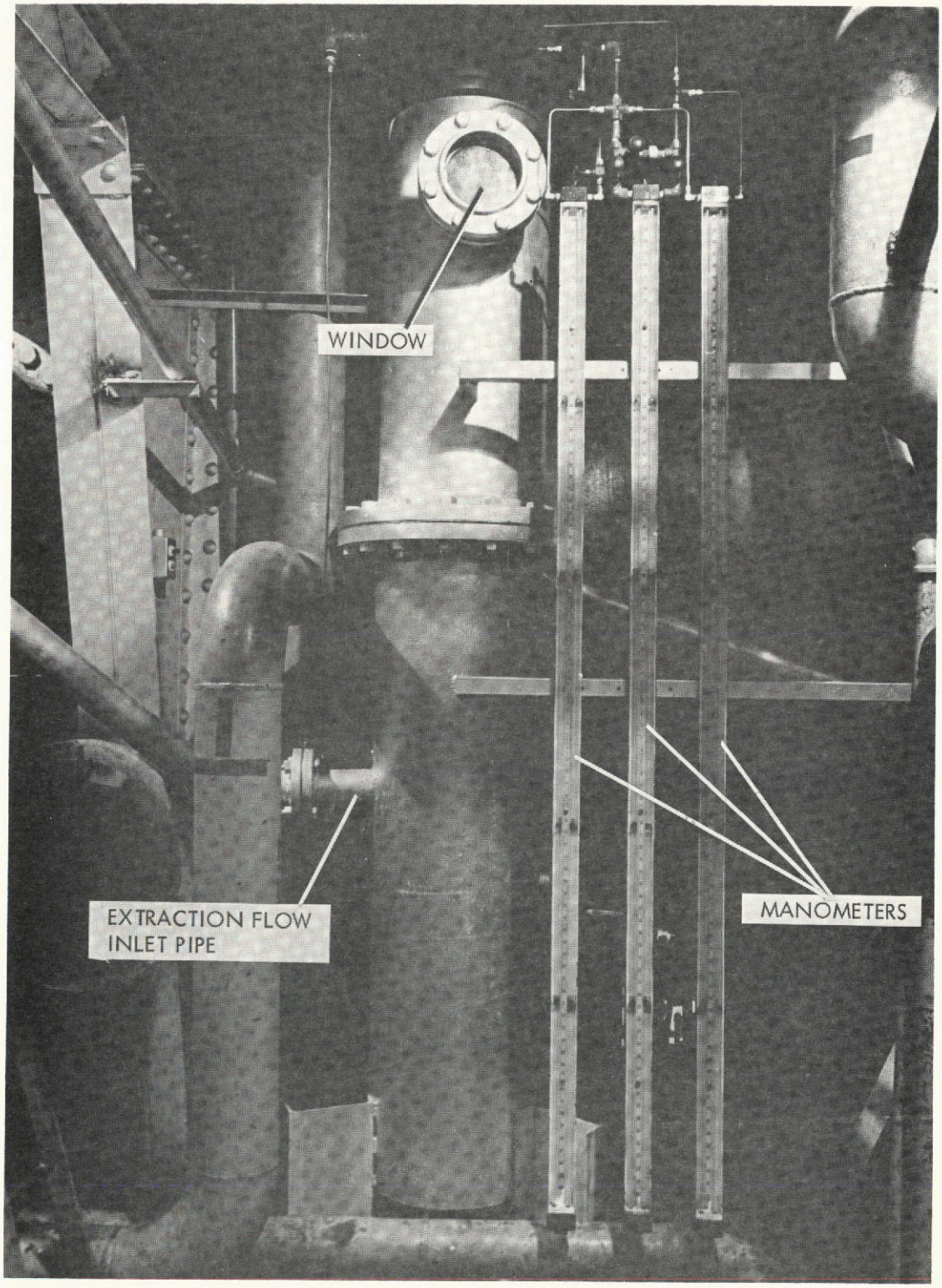

Figure 11. Moisture Separator and Measurement Tanks

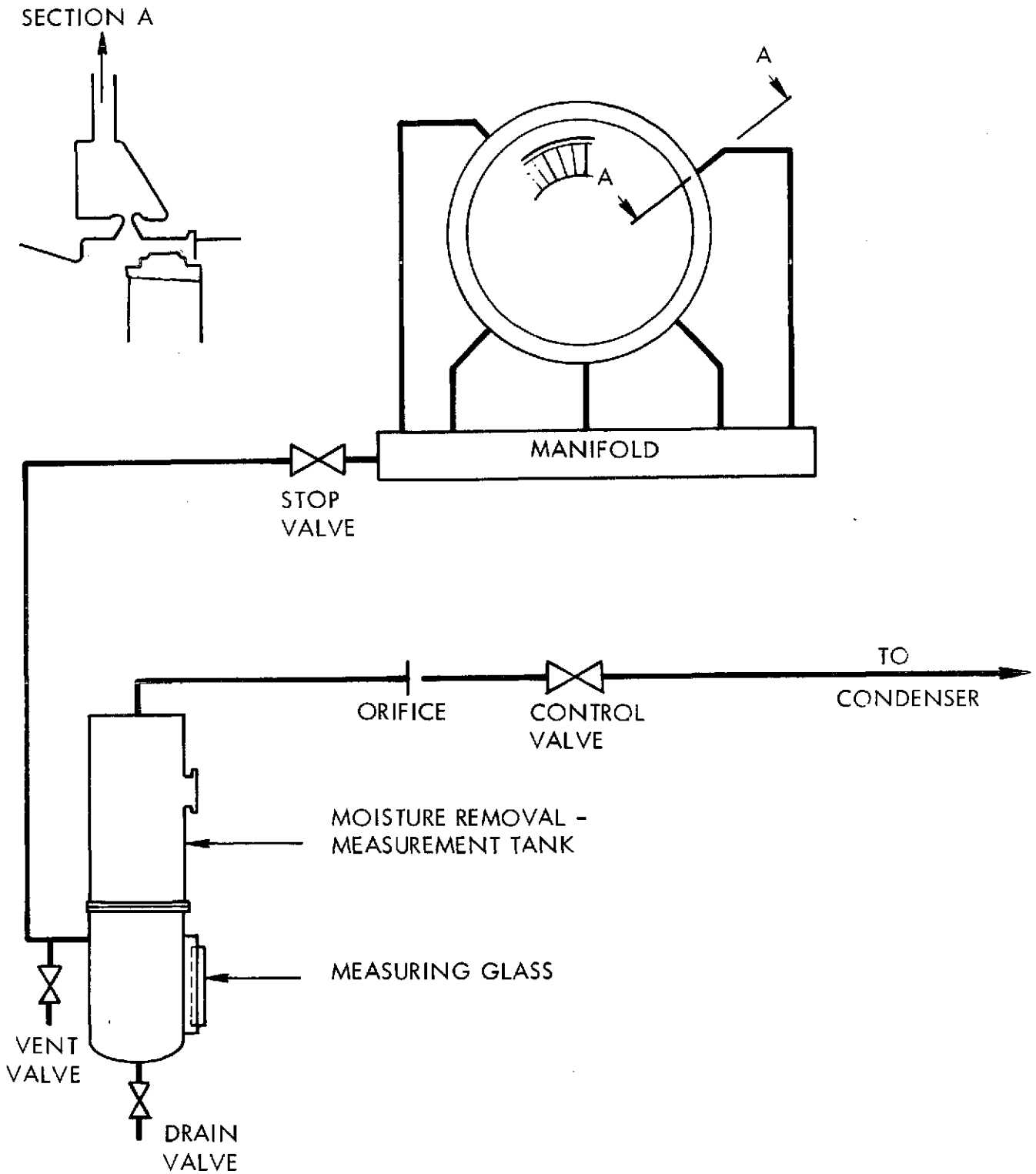

Figure 12. Fourth Stage Rotor Casing Slot Removal System

5.0 PHOTOGRAPHIC EQUIPMENT

Photographic System Design Considerations

An important consideration in the photographic system design was to avoid disturbing the flow being photographed with the instrumentation. Tests were performed in a two-dimensional high Reynolds number air cascade using blading similar to that of the fourth stage stator to investigate the effects of placement of the instrumentation on the flow. Results of these tests indicated that small diameter instrumentation could be placed in certain locations in the stator-rotor blade axial space without seriously disturbing the flow either on the surface or in the wake of the blade being photographed. These tests showed further that a large cutout in the adjacent stator blade could be tolerated without seriously affecting the flow on the blade being photographed. These criteria were used as guidelines in the placement of the optical instrumentation in the turbine. The cascade tests are discussed in greater detail in Appendix A1.

Another important consideration in the photo system design results from the fact that the sub-micron diameter fog droplets scatter and attenuate the light. Rough calculations indicated that at low pressure levels there will be only small attenuation by the fog. However, at high pressures, the calculations indicate substantial light attenuation. These results are qualitatively consistent with observations made in steam turbines. Therefore, to minimize effects of the fog on light attenuation and scattering, the lighting to subject, and subject to borescope distances were kept as small as possible without significantly affecting the flow.

Prior to photographic condensate flow in the test turbine, checkout tests of the optical systems were run at the NASA-Lewis Research Center[11]. Tests were run in a full scale wooden model of a section of the test stage that held the actual turbine blades. The photographic instrumentation was placed in the model in the same orientation as planned for the test turbine. The test results were encouraging, although the light attenuation due to the fog particles could not be simulated. Condensate flow was simulated with an aerosol using an air-water mixture. The photographic results indicated that for water flowing across a blade surface, the best contrast

can be achieved by utilizing a bare metal rather than a painted surface. However, a painted blade was also photographed and it was decided to use a painted blade in the turbine for the initial testing in order to maximize on the lighting and to gain some experience with painted surfaces in a steam turbine. The checkout photo tests also demonstrated that for front lighted drop photography, which was to be done at the exit of the last rotor blade, best results could be achieved with a black background. Therefore, the last rotor blades, after final assembly in the rotor, were painted a flat black.

General Instrumentation Description

The general photographic instrumentation approach was based on the use of borescopes and fiber-optic light tubes. Figure 13 shows the borescope used. It has a fixed mirror and two camera adapters; one with a Fastax bayonet and the other with standard C-mount threading. The magnification of the borescope is 0.2 at an object to borescope centerline distance of 2.5 cm (1.0 inch). The borescope field of view is approximately 53°. Its length is approximately 32.8 cm (12.9 inches).

Figure 14 shows the fiber-optic light tubes used for the blade surface photography. The light tubes have a rigid section clad with stainless steel tubing, a flexible section sheathed with PVC, and a quadrifurcated section with rigid plastic ends to efficiently gather light from the light source. One light tube has a mirrored tip to direct the light 90° to the light tube axis. The other light tube shown in Figure 14 has no mirror so that a cone of light shines outward with the cone centerline parallel to the light tube axis. The rigid stainless steel clad section of the light tubes, which are inserted in the turbine, are 1.427 cm (0.562 inch) in diameter. These light tubes are never inserted directly in the turbine flow path, so their diameter can exceed 0.953 cm (0.375 inch) the size used in the cascade tests without disturbing the flow being photographed. The overall length of the light tubes is approximately 91 cm (3 feet).

The light source selected for the blade surface photography and also used for back-lighted drop photography is the EG&G Model 501 high-speed strobe. The EG&G Model 501 consists

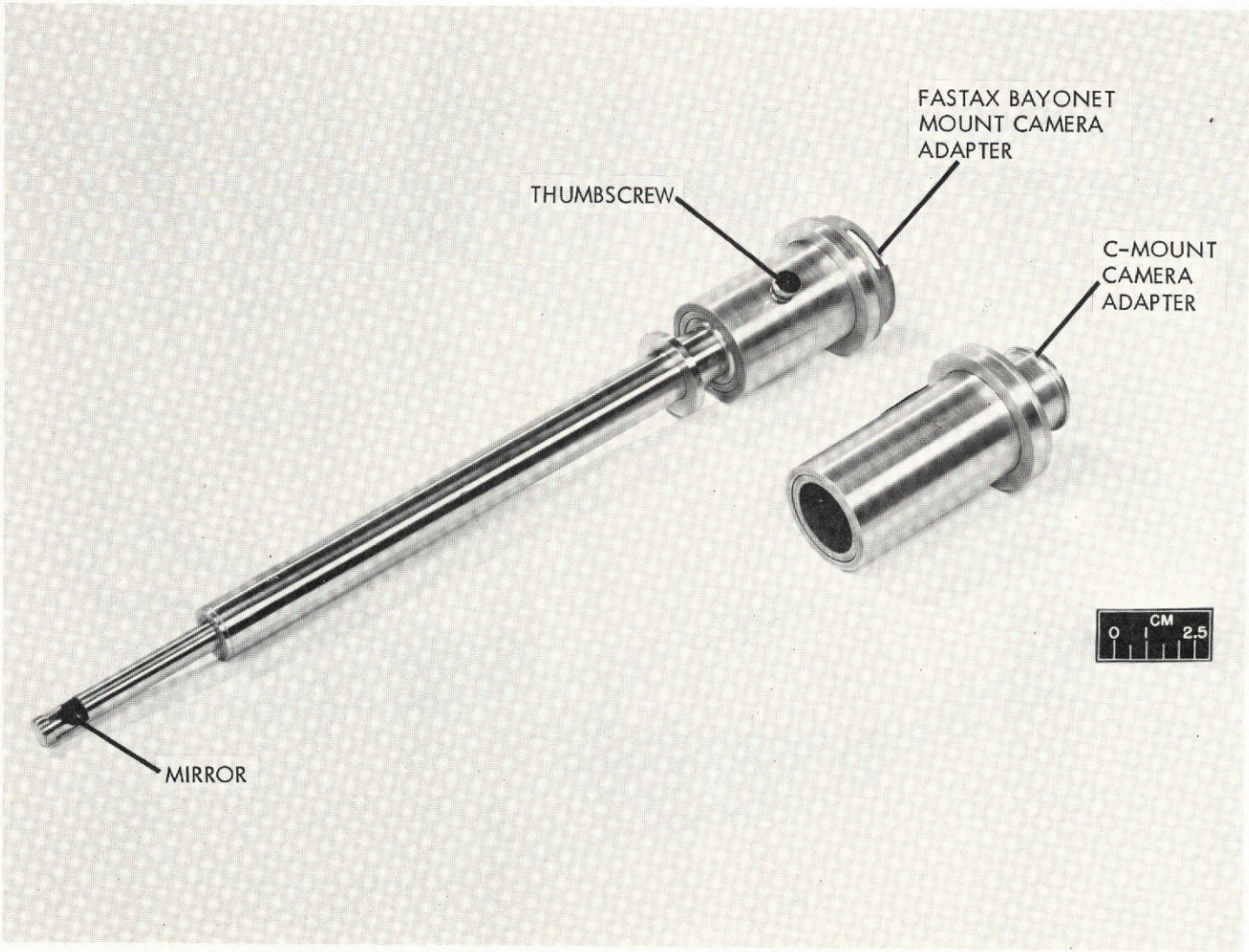

Figure 13. X0.2 Borescope

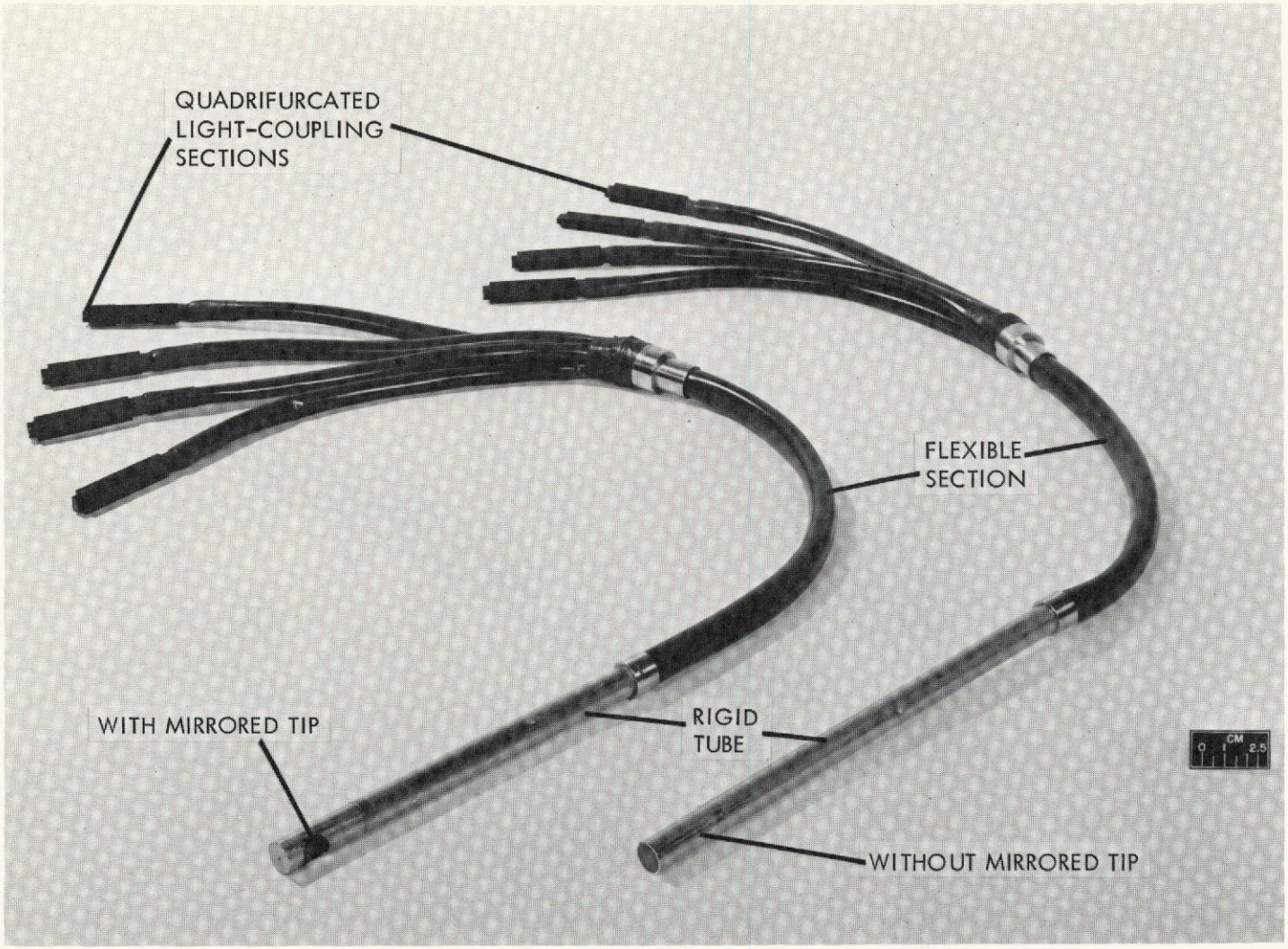

Figure 14. Fiber Optic Light Tubes

of a power supply, modulator, and timer unit housed in a cabinet plus lampholders and cables. The short-duration flash of the strobe stops the motion of the flow and gives the same illumination with a camera operating at different framing rates. Up to 6000 flashes per second are possible with the EG&G Model 501.

A variety of xenon flash tubes are available for use with the EG&G Model 501. Two flash tubes selected for this application are the FX-11-0.125 and FX-12-0.025, shown in Figure 15. Both flash tubes are 0.61 cm (0.21 inch) in diameter and approximately 9.53 cm (3.75 inches) long. The FX-11-0.125 has a 3.1 mm (0.125 inch) gap in a 4.0 mm (0.157 inch) inside-diameter quartz tube. The FX-11-0.125 and FX-12-0.25 flash tubes are filled with xenon to a pressure of 2×10^5 Pa (2 atmospheres) and 1×10^5 Pa (1 atmosphere), respectively.

The EG&G Model 501 has three capacitance settings, 0.01, 0.02, and 0.04 microfarad, for varying the flash tube light output. For flash duration and light output see Table 1 for the three capacitance settings[11]. With a capacitance setting of 0.01, microfarad on the FX-11-0.125 and FX-12-0.25 flash tubes, it is recommended that operation is limited to bursts of 500 and 100 flashes, respectively, to prevent overheating of the electrodes and quartz capillary walls and insure long flash tube life[11]. However, balancing turbine operation cost against flash tube costs, it was decided to exceed the recommended number of flashes. Most films were run at 0.02 and 0.04 microfarad with bursts of 1200 and 600 flashes, respectively. Approximately 95 rolls of film were shot which consumed seven flash tubes.

To use these small flash tubes, a coupling transformer unit is required. It has a 5 to 1 voltage stepdown ratio with the lamp on the low voltage side. The 2000 volts produced on the flash tube is insufficient for starting, so an 8000 volt starting pulse is obtained with a trigger electrode or starting coil. The transformer unit with a Lucite adapter to hold the fiber-optic light tube ends is shown in Figure 16. Since the flash lamps get very hot, a stream of cooling air can be passed between the flash lamp and the fiber-optic light tube ends to help keep the fiber-optic ends from getting too hot.

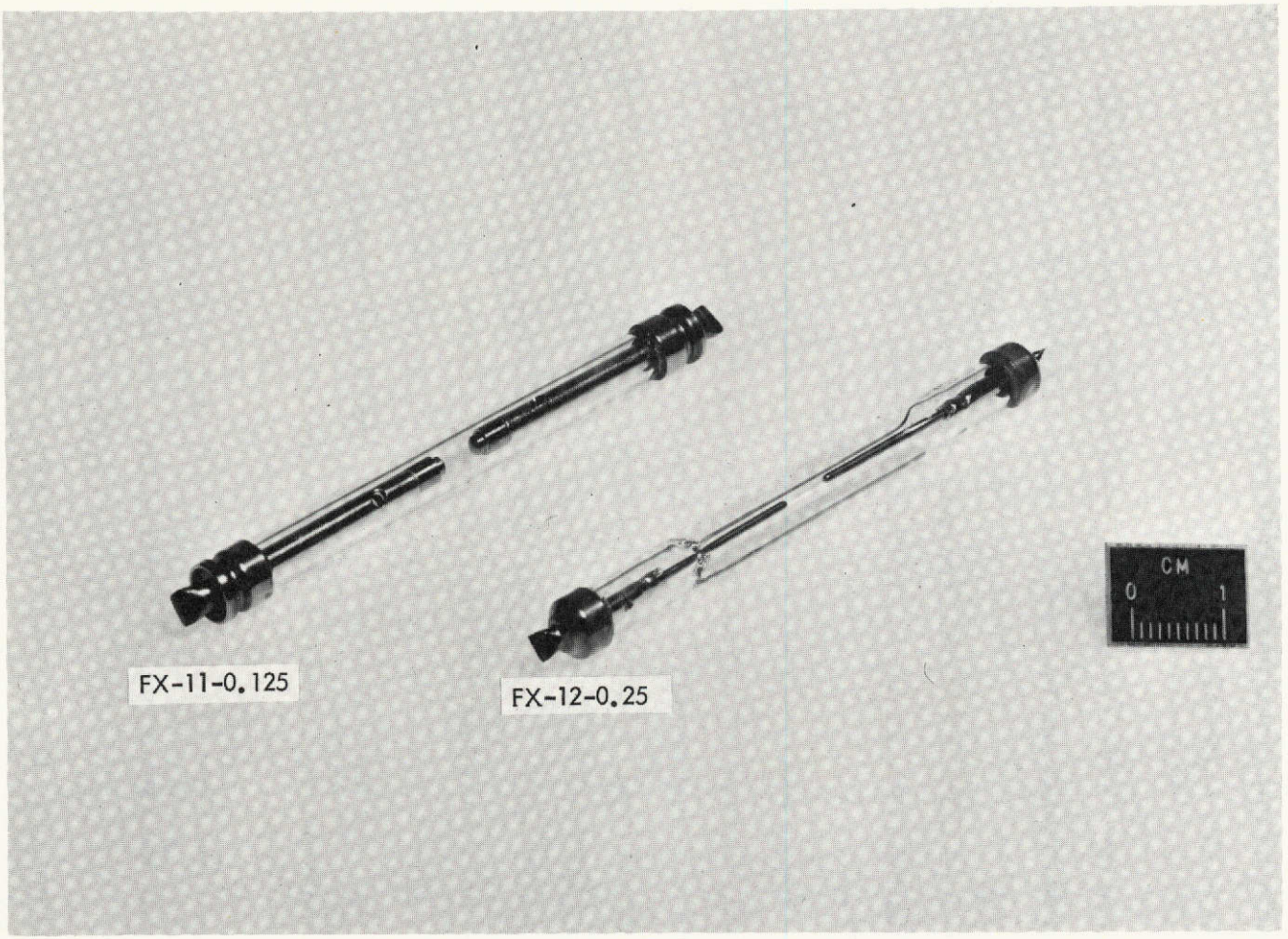

Figure 15. Xenon Flashtubes

TABLE 1

FLASHLAMP CHARACTERISTICS

Flash Lamp	Capacitance, F	Light Output, cp-sec	Pulse Width*, microsec
FX-11-0.125	0.01	0.39	0.9
	0.02	0.97	1.4
	0.04	1.67	2.2
FX-12-0.25	0.01	0.38	1.2
	0.02	0.90	1.4
	0.04	1.57	2.2

*At one-third peak amplitude

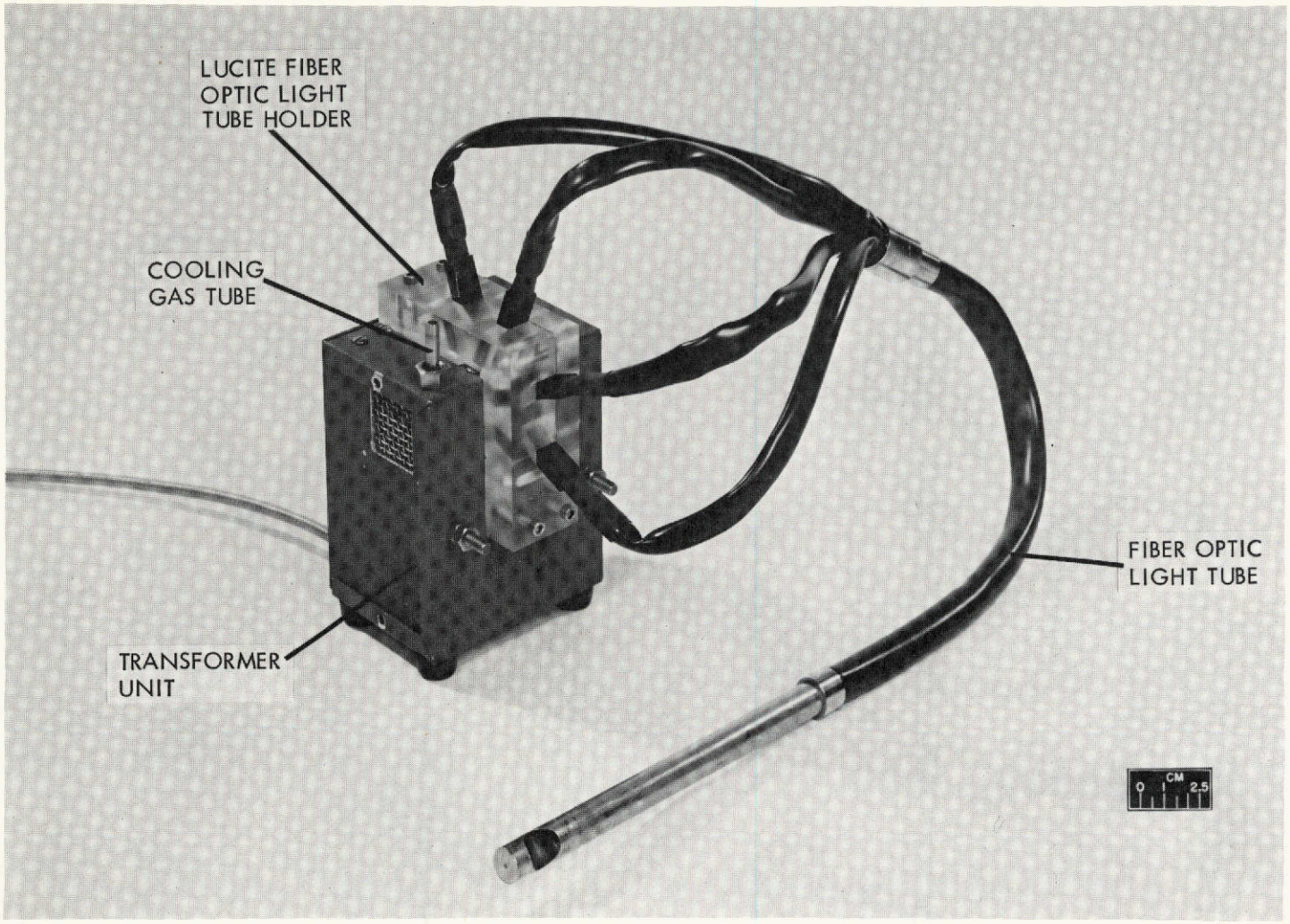

Figure 16. Modified Transformer Unit

A cross-sectional sketch showing the arrangement of the light tube ends around the flash lamp is shown in Figure 17. The flash tube and light tube ends are separated by a space of approximately 0.16 cm (0.0625 inch). Because there is an 8000 volt potential on the trigger electrode, the cladding on the light tube ends and the light tube holder were made of non-metallic materials.

The camera selected for the blade-surface photography was a 16 mm Fastax WF3 camera. A reluctance pickup on the Fastax camera is used to synchronize the flashing of the EG&G 501 to the camera shuttering. With a goose attachment, high-speed photography (up to 8000 flashes/second) can be obtained. All movies were run at 3000 flashes/second. A framing camera was selected for the rotor spray and removal slot photography and one drop photography technique.

5.1 ROTOR SPRAY AND REMOVAL SLOT PHOTOGRAPHY

The liquid in the turbine that is collected on the rotor blades is quickly spun to the blade tip shroud by centrifugal force and is thrown off at high velocity. Because of the high peripheral speed of the rotating blades, the drops are well atomized but still large compared with the fog drops. The purpose of the rotor spray photography was to qualitatively photograph the course of the spray with and without suction applied at the casing slot at the trailing edge of the rotor blade row.

Figure 18 shows a model simulation of the rotor view. A framing camera was used at framing speeds of 20 to 80 frames/second. The lighting distances for this view were relatively large compared to other views and the fiber-optic light tube and strobe system was found to be marginal. Therefore, light tubes containing small, high intensity, tungsten-halogen lamps were used to directly illuminate the view instead. Figure 19 shows one light tube along with the 8-1/2 volt, 62 watt (45.7 ft-lb/sec) tungsten-halogen lamp it contains. The light tube diameter is 1.426 cm (0.562 inch). The lamp is exposed to the steam flow, but the electrical leads are sealed from the steam by high temperature epoxy. A second light tube with a 1.9 cm (0.75 inch) diameter was used in addition to the 8-1/2 volt light tube. This tube contained a 120 volt, 250 watt (184.4 ft-lb/sec) tungsten-halogen lamp. The x0.2 borescope was used. Figure 20 shows the location of the borescope and light tubes relative

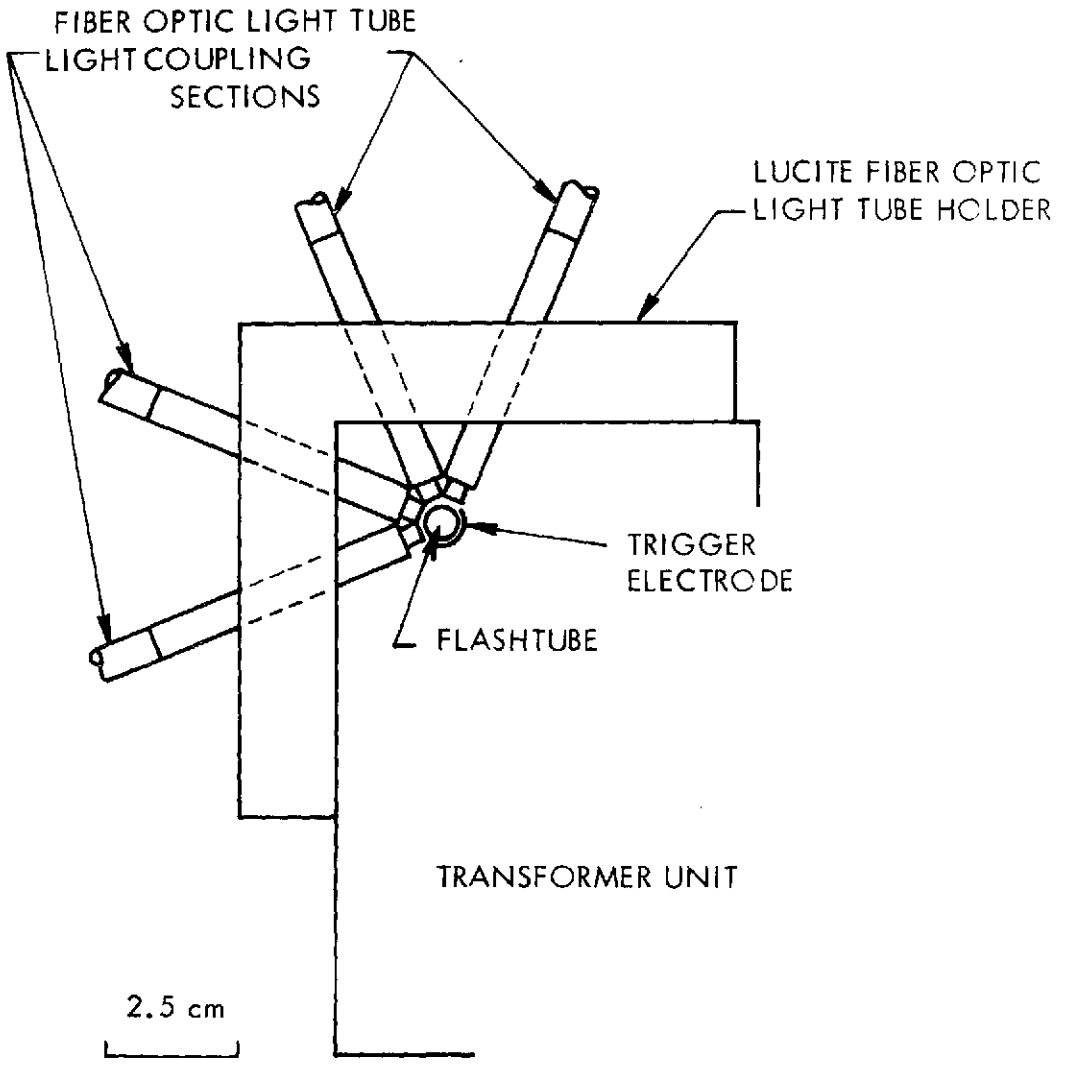

Figure 17. Arrangement of Fiber Optic Light Tube Ends Around Flashtube

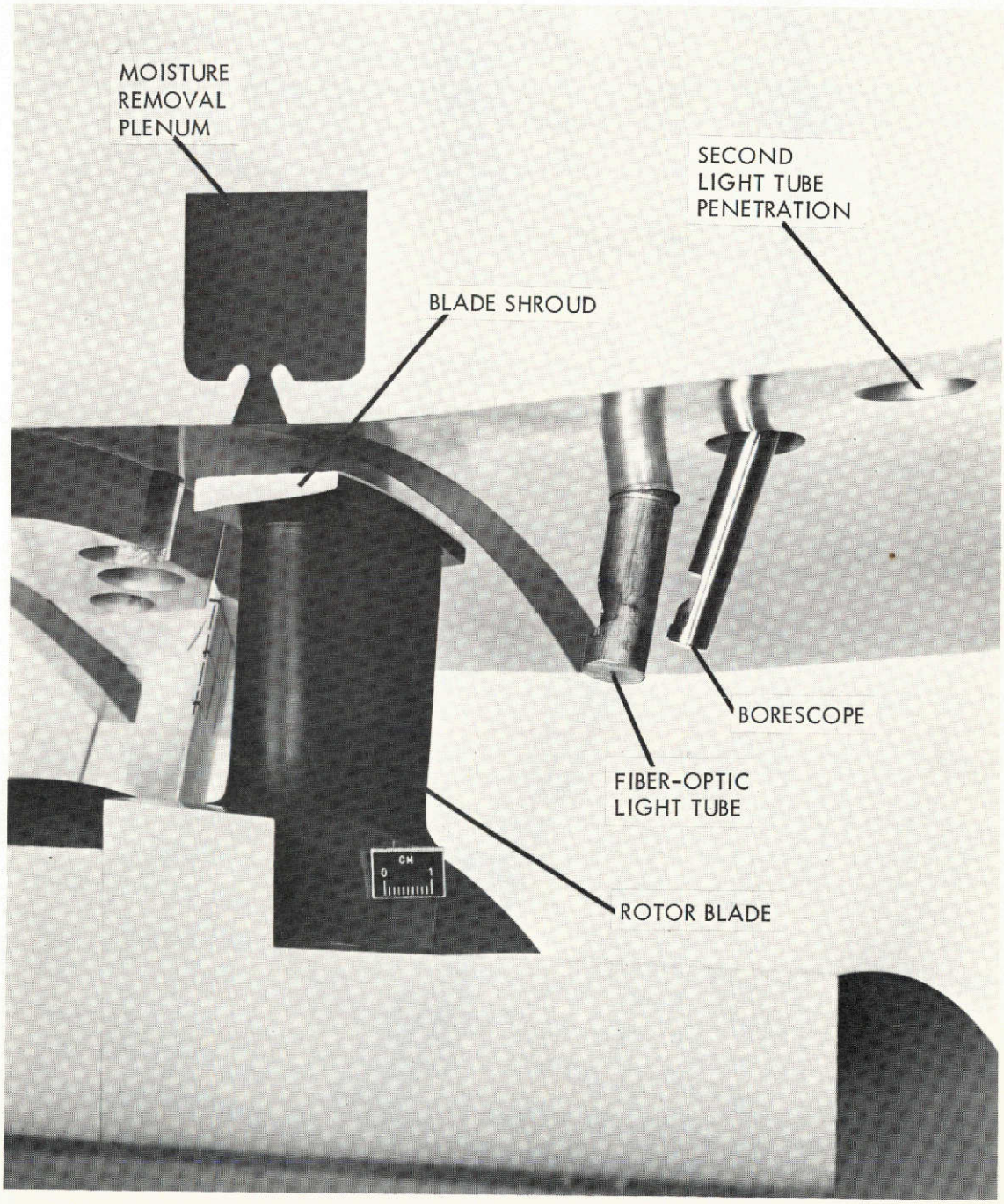

Figure 18. Rotor Blade Row View Configuration

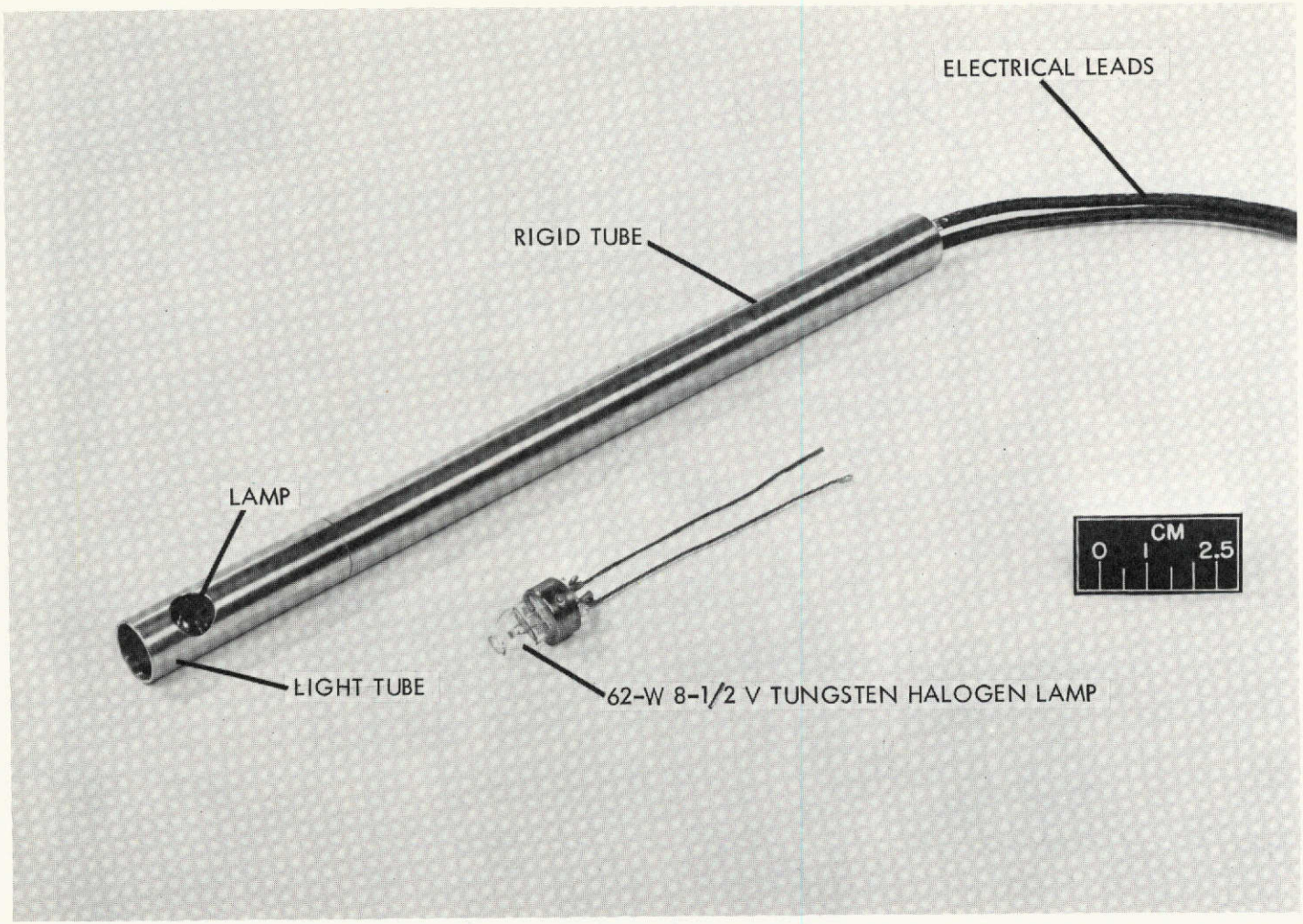

Figure 19. Tungsten - Halogen Light Tube

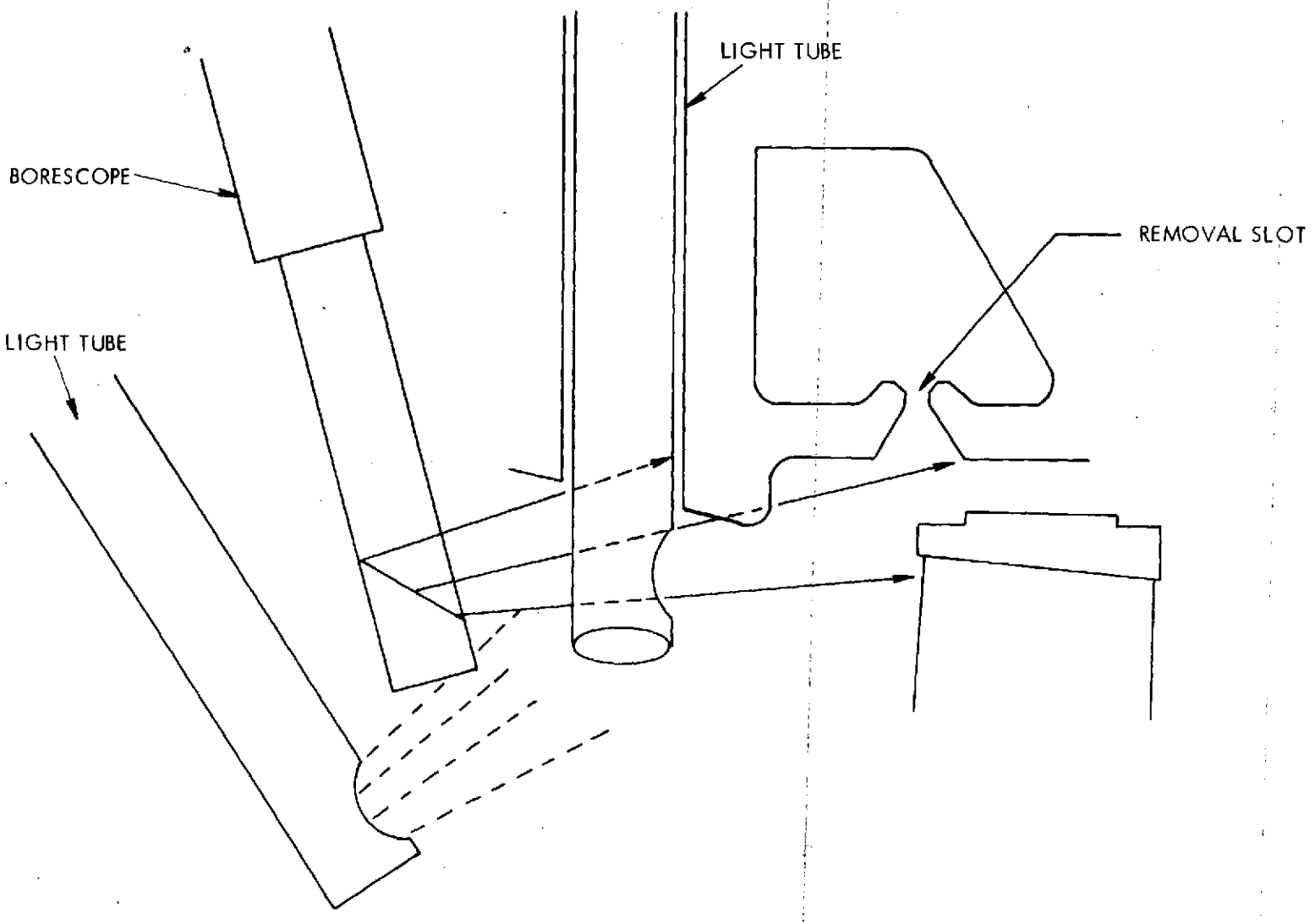

Figure 20. Borescope and Light Tube Location for Rotor View

to the rotor blade. Both light tubes can be used simultaneously.

5.2 STATOR BLADE PRESSURE SURFACE PHOTOGRAPHY

The x0.2 borescope and Fastax camera were used for the pressure surface photography along with the fiber-optic light tube with the mirrored tip shown in Figure 14. Figure 21 shows a model simulation of the pressure surface view.

5.3 TRAILING EDGE PHOTOGRAPHY

The x0.2 borescope and Fastax camera were used for the trailing edge view along with the fiber-optic light tube without mirrored tip as shown in Figure 14. A model simulation of this view is shown in Figure 22.

5.4 STATOR BLADE SUCTION SURFACE PHOTOGRAPHY

Figure 23 shows a model simulation of the stator suction surface view. All movies of the suction surface were unsatisfactory due to excessive moisture collection on the borescope mirror. The system used was the same as for the trailing edge view which included the x0.2 borescope, non-mirrored fiber-optic light tube and the Fastax camera.

5.5 DROP PHOTOGRAPHY

Two types of backlighted drop photography were planned for this test program. One technique was to use a x1.5 borescope, a framing camera and an EG&G Model 2307 double flash light source. The objective of this view was to take a rapid succession of single (or double) exposure per frame stop action pictures of the atomization of collected moisture discharged from the stator blade trailing edge.

The EG&G 2307 light source flashes when a spark is generated across tungsten electrodes mounted in a quartz or Pyrex tube and separated by an air gap. The light source can be operated with a single flash or a double flash separated by a variable time interval from 5 to 100

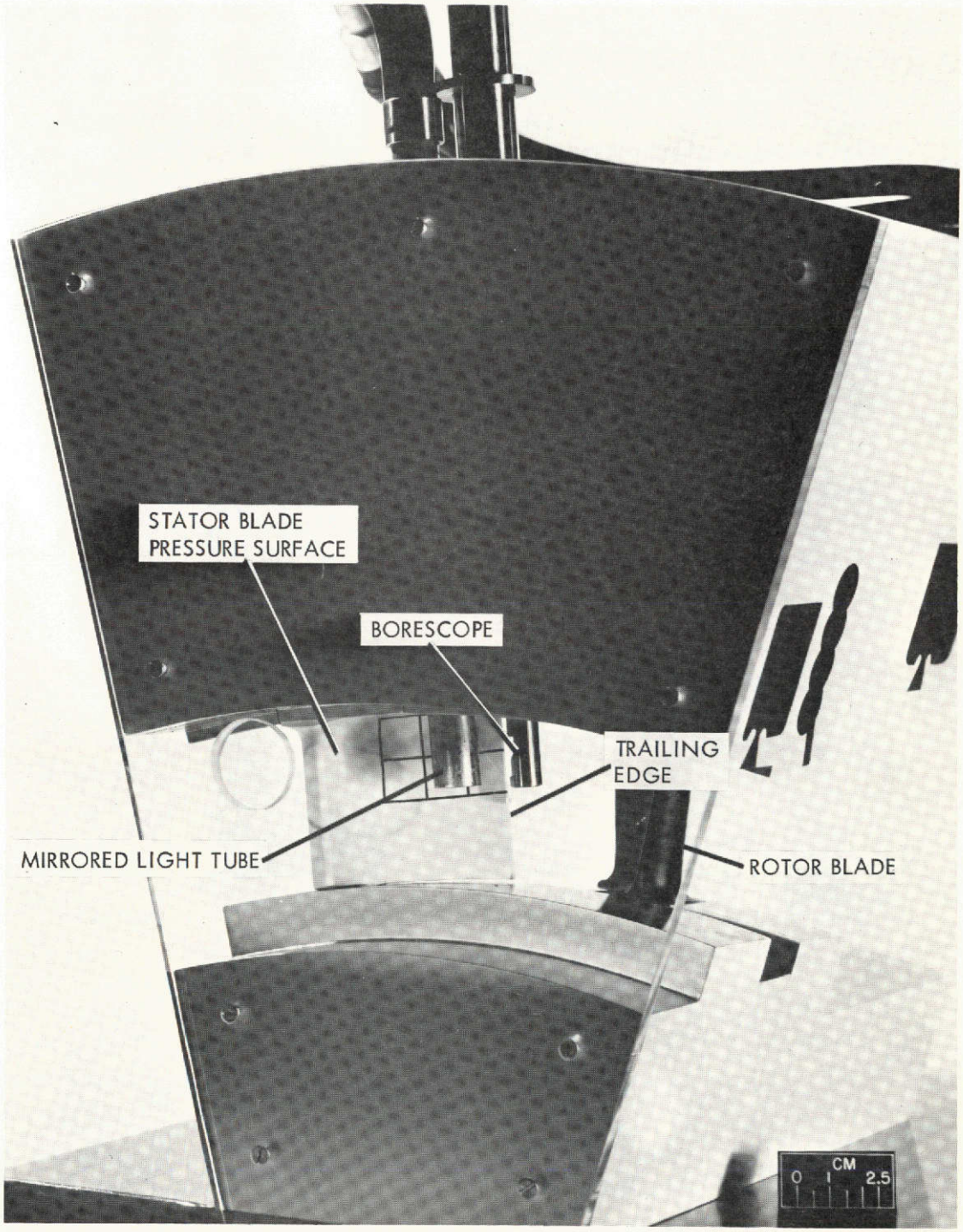

Figure 21. Pressure Surface View Configuration

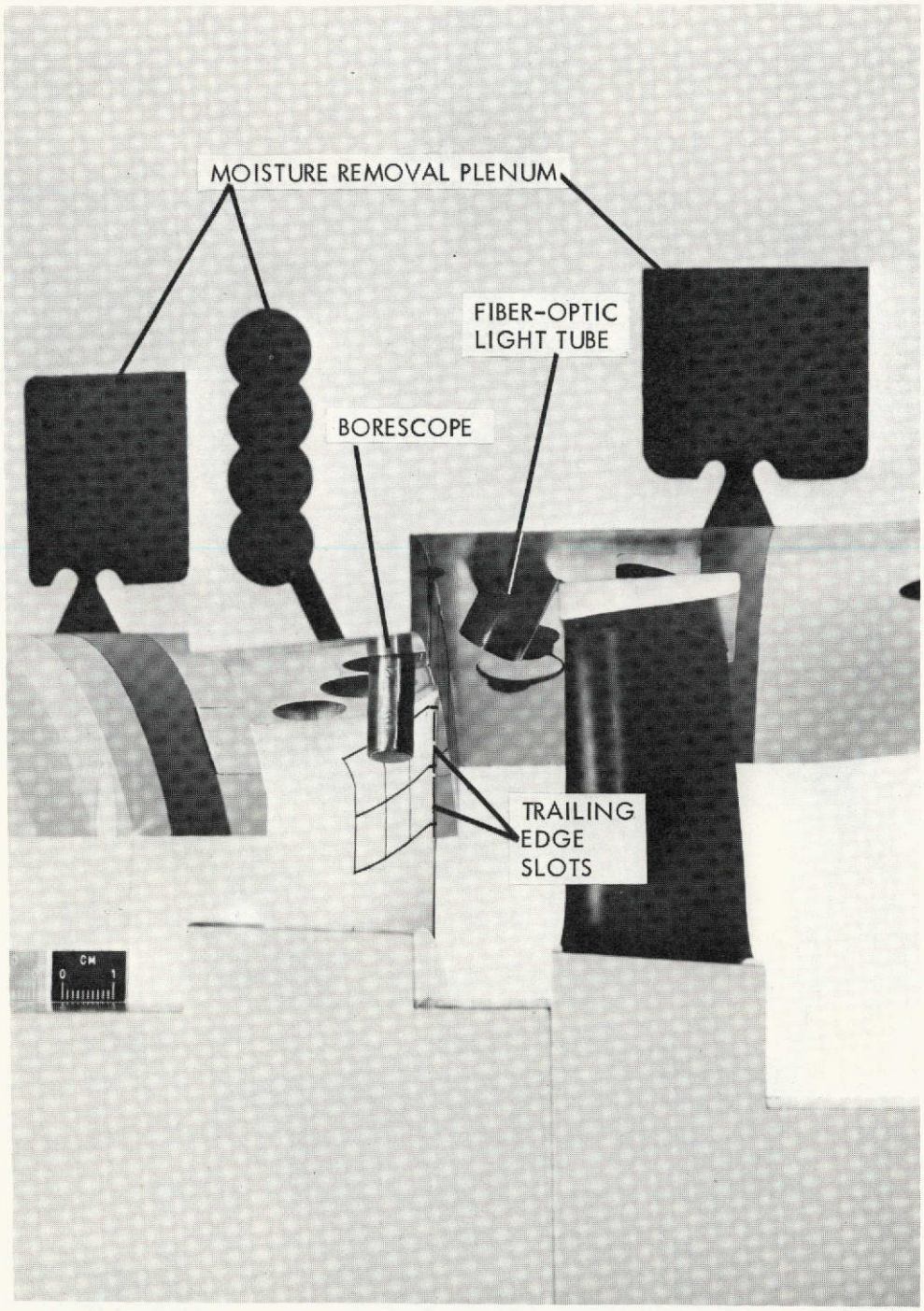

Figure 22. Trailing Edge View Configuration

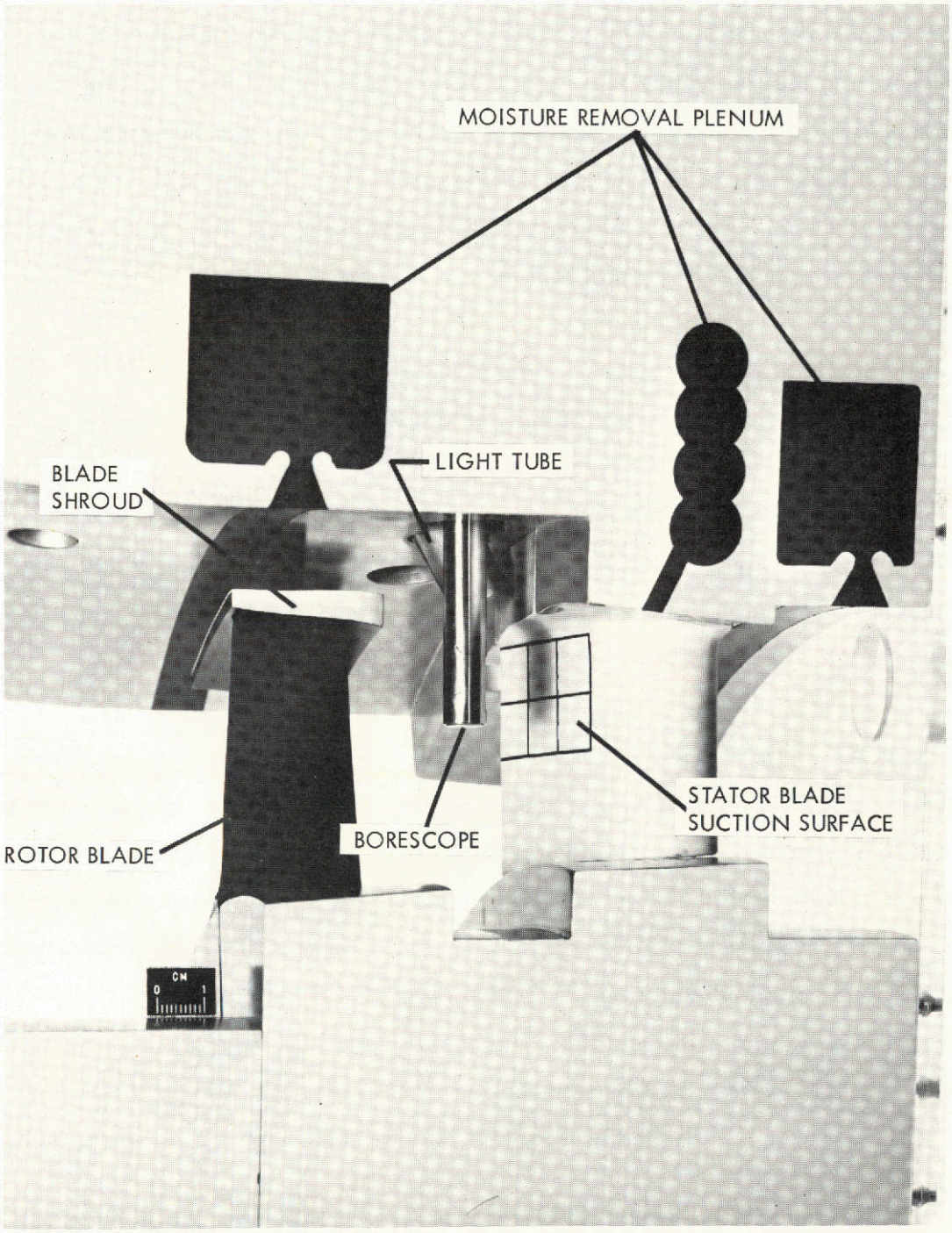

Figure 23. Suction Surface View Configuration

microseconds output of each flash when operated as a double-flash source are approximately 0.15 microsecond and 0.04 lumen-sec (0.003 cp-sec) can be operated as a single-flash light source either by setting the time delay to zero or by disconnecting half the discharge circuitry. If the time delay is set to zero, the flash duration and light output are approximately 0.4 microsecond and 0.08 lumen-sec (0.006 cp-sec) respectively. If half the discharge circuitry is disconnected the single-flash duration and light output are about the same as for each flash when operated as a double-flash light source.

Because of rather low light output provided by the EG&G Model 2307, it was felt that transmitting the light through a fiber-optic light tube would not provide sufficient illumination. Therefore, a specially constructed light tube was made with the tungsten electrodes mounted inside a sealed, stainless steel tube that could be placed inside the turbine to directly illuminate the blade wake. The light tube is shown in Figure 24. The light tube has a 0.953 centimeter (0.375 in.) diameter and is approximately 27.7 centimeter (10.9 in.) long. A lens is located in the tip section to reduce the divergence of the light from the spark flash.

Although the EG&G 2307 light tube is a convient way of obtaining both single- and double-flash photographs, its low light output is a serious handicap. A fiber-optic light tube was constructed that could be used with a variety of other light sources for single- or double-flash photography. The fiber-optic light tube is shown in Figure 25. It consists of a rigid stainless-steel clad section 0.953 centimeter (0.375 in.) in diameter, a tip section containing a mirror, a flexible section with polyvinyl-chloride (PVC) sheathing, and a rectangular light-coupling section sheather with a rigid plastic covering. The overall length of the light tube is 91 centimenters (3 ft). The ends of the glass fibers are potted in high temperature epoxy, ground flat, and polished. The fibers are not aligned as would be required for image transmission.

One light source selected for use with the fiber-optic light tube is the EG&G Model 501 high-speed strobe. When using an FX-11-0.125 xenon flash tube with a capacitance setting of 0.01 microfarad, the light output is 5 lumen-sec (0.4 cp-sec), more than 60 times that of the EG&G 2307. However, the flash duration is longer, 0.9 microsecond, so that small drops

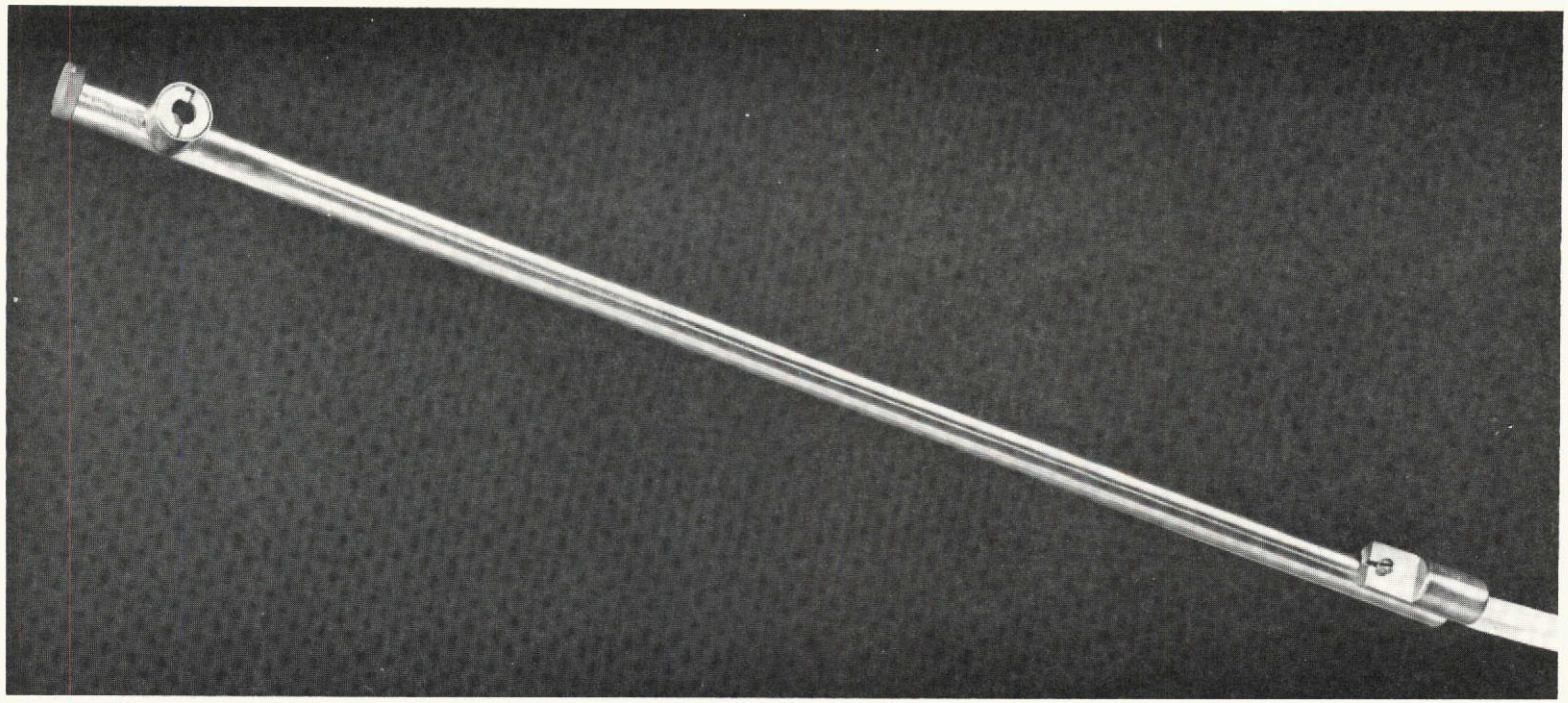

Figure 24. Light Tube for Single Flash and Double Flash Operation

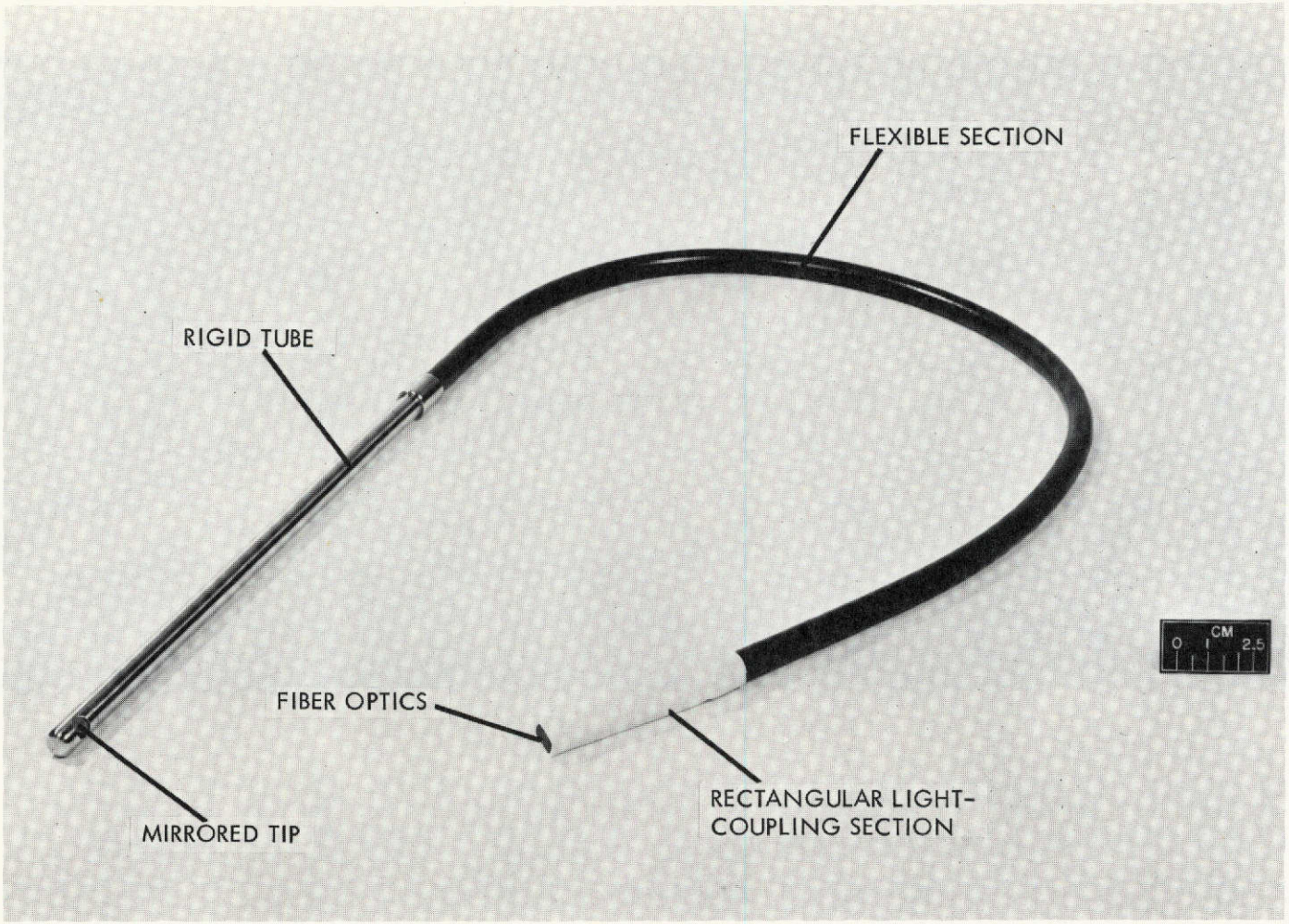

Figure 25. Fiber Optic Light Tube

traveling at high velocities are not "stopped" by the flash. Without the double flash, direct drop velocity measurement could not be obtained.

The custom-made borescope intended for the drop photography is similar in appearance to the x0.2 borescope shown in Figure 13. The borescope has a magnification of 1.5 at an object to borescope centerline distance of 2.54 cm (1 inch).

A plan view of the configuration of the photographic hardware in the turbine is shown in Figure 26. The borescope is located in a cutout portion of the adjacent blade near the blade trailing edge. There are three positions for the light tube to photograph drops in the blade wake at approximately 0.1, 0.5, and 1.0 cm (0.04, 0.2 and 0.4 inch) downstream of the trailing edge. A retractable transparent target is used for focusing of the borescope and camera. It is air actuated and retracts by a spring built into the actuator mechanism. Back-lighting was selected to minimize the amount of light required for proper film exposure.

The second technique planned for backlighted drop photography utilized the x0.2 borescope and the Fastax camera at 3000 frames/sec. The light source was the EG&G 501 strobe. Movies were taken utilizing the 0.95 cm (0.375 inch) fiber optic tube and also the 1.43 cm (0.562 inch) light tube. Figure 27 shows a plan view of the borescope and light tube arrangements for this configuration. Because of the success in obtaining quantitative as well as qualitative data using this configuration and the difficulties anticipated in obtaining still photographs using the x1.5 borescope, the still photography was not attempted.

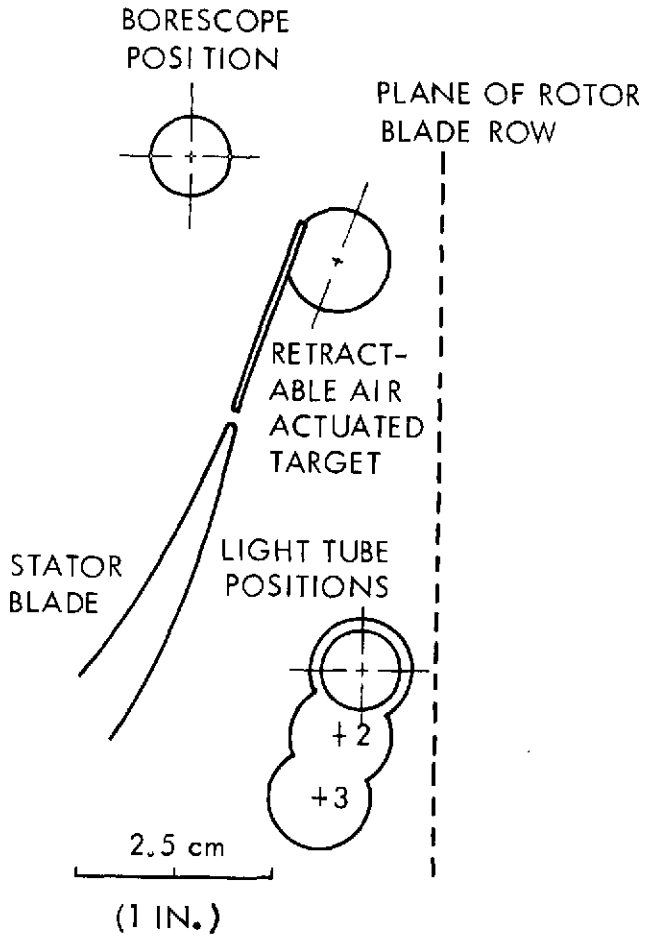

Figure 26. Plan View for Drop Photography Configuration - X1.5 Borescope

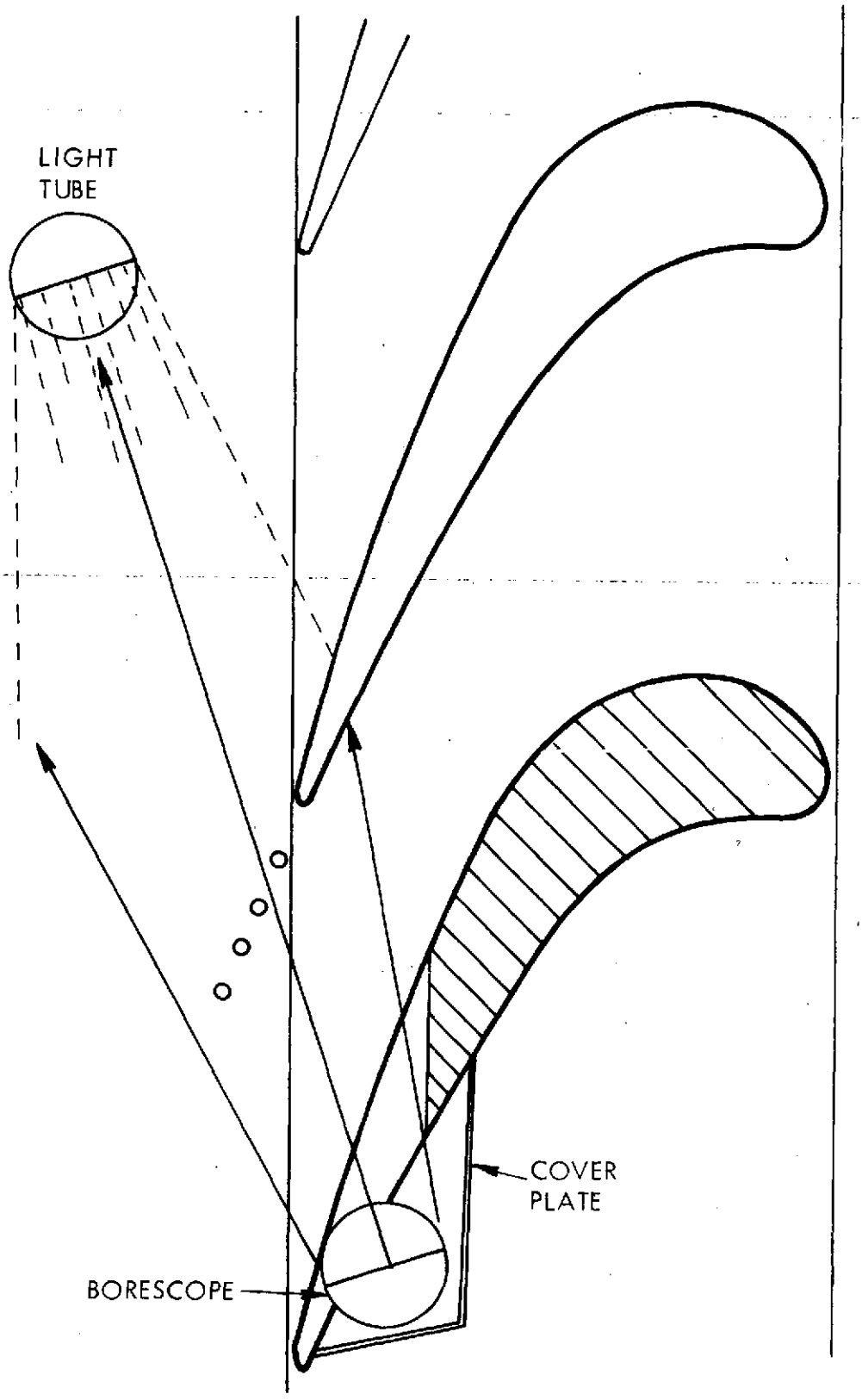

Figure 27. Plan View for Drop Photography Configuration - X0.2 Borescope

6.0 TURBINE-PHOTO SYSTEM INTEGRATION

Penetrations through the turbine walls to accommodate the rigid borescopes and light tubes were required at a number of locations to encompass the variety of photographic views. Seals were needed to prevent leakage around the borescopes and light tubes.

Due to the double-wall construction of the turbine, special care was needed in the design of these seals. Since the optical systems are relatively fragile compared to the turbine components, the sealing systems were designed to "float", that is, allowed to move in a fixed plane. Allowing the seals to move also somewhat reduced the manufacturing tolerances required in the drilling operations of the turbine outer and inner casings. Figure 28 shows the sealing arrangement used for one borescope location. In this example a seal which is fixed in position is used at the outside of the inner casing. A "floating" seal is used at the outside of the outer casing. This seal is held in place radially by the seal retainer shown. O-rings are used to seal around the borescope and at the face of the "floating"seal. A clamp on the outside of the turbine seal assembly holds the borescope in place. Eleven seal assemblies, similar to the one shown, are used in the turbine for the photographic instrumentation.

Figure 29 is a photograph of the fourth stage stator blade row. The penetrations for photographing the blade suction surface and trailing edge are shown. The blade being photographed was painted white for the initial tests to reduce the amount of illumination required for proper film exposure. A black grid helps orient the viewer. The paint failed to adhere everywhere to the blade surface. Some chipping occurred but the predominant failure was a separation of the paint in sheet form. The paint was applied by spraying and, in retrospect, a dipping process may have been more effective. The blades were painted prior to assembly in the inner casing.

At three locations in the turbine, the borescopes are inserted on radial lines into the stator blade airfoil section. Since the blades are placed individually into the inner casing to form the blade row, careful procedures are required to insure proper hole alignment between the

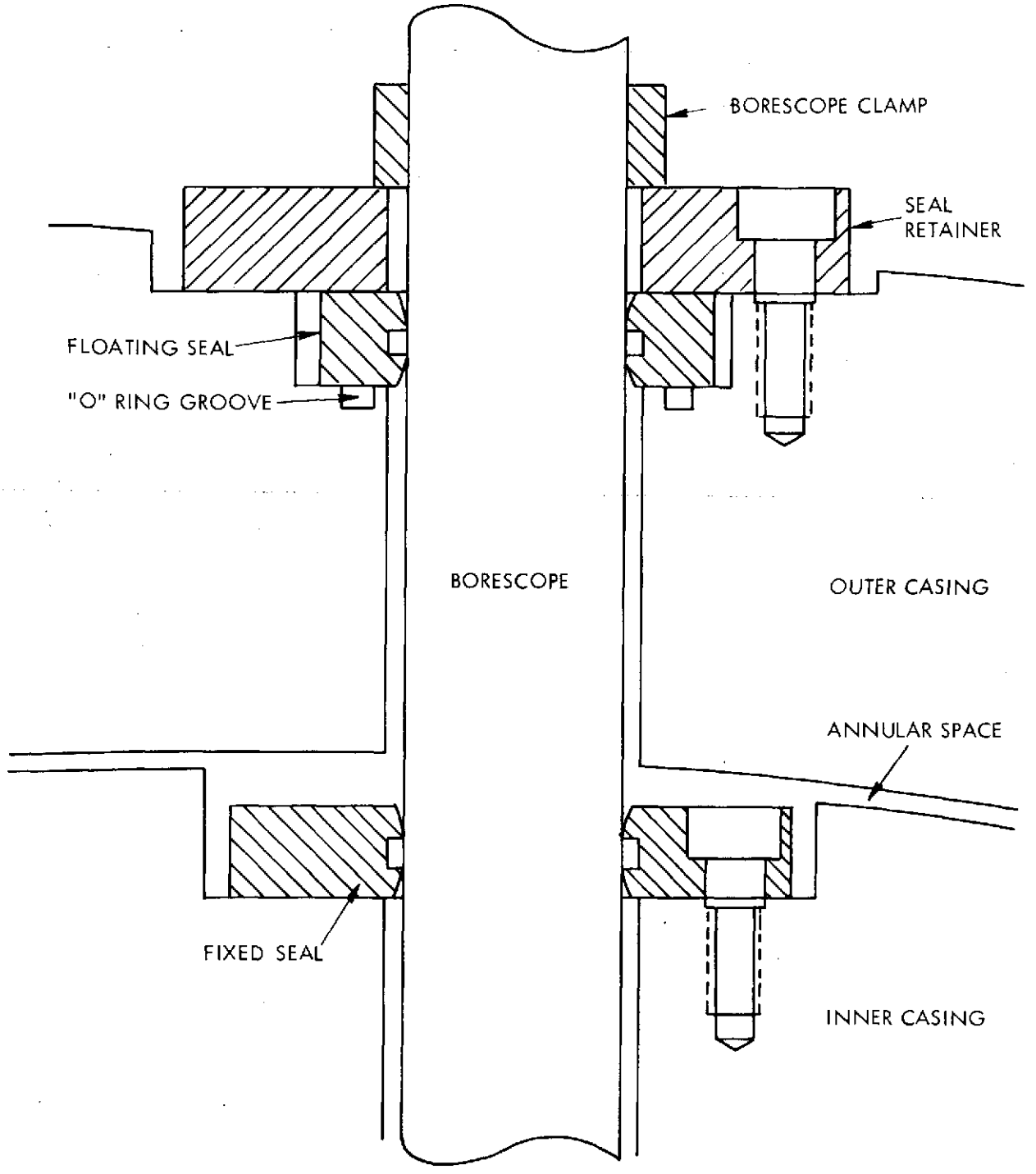

Figure 28. Borescope Sealing

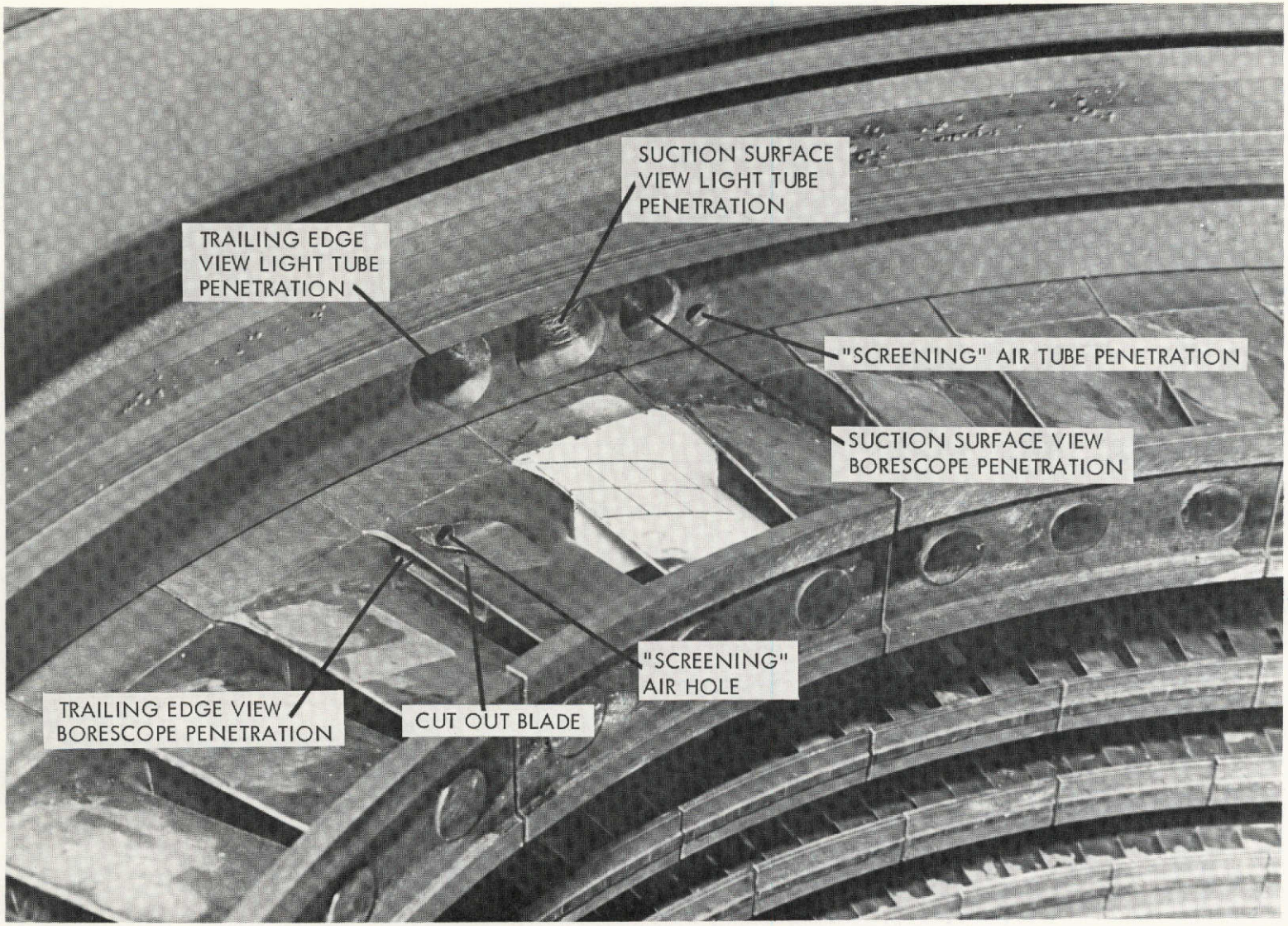

Figure 29. Fourth Stage Stator Blade Row

inserted blade, inner casing and outer casing. A cut-out stator blade is shown in Figure 30 prior to installation in the turbine. The inserted tubes simulate a borescope and light tube.

While most of the liquid in the turbine is in the form of submicron diameter fog droplets, the small percentage that is collected by blade and casing surfaces can run over the borescope mirrors and obscure the view. To keep the borescope mirrors free from liquid, there is, at each borescope location in the turbine, a small hole or tube which directs a jet of "screening" gas over the borescope mirror. Depending on which view is being photographed, either filtered shop air or higher pressure bottled Nitrogen gas was used. The screening gas, prior to entering the turbine, is heated to 423°K (270°F). The screening gas proved effective at all locations except the suction surface view. Occasional drops could be observed on the borescope mirrors but this did not detract from the quality of the films. Observations with and without the screening gas was very convincing that the gas was essential for successful photographic results.

Considering the suction surface view, the screening gas was clearly inadequate. This was the most challenging location from a design point of view because of the orientation of the borescope mirror to the flow. Figure 31 shows a plan view of this system. During turbine operation it was determined that by rotating the borescope to look directly into the screening gas the mirror would stay clean. However, when facing the suction surface the mirror collected considerable moisture and no meaningful observations could be made.

In order to accommodate the penetrations of the borescopes, light tubes, screening gas lines and moisture extraction pipes, 79 holes were drilled into the inner and outer casings and some individual blades. In most cases, due to the double wall construction of turbine, many of these holes had to match each other at final assembly. In certain cases, three holes had to fall in line with each other. Also in certain cases, deep drilling and unusual angles were encountered.

Of the 79 holes drilled only one was in error such that it affected the photographic results.

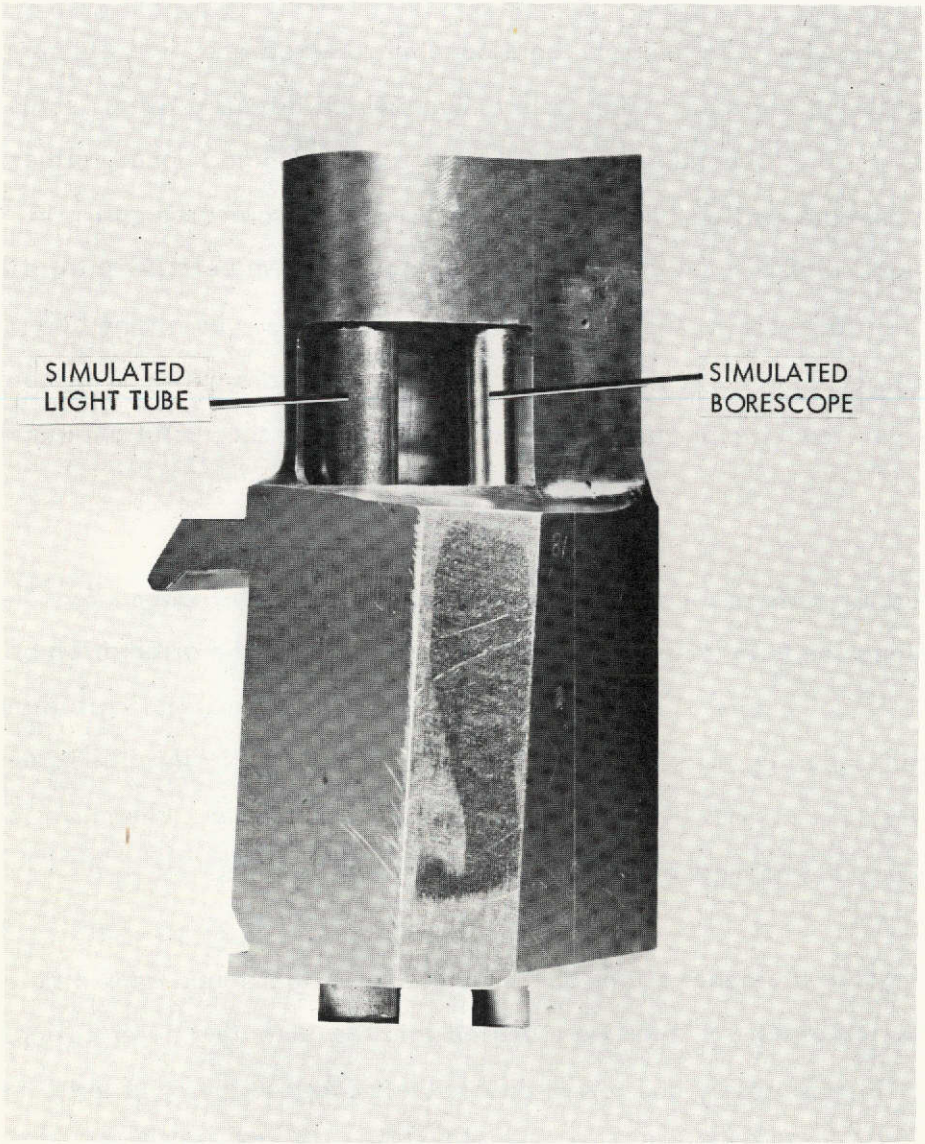

Figure 30. Stator Blade with Cutout for Optical System

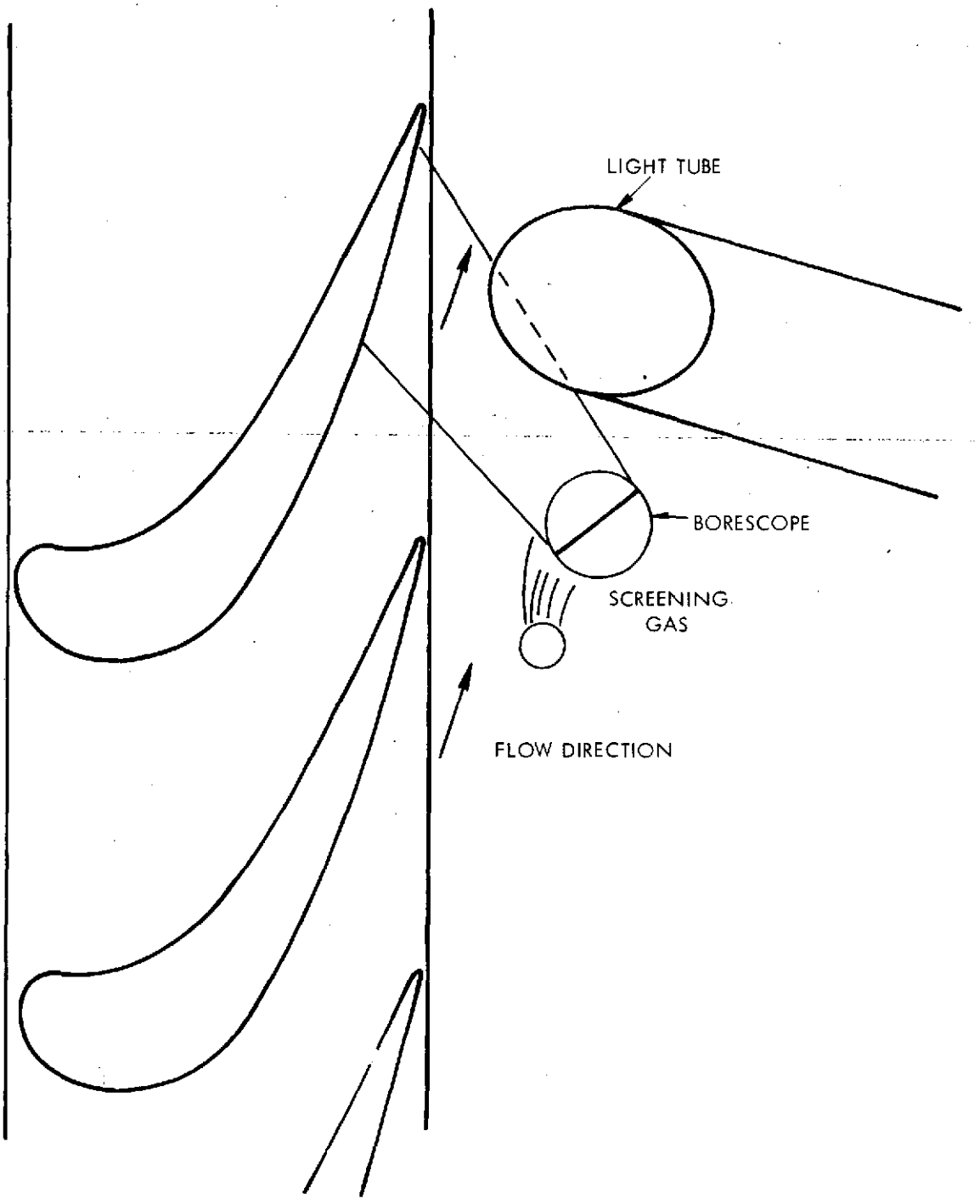

Figure 31. Suction Surface Screening Gas

The light tube penetration hole in the inner casing for the trailing edge view was drilled such that optimum lighting could not be achieved. As a result the lighting was less than required for photography of the fourth stage stator trailing edge slots. In order to amellorate this situation one of the straight through light tubes was modified by cutting the end at an angle in order to deflect the light 22° from the light tube axis. This was successful although only the two outermost slots received sufficient illumination for proper exposure of the photographs.

The camera mounting system is shown in Figure 32. Also shown is the borescope and light tube in the trailing edge position, the light source and the EG&G 501 control console. The mounting brackets provide motion in the radial and axial direction. The camera can be rotated in the transverse plane by loosening a mounting screw in the camera base. Focus is achieved by moving the camera in the radial direction. Two methods of focusing were tried, one utilizing a focus leader and the other by the parallax method. The latter proved more successful. For focusing, the strobe light is replaced by a 500 watt (369 ft-lb sec) projector lamp. The lamp was cooled by shop air and heat resistant glass was used to protect the ends of the fiber optic light tube.

As previously mentioned the photographed blades were painted white prior to the photo check-out tests but the paint deteriorated in a relatively short time. Therefore, prior to the actual photo tests all paint was removed and the blade surfaces restored as best possible to the original machined condition. The last rotor blade row was painted black and the shroud white for orientation purposes when viewing the film. This paint scheme was retained throughout the test program and, although some paint was lost, it is believed, (based on the results presented in Reference 11), that visualization was enhanced by painting the blades black.

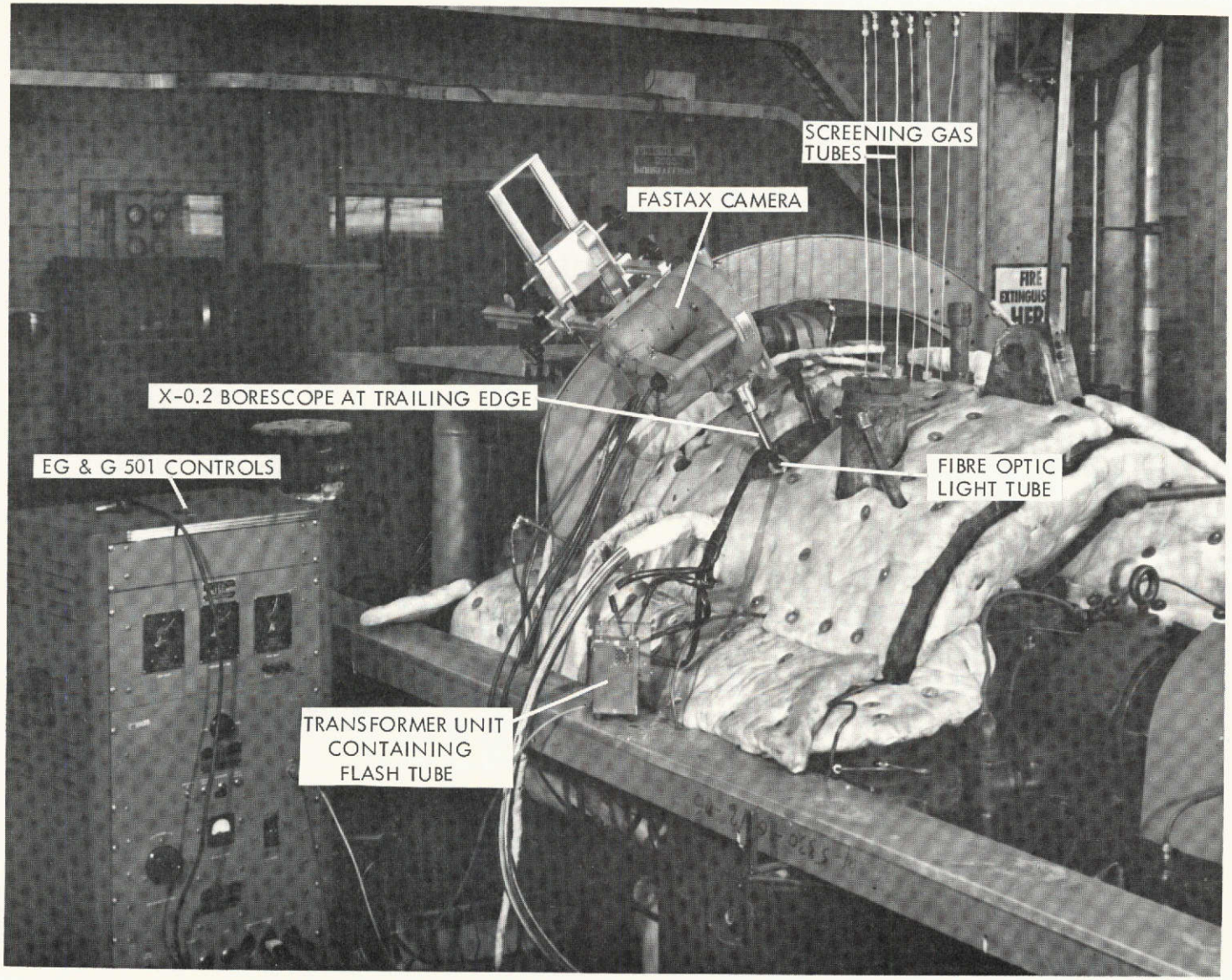

Figure 32. Photographic Equipment when Testing

7.0 TEST RESULTS

This section reports results of photographic, moisture removal, and efficiency tests.

7.1 PHOTOGRAPHIC OBSERVATIONS

As was discussed in Sections 5.0 and 6.0, six locations or types of photographic observations were planned. Four views produced worthwhile results. These are views of: 1) the fourth rotor blading and casing moisture removal slot above the rotor, 2) the pressure surface of the fourth stator blade, 3) the trailing edge of the fourth stator blade and trailing edge moisture removal slot, and 4) backlighted views of the breakup and transport of the drops torn from the trailing edge of the fourth stator. These views, because of the intense nature of the fog in the turbine (see Appendix A3), did not reproduce well as prints for illustration purposes. Therefore, sketches are used, where appropriate, to illustrate what was observed from viewing the negatives on a film analyzer or by movie projector. Results for the other two views were not obtained for reasons discussed previously in Section 5.0.

In all cases, successful photographs in the turbine were difficult to make. Even with the high intensity light sources used, the lighting was extremely limited. For the blade surface photography, for example, the two highest intensity settings on the EG&G Model 501 High Speed Strobe were required for adequately exposed photographs using Tri-X film. In some instances, the film had to be push-processed as well. The liquid in the stator blade and wake photography was fast moving and required high framing rates to adequately record the liquid flow. Because of the limitations on the number of flashes per burst dictated by flashtube life considerations, only a very short time period could be photographed in each film. Keeping the borescope mirror free from liquid was successful for all but one view although a hazy film would accumulate on the borescope mirror if photographs were not taken in as expeditious manner as possible. Focusing the cameras under turbine operating conditions was a difficult task because of the fog in the turbine and the sensitivity of focus to camera/borescope travel during the focusing process. Because of these difficulties, a considerable "learning period" was required in taking photographs in the turbine and many unsuccessful rolls of film were taken while mastering these

difficulties. Without the photographic checkout tests performed prior to turbine testing, the task would have been even more formidable. In spite of the difficult nature of the photography attempted, a sufficient number of films of good quality were obtained. Careful study of these films resulted in some valuable deductions about the condensate flow. The observations and deductions made are discussed in the following paragraphs for each view where successful photographs were obtained.

7.1.1 Fourth Rotor Blade View

Moisture collected on the face of the removal slot was clearly visible in the low speed movies utilizing the framing camera. Figure 20 orients the viewer to this photographic view. The best frame speed was 60 fr/sec when both incadescent lights were operating. Referring to Figure 33, motion of the liquid on the slot face was detectable in the tangential direction although no deductions could be made as to the velocity of the liquid. Very little change was observed in the quantity or motion of the liquid on the slot face when the removal slot was activated (although the width of the water rivulet seemed to narrow slightly and move outward radially). There were no indications that the liquid was going into the annular collection chamber. The tangential motion of the liquid was in the same direction as the turbine rotor which, of course, is the direction of the drops being thrown off the fourth rotor blade shroud.

Considerable loss of quality occurs in the printing process. In the original films, a fairly uniform distribution of fog over the entire viewing area could be seen. This is consistent with visual observations made when the camera was replaced with an eyepiece. Also observed visually was a pulsing sensation in the density of the fog clearly indicating an unsteady character to the turbine flow.

7.1.2 Pressure Surface View

Figure 34 orients the viewer for the pressure surface view. Very little moisture could be observed as can be seen on Figure 35. The photo is of sufficient quality to show machining marks and two calibration lines located 0.64 cm (0.25 inch) apart. A ribbon of water

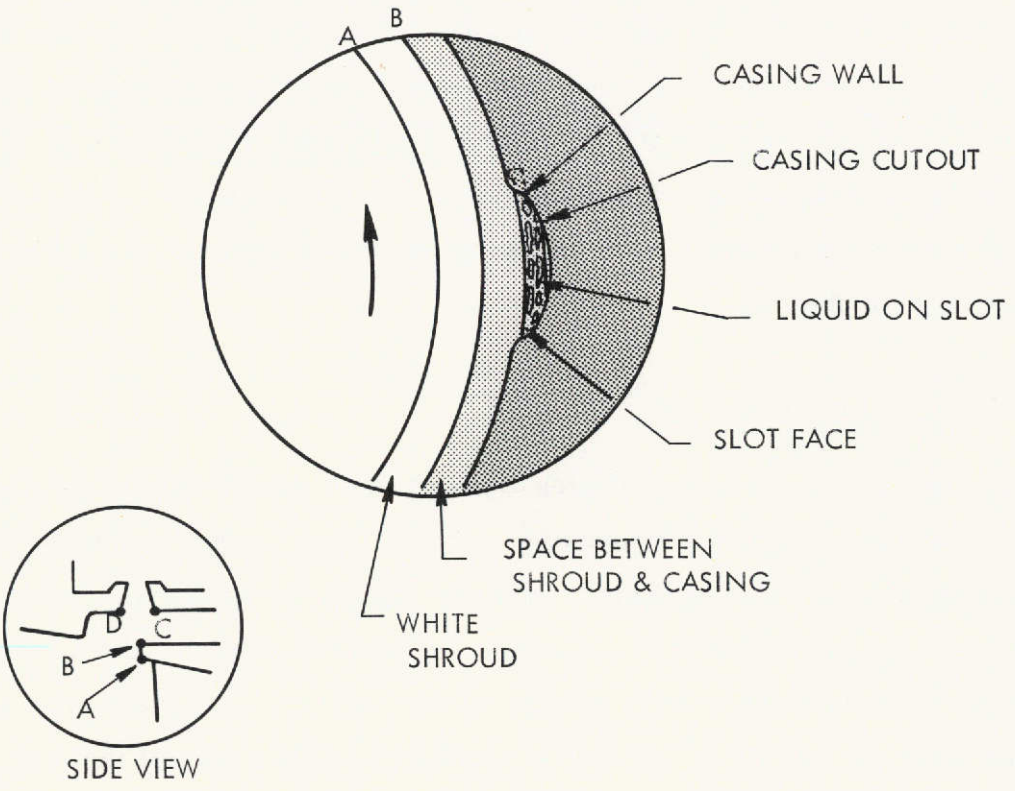

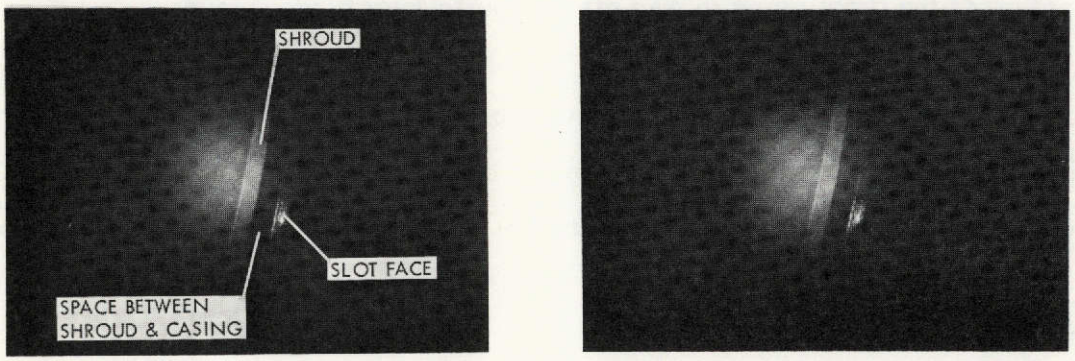

Figure 33. Photos - Rotor Blade Exit and Removal Slot

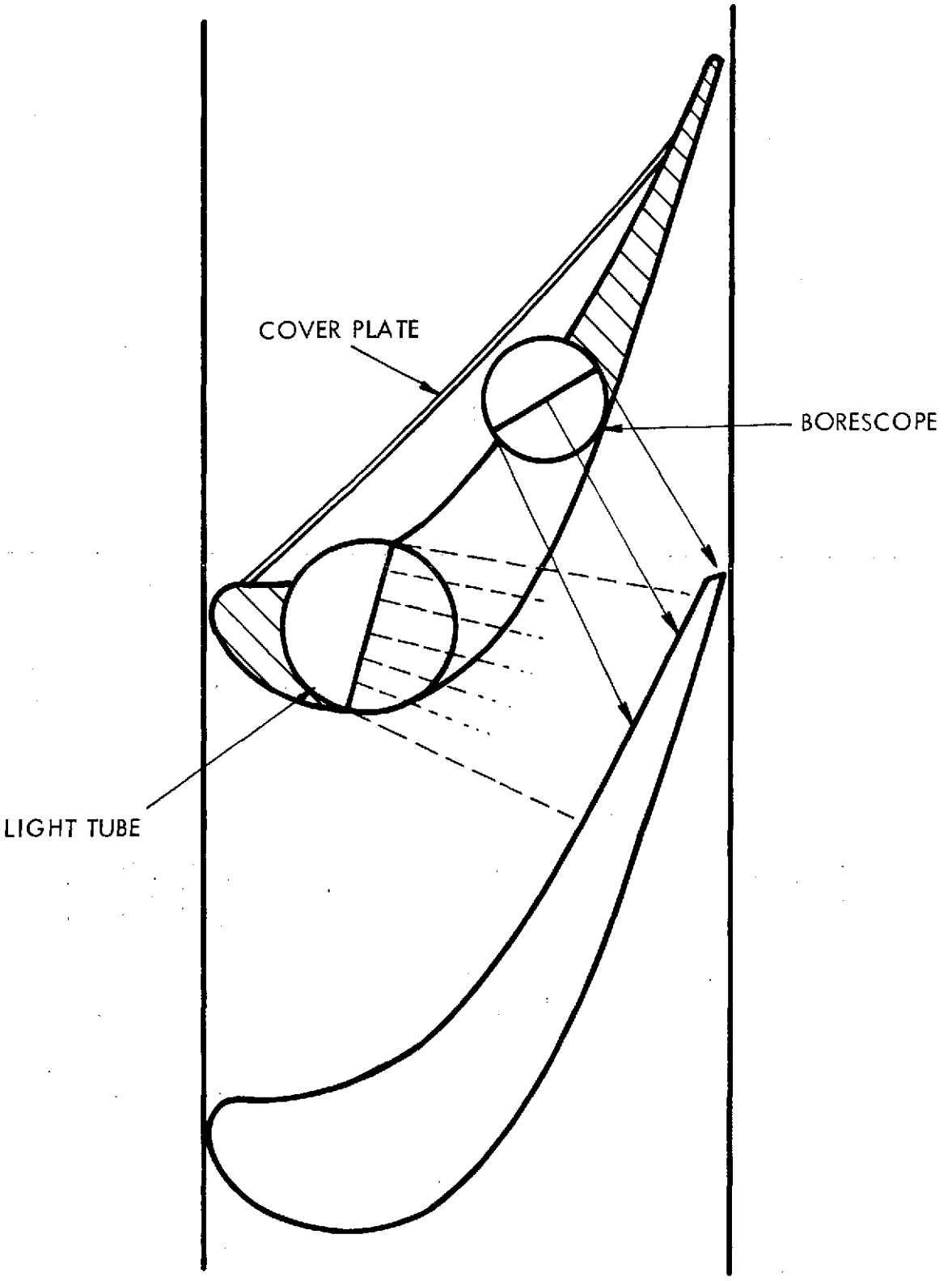

Figure 34. Pressure Surface View - Schematic

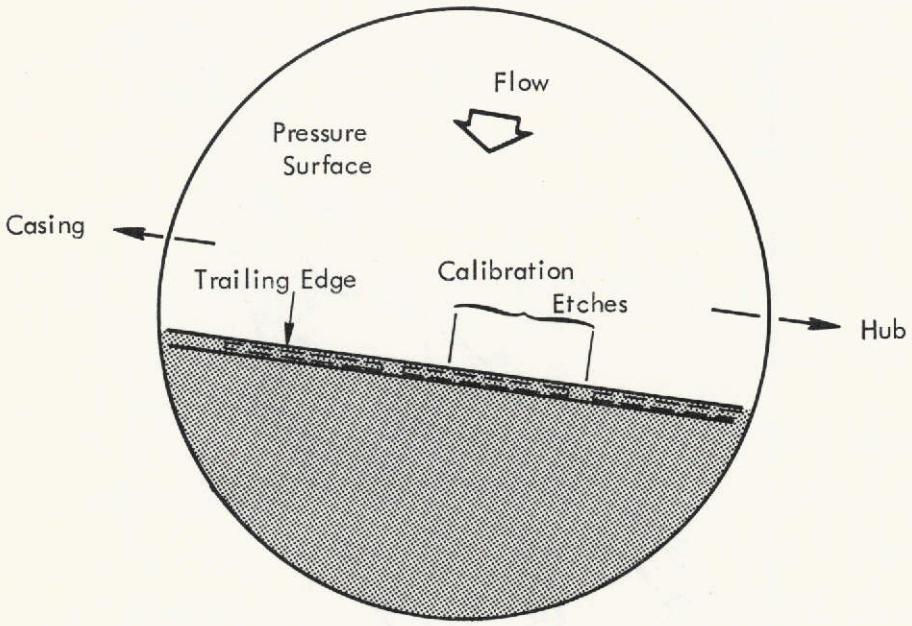

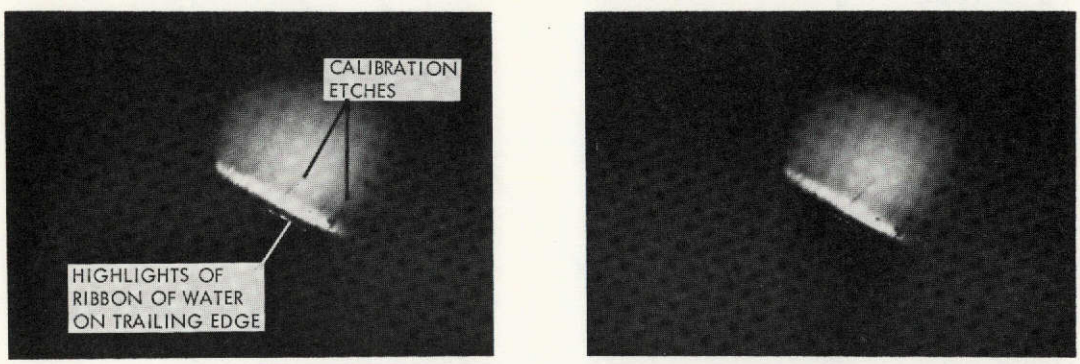

Figure 35. Photos - Pressure Surface View

clinging to the trailing edge can clearly be seen in the film but this feature is lost in the photographic printing process. No rivulets of moisture on the blade surface can be seen in the film. However, the quality of the film was not sufficient to rule out the possibility of a thin film existing over most of the blade surface. It can be stated that the condensate collected on the concave surface does not move to the trailing edge in the form of rivulets and perhaps a major portion of the condensate is swept towards the end walls due to secondary flow.

7.1.3 Trailing Edge View

Figure 36 orients the viewer for the trailing edge view. This view proved to offer the most informative qualitative information. Large drops could be seen being shed from the trailing edge and in some series of frames drop breakup can be observed. The predominant amount of moisture leaves the trailing edge near the juncture of the trailing edge and casing wall. The observation that most of the moisture departs the trailing edge near the outer boundary proved to be valuable information for locating the light tubes when taking backlighted drop photography.

The effects of secondary flow are evident in the direction imparted to the drops leaving the trailing edge near the outer diameter. A strong radially inward velocity is observed in a very consistent manner. Similarly, liquid clinging to the trailing edge moves inward and rather regularly departs the blade at around the 3/4 blade height position. Figure 37 shows a series of frames where, in Frame #3, a drop could be seen just prior to departing the trailing edge while in Frame #4, drops could be seen near the 3/4 blade height position.

The most significant conclusion reached from these high speed movies was that all moisture on the stator blade surfaces was not removed when suction was applied to the trailing edge slots. The amounts of moisture measured externally in the separator system, although admittedly less than that predicted according to the model used, were encouraging and without the film information the conclusion may have been reached that the removal slots were very effective

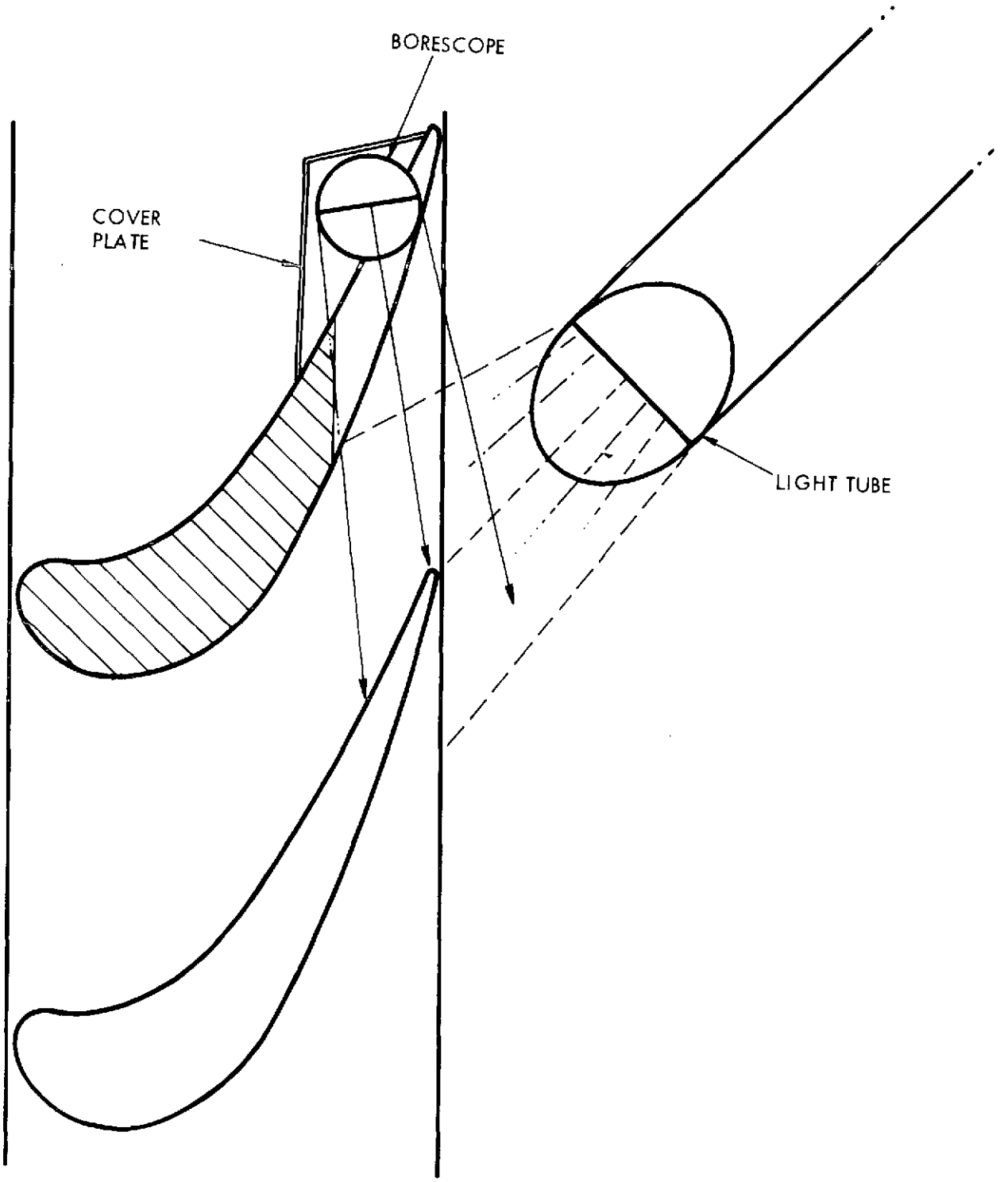

Figure 36. Trailing Edge View - Schematic

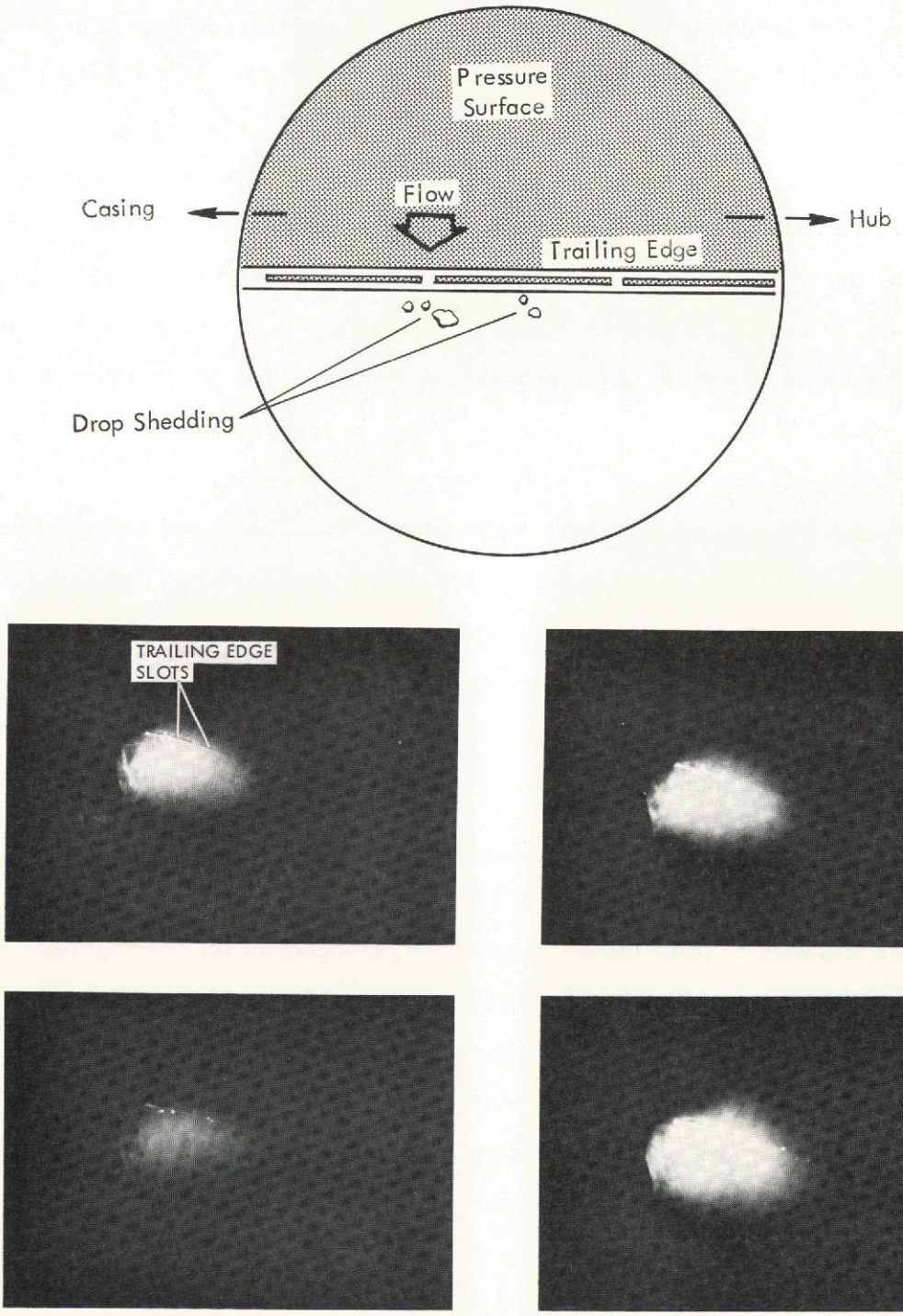

Figure 37. Photos - Trailing Edge View

in eliminating large drop shedding from the trailing edge. However, comparison of films with suction on and off showed large drops departing from the junction of blade and casing for both conditions.

The most likely explanation for the fact that the slots did not remove all moisture for this turbine geometry is the strong secondary flows that drag the moisture from the pressure surface across the casing to the suction surface resulting in a concentration in the corner of blade and casing. Figure 38 shows a schematic of the probable movement of the liquid along the casing wall.

The liquid seems to concentrate in rivulets at the junction of the blades and casing. This liquid can be torn off the casing as large drops under the impress of the vapor drag and cause considerable damage to rotor blades and shrouds. In this turbine, separation of the liquid directly from the casing was not observed. Rather, the liquid seems to depart at the junction of the blade and casing or to run down onto the stator blade surfaces in the vicinity of the trailing edge under the impress of vapor secondary flows where it is then torn from the trailing edge.

7.1.4 Backlighted Drop Photography

Shown in Figure 27 is a schematic of the instrumentation arrangement for the backlighted drop photography. As previously mentioned, all drop photos were taken with the x0.2 borescope thus limiting the size of the smallest drops that could be detected to around 60 microns. All movies were taken with the Fastax Camera at 3000 frames/second. Both TRI-X and PLUS-X film were used. The lighting was adequate to give good results with the PLUS-X film which is a more desirable film for measuring the drop sizes.

In some frames of the high speed movies, globs of water are seen torn from the trailing edge and in subsequent frames the breakup can be observed. In these instances, the radial motion inward of the liquid can be clearly detected. Qualitative information such as this can be made in a "halo" surrounding a bright light circle which is the light tube mirror. The accuracy of

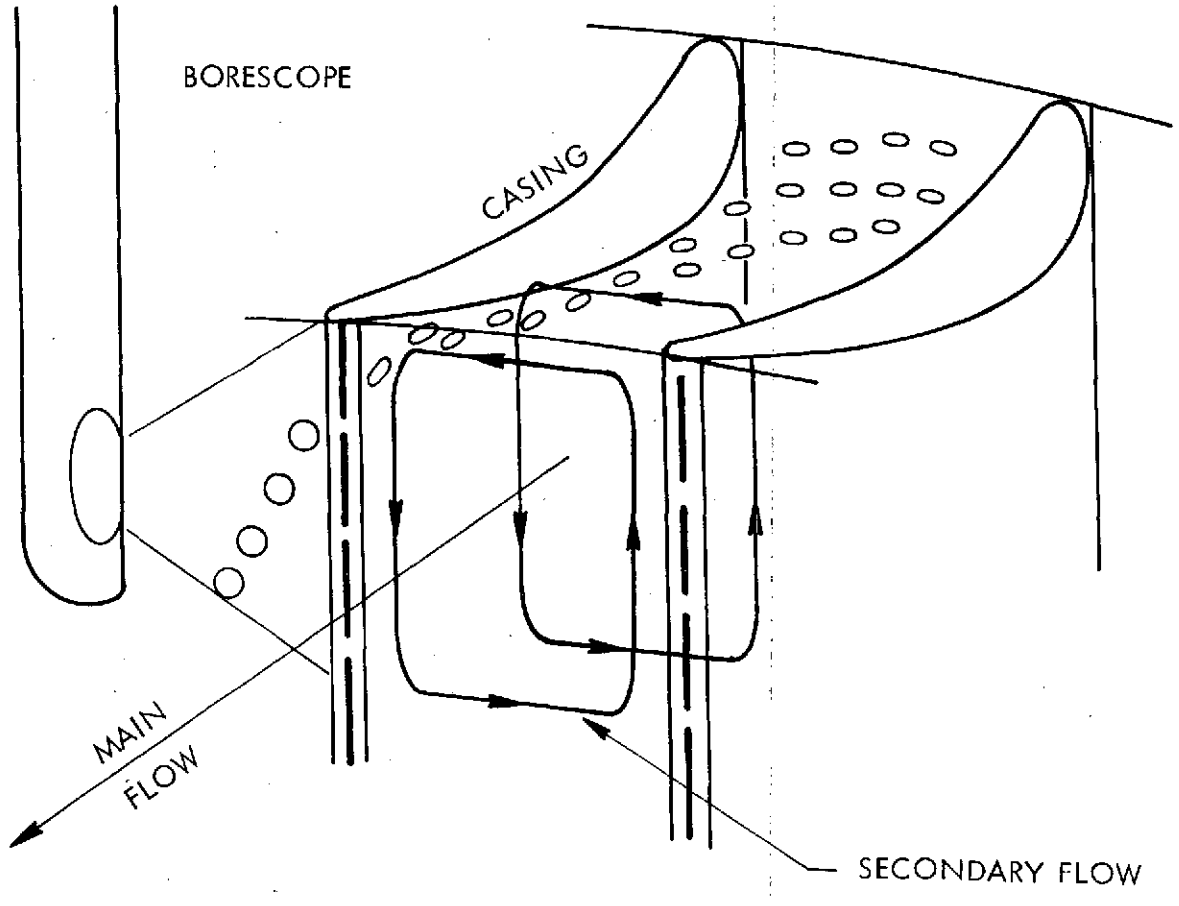

Figure 38. Secondary Flow Affect on Drop Movement

quantitative data in this region is somewhat questionable, even when viewed on film analyzer, since light reflections give the drops a "soap bubble" appearance indicating the drops may be acting as lenses. Shown on Figure 39 are two frames covering a time span of 1/600 second. Again, the difficulties of reproducing the frames are apparent for significantly more detail can be seen upon close examination of the original movie films. (In fact, the "halo" area cannot be seen in the reproduced photograph.) There are additional frames between and adjacent to those shown in Figure 39 which show additional details of the drop shedding. Some of the shading noted in the circle of light is due to a combination of factors such as imperfections in the fiber optics and the collection of dirt and water on the light tube mirror. Screening gas was not used on the light tube mirrors. This particular series of frames was the largest concentration of liquid photographed during this test series. Other films showed several drops in single frames but never the quantity shown on Figure 39. Shown on Figure 40 is a schematic of a frame showing a relatively large glob of liquid prior to leaving the trailing edge. After detachment many individual drops can be seen traveling radially inward. The approximate size and shape of the glob was determined by tracing on a film analyzer. Shown on Figure 41 is a schematic of drops filmed just as they were detaching from the trailing edge. In this frame, larger drops of water appeared to be forming dumbell shapes prior to breakup into smaller drops.

Shown on Figure 42 is some quantitative measurements taken of drops in front of the circle of light. Only drops appearing in front of the circles of light were considered for quantitative measurement. In this area, the drops appear as black circles. In most frames that were closely examined, the drop diameters were consistent with the theory of drop atomization occurring within 0.5 cm (0.197 inch) downstream of the trailing edge. In this particular frame, however, two drops were measured at 600 micrometers (23600 micro-inches) at 0.66 cm (0.26 inch) downstream which is significantly larger than expected. Observations of the liquid discharged from the stator were confined to the region between the stator trailing edges and one centimeter downstream. The liquid does indeed depart the stators as rather large globs which are quickly broken up into smaller drops and accelerate from view. A detail difference from that implied by the model, as discussed in Section 3.0, is that the globs of liquid undergoing breakup do not move directly downstream but have a substantial radial inwards velocity component due to secondary flow.

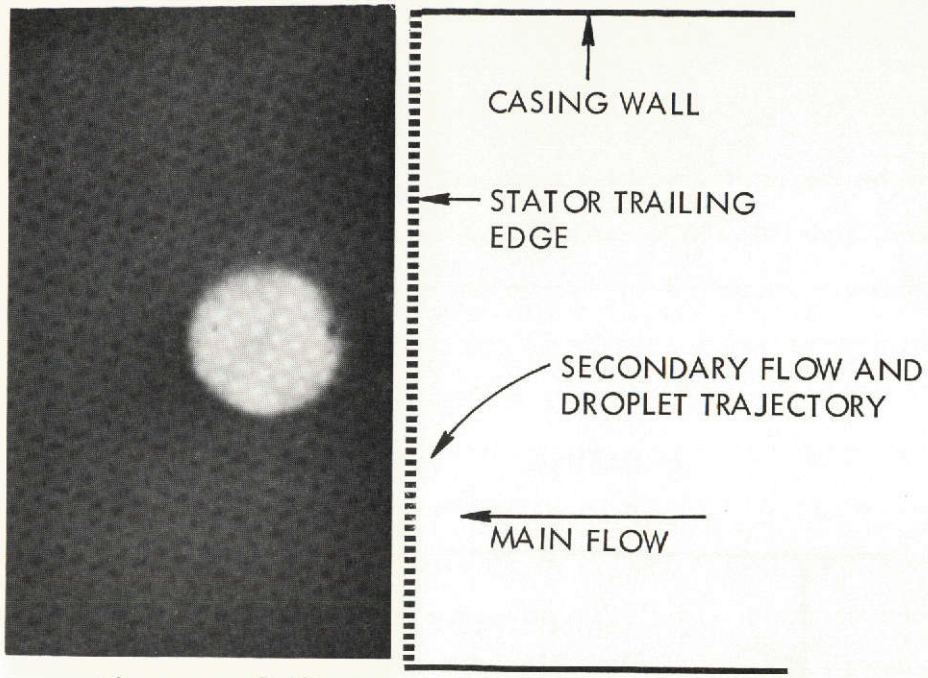

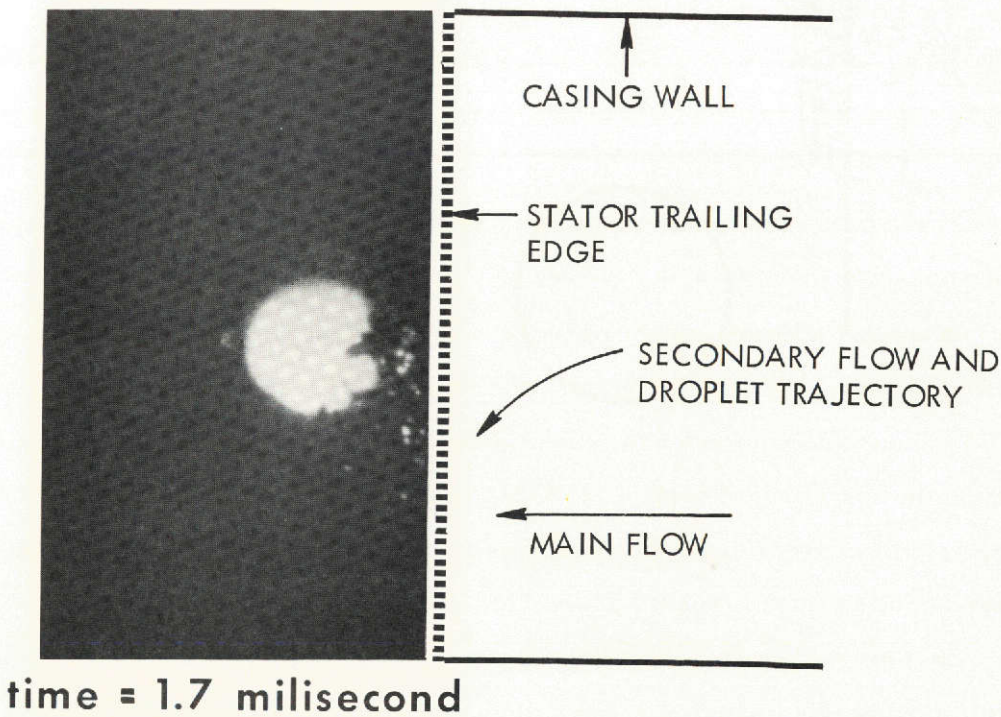

Figure 39. Backlighted Drops Leaving Trailing Edge

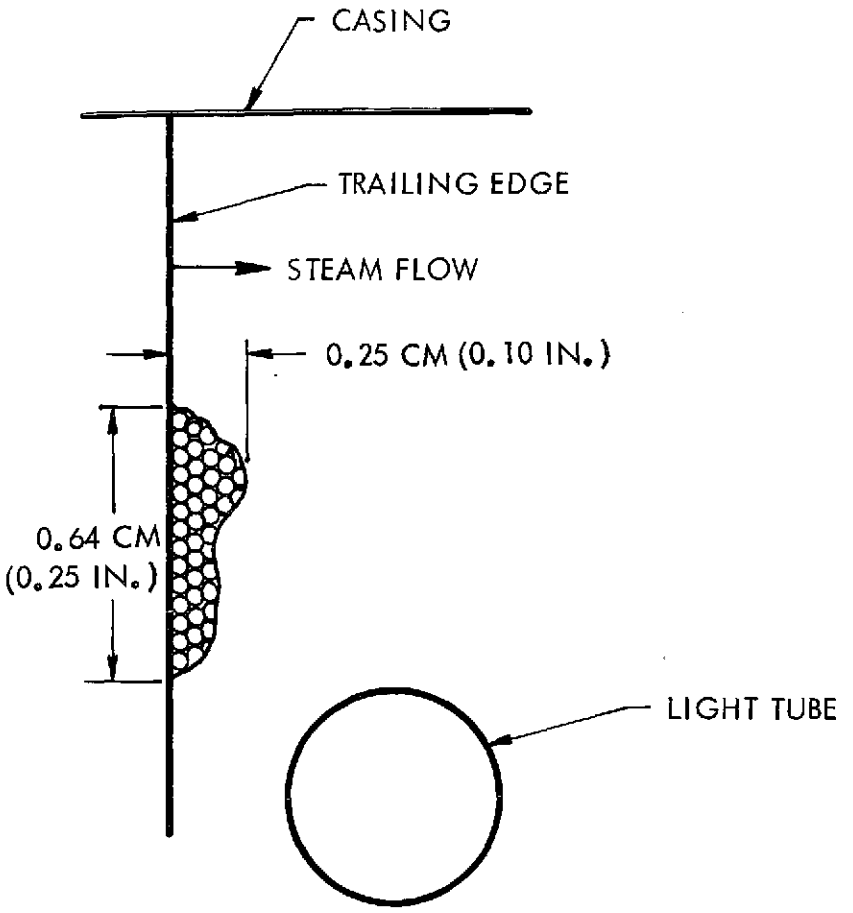

Film No. 32, Frame No. 842

Figure 40. Liquid Detachment at Trailing Edge - Schematic
(Film No. 32, Frame No. 842)

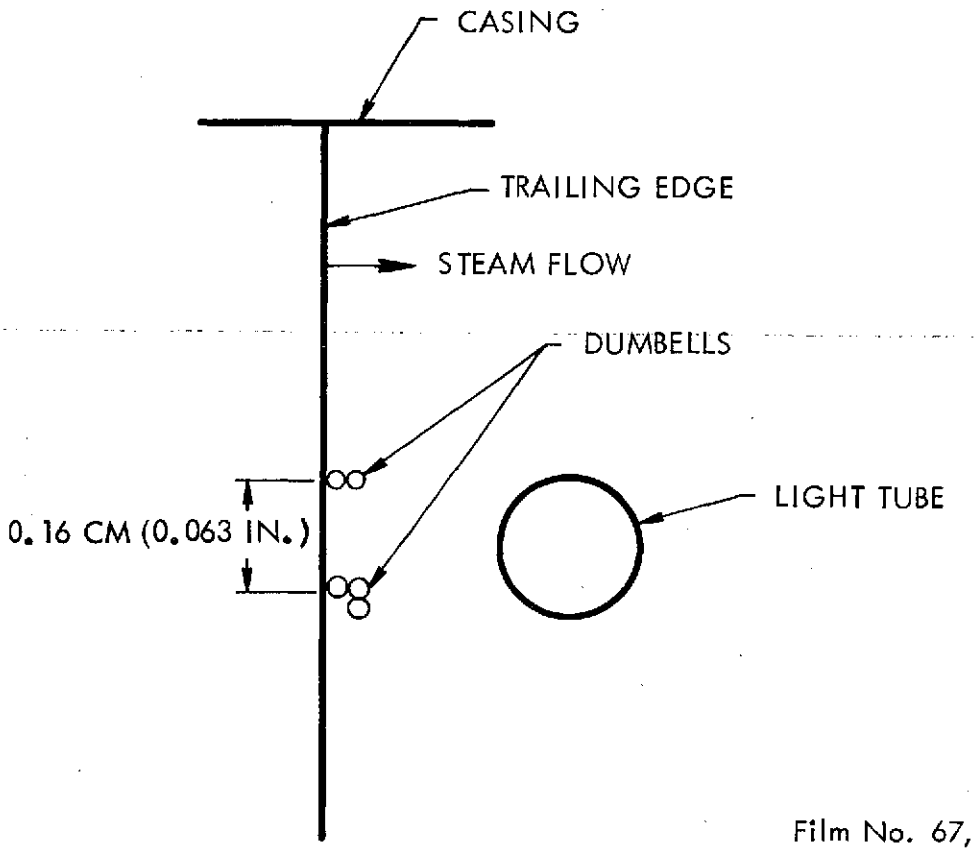

Figure 41. Drop Detachment at Trailing Edge - Schematic
(Film No. 67, Frame No. 571)

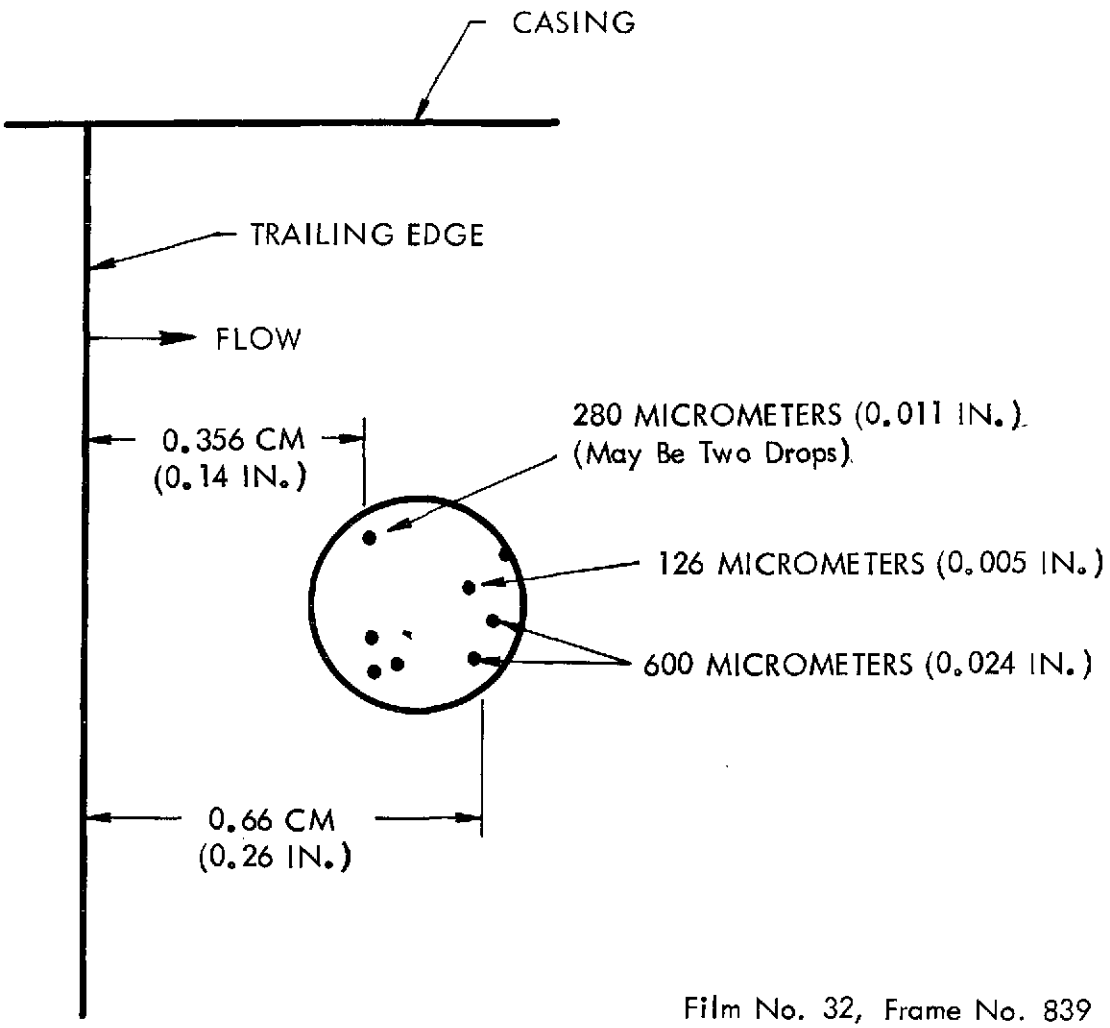

Figure 42. Backlighted Drop Measurements - Schematic
(Film No. 32, Frame No. 839)

7.2 MOISTURE REMOVAL

Figure 43 shows test results for moisture removal effectiveness through the slotted trailing edges of the fourth stator blade row. Effectiveness is defined as percent of exit equilibrium moisture removed. The moisture removal effectiveness is shown for varying vapor extraction rates. Shown also are the predicted removal rates. The predicted rates were based on the following: calculations of the amount of moisture collected on all upstream turbine surfaces based on NASA CR-1830; no moisture removal upstream of the fourth stator blades; 100% removal of all moisture on the outer half of the stator blades, the effectiveness of the removal system would be independent of the vapor extraction rate. The tested removal rates are less than predicted. Two of the test points were run at the time high speed movies were taken of the stator trailing edge. As discussed in the photographic test results, the movies clearly showed that all moisture on the blade, particularly near the outer diameter, was not removed.

One low density data point falls close to the predicted removal rate. This test point was the first run for the stator blade removal series but the conditions could never be repeated. The measurement of the moisture removed is believed to be quite reliable since the measurement technique is simple and from observations of the wire mesh in the tank, the separation of liquid from vapor appeared effective. One of the most difficult parameters to measure and control is the turbine inlet temperature. In order to achieve the high moisture levels in the test stage, the inlet temperature is maintained as close as possible to the saturation temperature while maintaining dry vapor at the turbine inlet. From experience, a minimum of $8^{\circ}K$ ($15^{\circ}F$) superheat is required and careful monitoring of temperature is required to avoid slipping into the wet region.

During a transition period of operation with some less experienced personnel, a medium density test was run where the inlet conditions were definitely in the two phase region. The results were most interesting since the trailing edge slots removed six times the predicted removal rate. Unfortunately, the moisture level into the turbine is unknown. Nevertheless, the test indicated the slots are capable of removing significant amounts of moisture. In view of this experience, it is believed the first test point, which falls near the predicted removal rate, is higher than the other points due to a slightly wet inlet condition.

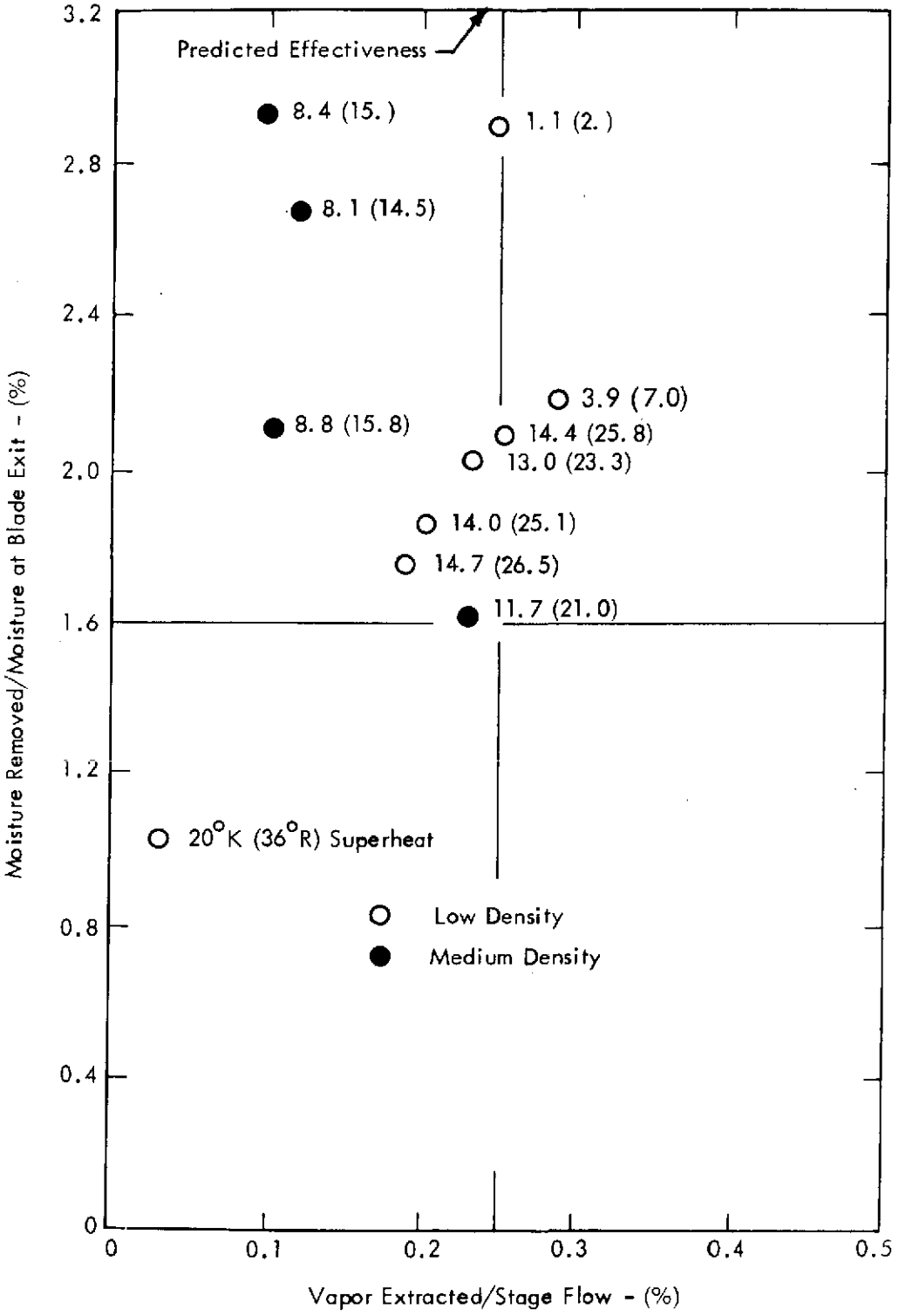

Figure 43. Moisture Removal Effectiveness - Stator Blade Slots

The inlet temperature is maintained by a desuperheater. Each data point shown on Figure 43 has an accompanying number designating the measured superheat at the turbine inlet. There appears to be some effect of superheat indicating some moisture may have been carried into the turbine inlet from the desuperheater. For the one test point discussed where the amount of liquid removed was very high (not shown on Figure 43), the inlet was unquestionably in the wet region. This test point, in addition to the apparent effects of inlet superheat on effectiveness illustrates how different conclusions may be reached as to moisture removal effectiveness when moisture is injected into a test turbine as opposed to when the moisture is naturally formed through the turbine expansion process. The test points centered around 14°K (25°F) superheat appear meaningful and show a trend of improved moisture removal with increasing vapor removal, contrary to the model assumed. The two films denoted 32 and 66 were taken for these steam conditions. The photographs shown on Figure 39 are reproductions from film 32.

Shown on Figure 44 is the removal effectiveness of the casing slots behind the third and fourth rotor blades. Also shown are the predicted amounts of moisture collected on all turbine surfaces according to the analytical model[5]. The third rotor blade casing slot (3R) removed up to nearly 70% of the predicted amount of moisture available, although considerable scatter is evident in the data. The fourth rotor blade casing slot (4R) performance was poor. The same philosophy was followed in the design of the slot and annular collection chamber as in 3R and no explanation for the differences are immediately evident. The amount of superheat again appears to be a factor in the 4R slot performance and to a lesser degree in the 3R slot performance.

The standard speed movies at the fourth rotor blade exit tend to verify the low removal rate of the casing slot. However, the quality of the films are not sufficient for absolute confirmation. The effectiveness of the moisture-separator measurement tanks is believed quite good based on past experience with these devices, the observations through the portholes, and the demonstration that considerable moisture can be separated when the turbine inlet was wet.

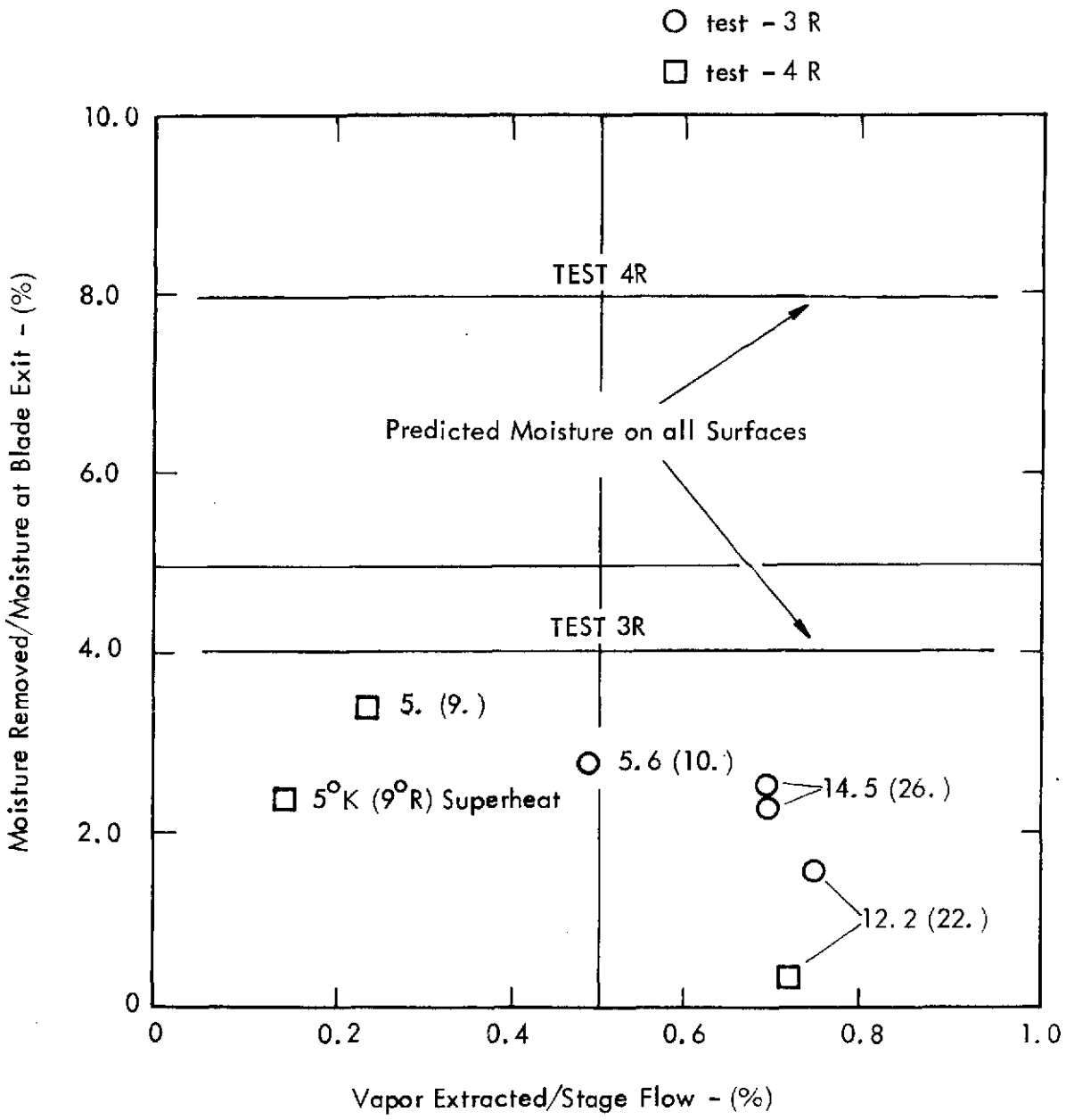

Figure 44. Moisture Removal Effectiveness - 3R and 4R Casing Slots

Some additional testing was done on the 4R removal system utilizing a sodium tracer technique. This was not in the original test plan and the equipment used was designed for testing of large nuclear turbines. Due to the small size of the test facility and the correspondingly small mass flows, precise agreement was not expected between the sodium measurements and the separator tanks.

In order to have sufficient quantities of liquid to be sensed by the sodium tracing method, a test was run with wet steam at the turbine inlet. This was similar to the conditions discussed previously regarding the trailing edge slot removal where the removal effectiveness increased significantly for wet steam at the turbine inlet. The 4R casing slot responded in a similar way to the wet steam inlet, as did the trailing edge slots, wherein significant amounts of moisture were removed. The sodium tracer technique confirmed the increased moisture removal. However, the tracer technique indicated 38% less moisture removal than the measuring tank. The difficulties encountered in maintaining steady turbine operating conditions with wet steam inlet contributed to the disagreement between the two measurement techniques.

7.3 EFFICIENCY

Although the original contract did not provide for determining moisture affects on turbine thermodynamic performance, the scope of the contract was expanded at a later date to include these tests, since this information is of considerable interest.

The turbine, however, was not designed nor instrumented with the intention of running a sophisticated performance test program. Likewise, optimum performance was not sought. The original intent was solely to design a turbine with well ordered flow to expand sufficiently far into the two phase region to permit photographic observations to be made.

To determine the effects on turbine performance due to moisture, other variables that affect performance must be considered and held constant as best possible. Two important parameters

are Mach Number and flow incidence at blade inlets. Although these parameters cannot be held constant over a range of moisture levels, the effects can be minimized by judicious selection of operating conditions.

Shown on Table 2 are the Mach Numbers at each blade exit for the different levels of moisture and the flow inlet angles to each blade. These conditions were achieved by varying turbine speed from 98 Hz (5900 rpm) to 118 Hz (7060 rpm).

Performance tests were run at nominally 1%, 4%, 6% and 8% moisture levels at turbine exit for medium and low density. Figure 45 shows the efficiency ratio for the wet and dry conditions up to an average moisture level across the turbine of 4%. Although there is considerable scatter in the data, the deterioration in turbine performance is quite apparent. Further, a non-linear deterioration in performance is indicated. A line showing a performance penalty of one percentage point per point of weighted average moisture, a commonly used first approximation, is shown for comparison.

TABLE 2

VARIABLE MOISTURE PERFORMANCE MEDIUM DENSITY TESTS

Exit Mach Number Comparison

Mach Number - Dimensionless

Exit Mois	1C	1R	2C	2R	3C	3R	4C	4R
1%	0.682	0.714	0.714	0.829	0.809	0.729	0.772	0.600
4%	0.682	0.713	0.713	0.792	0.829	0.754	0.742	0.570
6%	0.676	0.695	0.733	0.838	0.818	0.741	0.724	0.553
8%	0.700	0.728	0.724	0.831	0.807	0.724	0.692	0.520

Inlet Angle Comparison

Angles - Degrees

Exit Mois	1C	1R	2C	2R	3C	3R	4C	4R
1%	90.0	32.8	31.9	33.4	29.8	36.8	50.9	52.6
4%	90.0	32.6	31.7	33.3	31.1	38.3	51.6	51.6
6%	90.0	33.1	32.9	35.3	31.0	37.6	50.6	51.1
8%	90.0	33.4	32.0	33.2	29.3	35.6	48.3	49.9

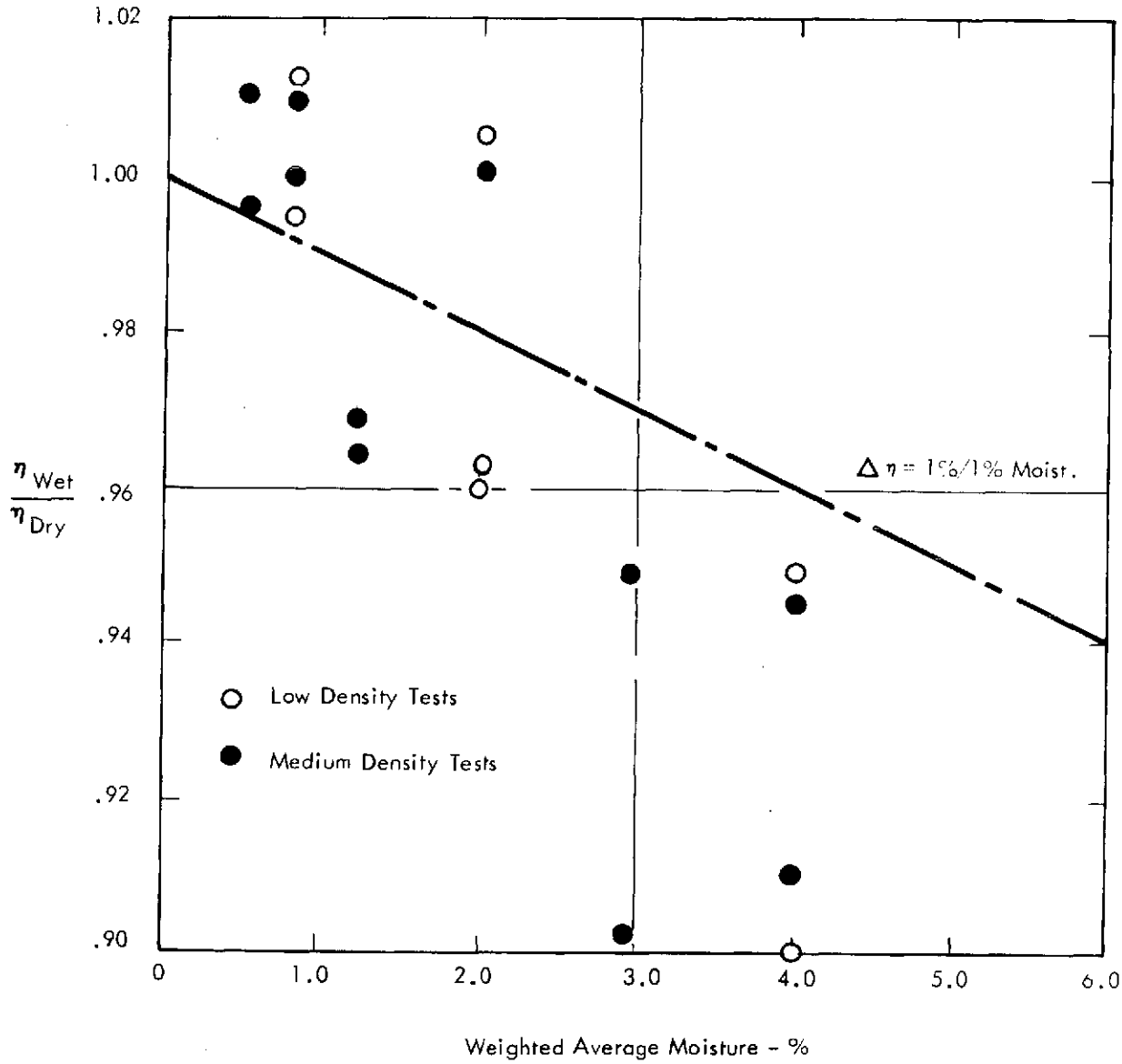

Figure 45. Efficiency Ratio for Wet and Dry Condition

8.0 CONCLUSIONS

Because of the intense fog present in the turbine, both high speed photographic and visual observations of flows on surfaces and the surfaces themselves were difficult to make. (The reproduction of the movie frames for reporting purposes resulted in the loss of much detail.) Careful study of the original films, however, led to some useful deductions. Resolution of the larger drops of water detached from the fourth stator, backlighted, was good and resolution of drops as small as 60 micrometers (2360 micro-inches) was achieved. From the results of testing, the following conclusions can be made:

1. The observed moisture flows in this turbine differed from that expected on the basis of descriptive material such as that given in NAS CR-1830 in important respects:

   - Moisture was not observed on the pressure surface in rivulet form. The existence of a thin film of moisture spread uniformly on the surface cannot be ruled out on the basis of the test results, however.

   - Moisture appears to concentrate at the junction of the blade and casing instead of being uniformly spread along the stator blade trailing edge.

   - The large globs of moisture torn from the stator blade trailing edge move radially inwards for a considerable distance before breaking up and moving downstream.

   - The moisture leaving the last rotor blade as a fog was uniformly distributed over the field of view. No concentrations of liquid could be seen departing the blade shroud and entering the casing removal slot.

   - There was little visual difference in the movement or in the amount of moisture observed departing the stator blade trailing edge with with or without trailing edge moisture removal. The quantities of moisture removed through the slots that were determined externally by tank measurement were encouraging. These data could have been erroneously interpreted as indicative of the successful removal of most of the potentially damaging liquid if the high speed movies had not shown that large drop shedding persisted when the removal slots were operating.

2. The dimensions of the large globs of liquid departing the stators and the diameters of the largest drops observed after secondary breakup of the globs were, in general, about the same as values calculated using the method of NAS CR-1830, although some exceptions were noted.

3. The amounts of moisture removed during operation of the suction slots in the stator trailing edges was about 70% to 90% of that calculated using the method from NASA CR-1830. However, the points at which 90% was achieved occurred only during tests with low turbine superheat. For this reason, the 70% level appears more representative.

4. The casing slot over the downstream edge of the third rotor blade shroud removed nearly 70% of the moisture available according to the method from NASA CR-1830. The fourth rotor blade casing slot removed very little moisture. Since the design philosophy for the third and fourth casing slots was the same, there is no obvious explanation for the discrepancy in the relative performances.

5. Although considerable scatter was present in the data, the turbine performance measurements over a range of moisture levels indicates a non-linear relationship between moisture level and performance degradation.

ACKNOWLEDGEMENTS

The authors wish to experss their appreciation to L. D. Tarvestad of Westinghouse Steam Turbine Engineering and P. R. Masterson of the Westinghouse Development Laboratory whose perserverance and dedication were essential in obtaining meaningful photographic data.

APPENDIX A1 - CASCADE TESTS

By

KIRIT J. DESAI
WESTINGHOUSE ELECTRIC CORPORATION

A1.0 INTRODUCTION

Due to the uncertainty as to the magnitude of the flow disturbance that might be caused by the light tubes and borescopes of the optical system in the test turbine, low speed air cascade tests were conducted with optical system probe simulations in the blade passage and downstream of the cascade blades to obtain experimental information on possible flow disturbances. The apparatus used is shown in Figure A1-1.

Wake velocity profiles were recorded by pressure traverse measurements at a downstream position, and static pressures were measured along the trailing edge of two cascade blades. From these measurements, the channel referred velocity and the wake velocity profiles were investigated both with and without optical system probes present.

A1.1 TEST APPARATUS AND PROCEDURE

The cascade blades used were a two times full size model of the third stage, 3/4 blade height section (height from the inner diameter position) of a three stage potassium test turbine. This blading was sufficiently similar to the test stage blading to obtain meaningful results and offered a convenient test setup.

The main consideration in designing the cascade test was to best simulate the flow field of the obstructed flow path of the test stage. To simulate the flow field, scaled probes were located in the cascade flow passages and inserted into one of the cascade blades as in the actual test turbine stage. Using the scale factor, the ratio of stator blade flow passage dimensions between cascade and turbine test stage, the probe size used was determined

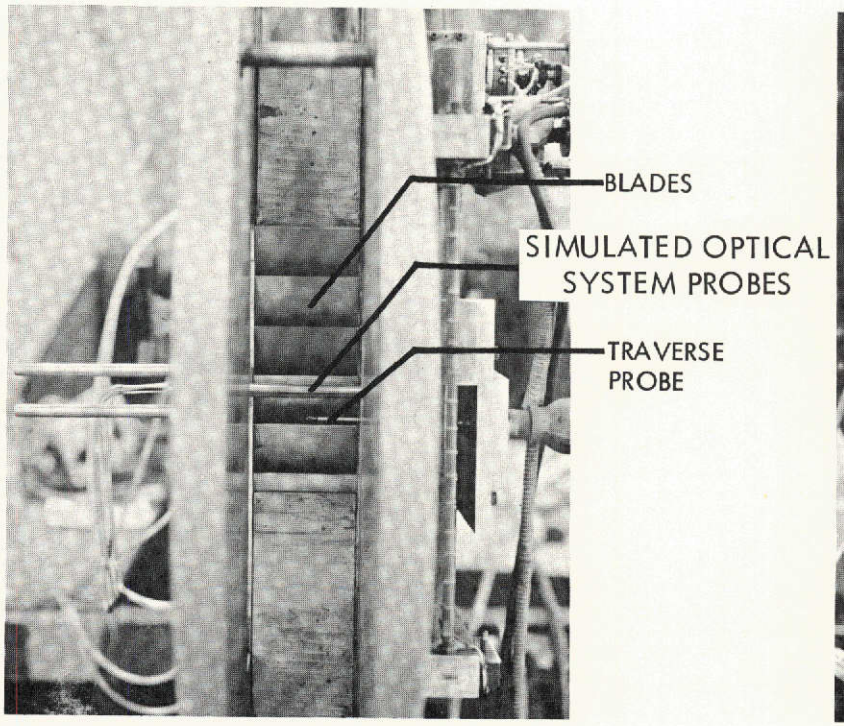

END VIEW

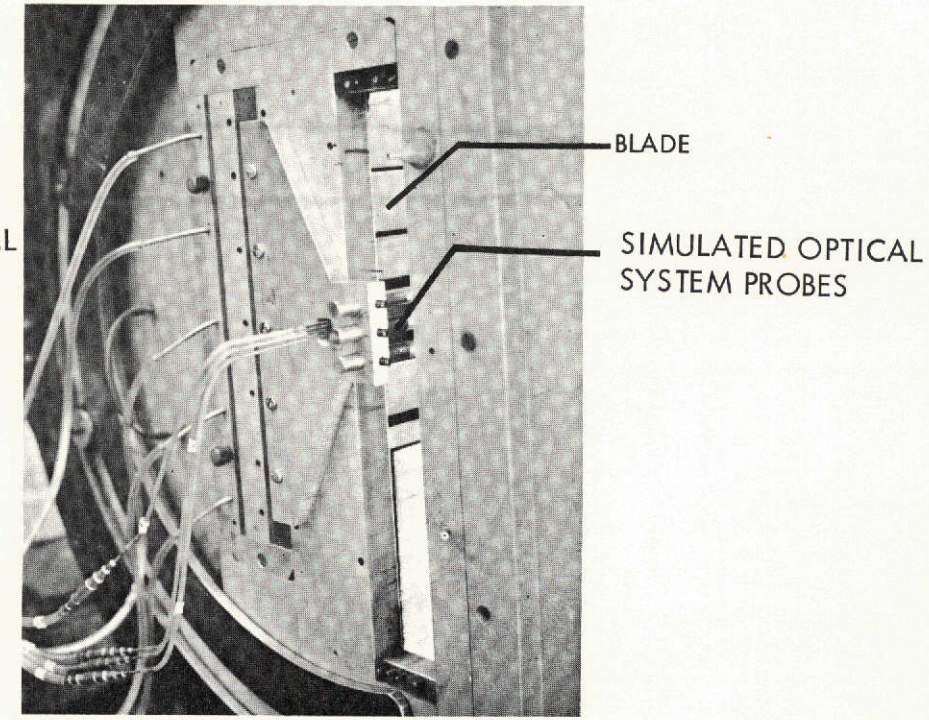

SIDE VIEW

Figure A1-1. Cascade for Flow Disturbance Tests

conservatively to be 0.95 cm (0.37 inch) in diameter. Figure A1-2 shows the plan view of the cascade and includes a tabular dimensional comparison between the projected test turbine fourth stage tip section and the cascade blade section.

Two blades were instrumented with static taps along their trailing edges; one with the taps on the concave surface and the other with taps on the convex surface. In order to minimize the end wall effects in the cascade and have reliable base data for comparison, it was decided against locating the taps at the 3/4 blade height position as in the test stage. As a result, the taps were staggered about the mean height position, the staggering of the taps to ensure added accuracy and reliability of the static pressure readings. One of the instrumented blades is shown in Figure A1-3.

A plan view of potential downstream optical system probe configurations, which permit observation of suction surface liquid flow toward the stator blade trailing edge, can be seen in Figure A1-4. The three probes can be inserted in the downstream flow field in any desired combination, as well as being inserted to any desired depth along the blade height. Figure A1-5 shows the details of the cut-out blade providing a view port for PLO probes that permit observation of the pressure surface liquid flow toward the blade trailing edge. The suction surface length of the cut-out portion was taken to be the same percentage of total suction surface length as in the actual test turbine blade. The PLO probe, located in the upstream flow passage in this configuration, can be inserted to any desired depth along the blade height.

Traverse measurements were taken in 0.013 cm (0.005 inch) steps in the pitchwise direction at mean blade height and 0.318 cm (0.13 inch) axial downstream positions. A Kiel total pressure probe operated by the automatic traversing rig was used for traversing downstream of the cascade. The overall shield diameter of the probe was 0.16 cm (0.06 inch). A total pressure probe and a thermocouple were located at the inlet to the cascade. The probes were connected to pressure transducers. The electrical signals from the transducers and from the traversing rig were fed to

	TEST TURBINE STATOR TIP SECTION		CASCADE NA53-8520" BLADE SECTION	
(PITCH)	S	= 4.18 CM (1.645 IN.)	S	= 3.58 CM (1.41 IN.)
(OPENING)	O	= 1.31 CM (0.517 IN.)	O	= 1.33 CM (0.524 IN.)
	O/S	= 0.3135	O/S	= 0.372
(EXIT ANGLE)	α	= 18.65°	α	= 21.8°
(PROBE DIAMETER)	D	= 0.953 CM (0.375 IN.)	D	= 0.953 CM (0.375 IN.)
	D/O	= 0.725	D/O	= 0.716
(TRAILING EDGE)	T_E	= 0.114 CM (0.045 IN.)	T_E	= 0.071 CM (0.028 IN.)

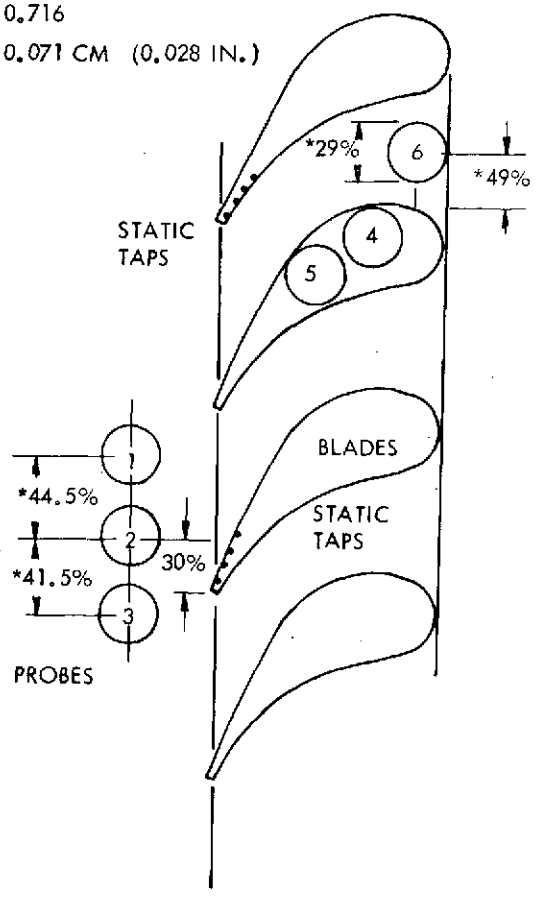

*WITH RESPECT TO PITCH

Figure A1-2. Optical Probe Simulations in Cascade

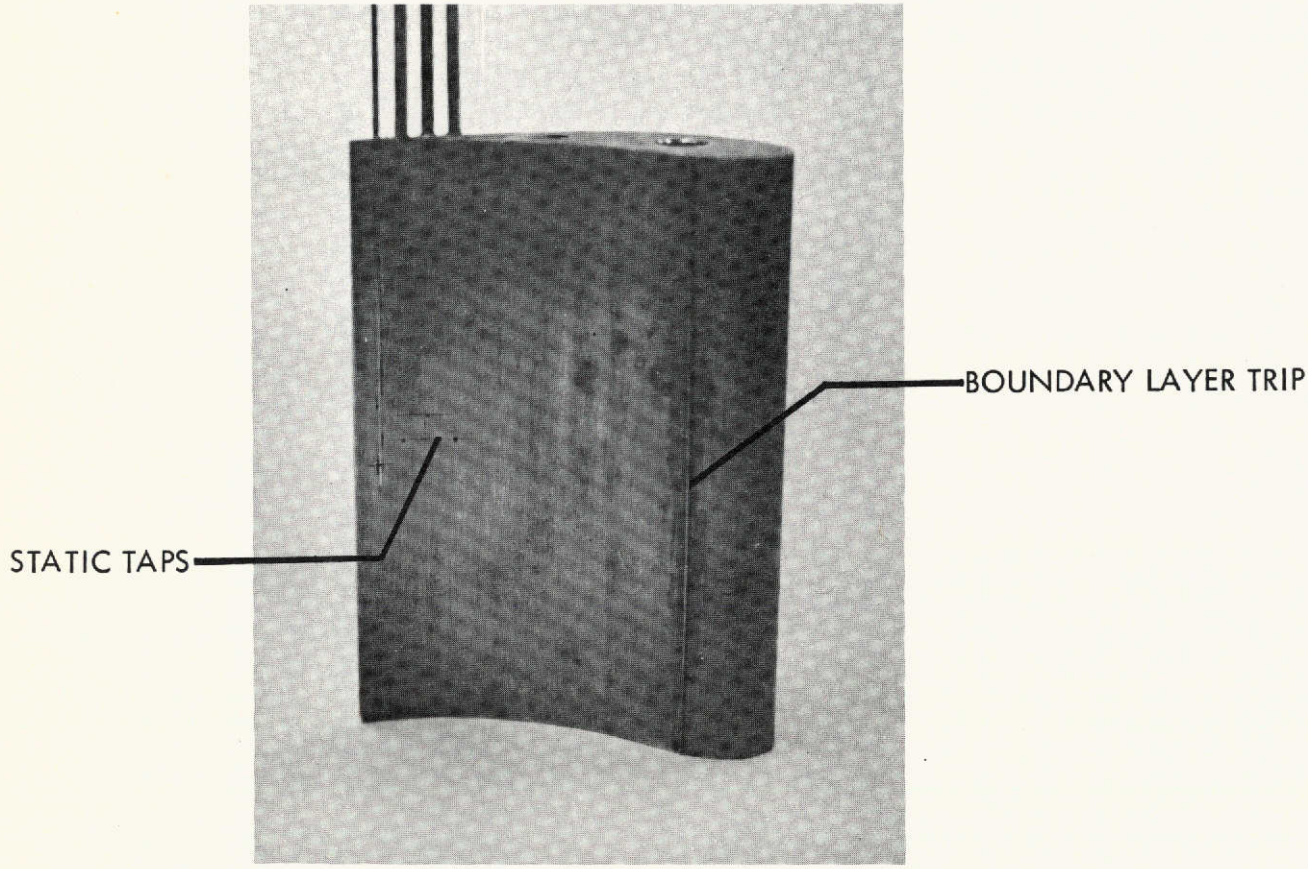

Figure A1-3. Instrumented Blade for Flow Disturbance Test

	TEST TURBINE STATOR TIP SECTION		CASCADE NA53-8520" BLADE SECTION	
		UNITS		
(PITCH)	S	= 4.18 cm (1.645 in.)	S	= 3.58 cm (1.41 in.)
(OPENING)	O	= 1.31 cm (0.516 in.)	O	= 1.33 cm (0.524 in.)
	o/s	= 0.3135	o/s	= 0.372
(EXIT ANGLE)	α	= 18.65°	α	= 21.8°
(PROBE DIAMETER)	d	= 0.953 cm (0.375 in.)	d	= 0.953 cm (0.375 in.)
	d/o	= 0.726	d/o	= 0.716
TRAILING EDGE)	t_e	= 0.1140 cm (0.045 in.)	t_e	= 0.011 cm (0.028 in.)

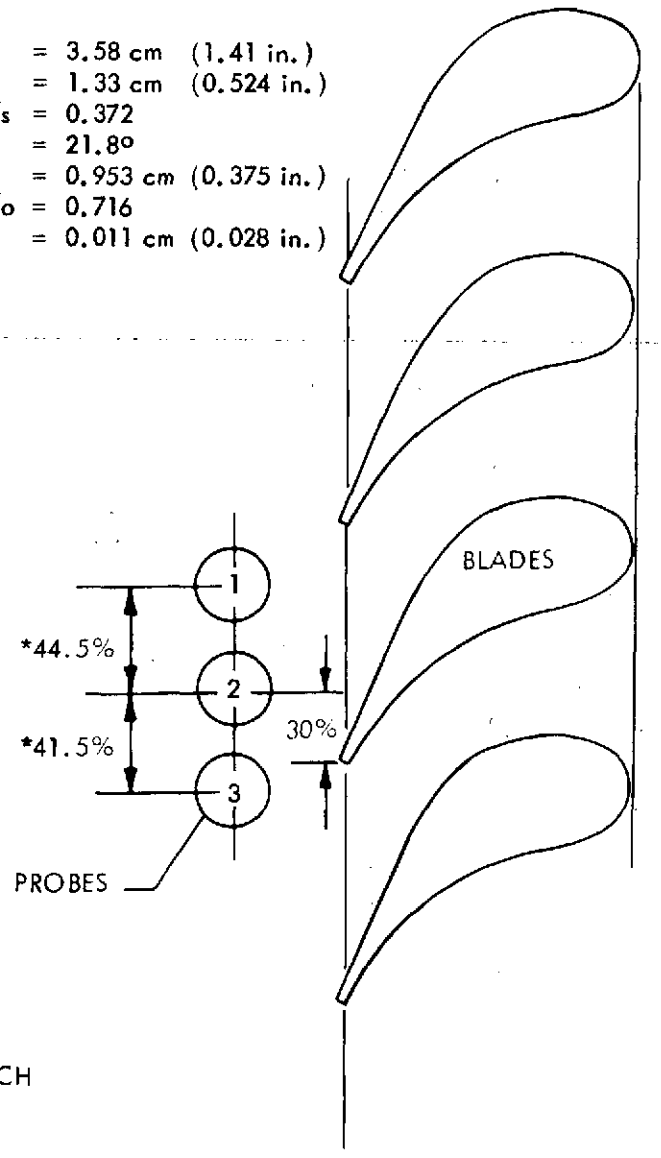

*WITH RESPECT TO PITCH

613071-48

Figure A1-4. Cascade Setup for Downstream Optical Probe Simulations

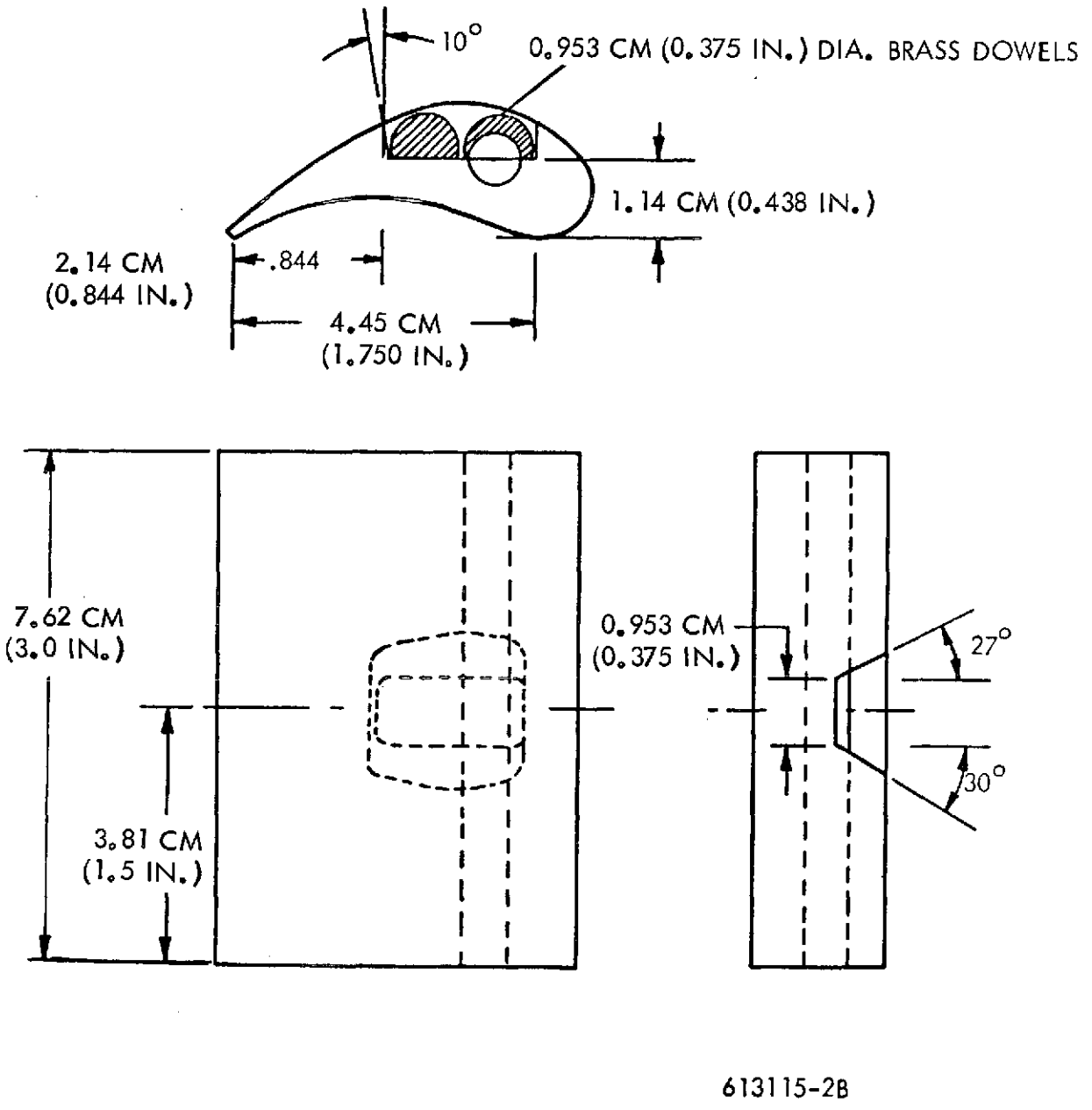

Figure A1-5. Cut-Out Blade

the computerized data acquisition system. The data which was recorded on computer magnetic tape was then fed to the high speed computer. Calculations were made to determine the point by point referred velocity by the following equation.

$$V_r = V/V^1 = \left[\frac{1 - (P_s/P_t)^{\frac{\gamma-1}{\gamma}}}{1 - (P_s/P_i)^{\frac{\gamma-1}{\gamma}}} \right]^{1/2}$$

where

P_s downstream static pressure

P_t downstream stagnation pressure

P_i inlet stagnation pressure

V downstream velocity

V^1 downstream velocity based on isentropic expansion from the inlet stagnation condition

V_r referred downstream velocity

γ specific heat ratio, 1.4

The computer output included plots of the actual and referred velocities across the length of traverse (pitchwise).

The static taps were connected directly to water manometers and the readings were taken manually.

All the tests were conducted at the same conditions; namely, $P_i - P_s$ = 66 cm (26 inches) of water (Mach No. = 0.33), and blade incidence angle 0 degrees.

A1.2 RESULTS AND DISCUSSION

By comparing the traverse results and the pressure readings with those of unobstructed flow results and analytical computations, it is possible to tell quantitatively the extent of flow disruption.

Figures A1-6 through A1-8 show blade surface referred velocities plotted against referred blade width for potential downstream locations, along with the results of theoretical computations for the unobstructed blade passage. As shown in Figure A1-6, there is good agreement between analysis and experiment on the basis of the no-probe baseline test. Figure A1-7 shows that a single optical probe in location No. 1 causes little or no disturbance of the suction surface flow. However, Figures A1-6 through A1-8 show that optical system probes in locations No. 2 and No. 3, individually or collectively, cause a great deal of disturbance of this suction surface flow. Traverse data, Figure A1-9, for optical system probes at location No. 1 also revealed the relatively small disturbance of this probe location on the flow. However, optical system probes Nos. 2 and 3, when in position with No. 1 respectively, did show deviations from normal unobstructed flow and distortions in the wakes were appreciable.

Figures A1-10 and A1-11 show that all the cut-out blade configuration tests, only the one with probes 4 and 5 in position, seemed to be satisfactory with respect to minimizing observed flow disturbance. While this test gives the least displacement of the blade surface velocities from those observed during base line test, the above statment is based more on the traverse results obtained than on the measured surface velocities. A comparison of all wake traverse tests for this configuration are given in Figure A1-12. Tests that had probe No. 6 in position showed the greatest disturbance of the channel flow; here again, the basis for the above statement is more on traverse data. The remaining tests, various combinations of probes 4 and 5 and the cut-out blade, showed little or no flow disturbance.

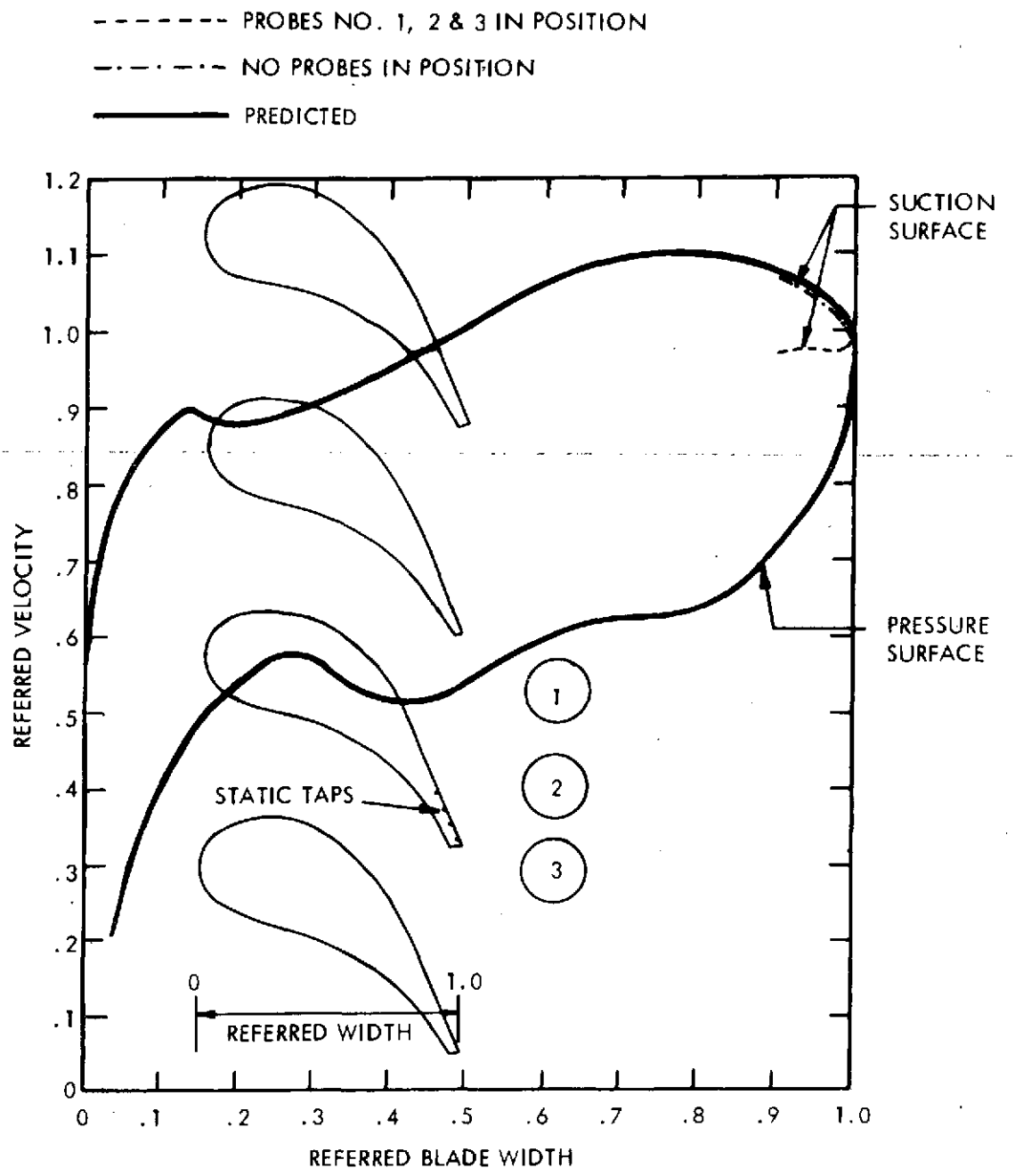

Figure A1-6. *Cascade Blade Surface Velocities - Downstream Configuration*

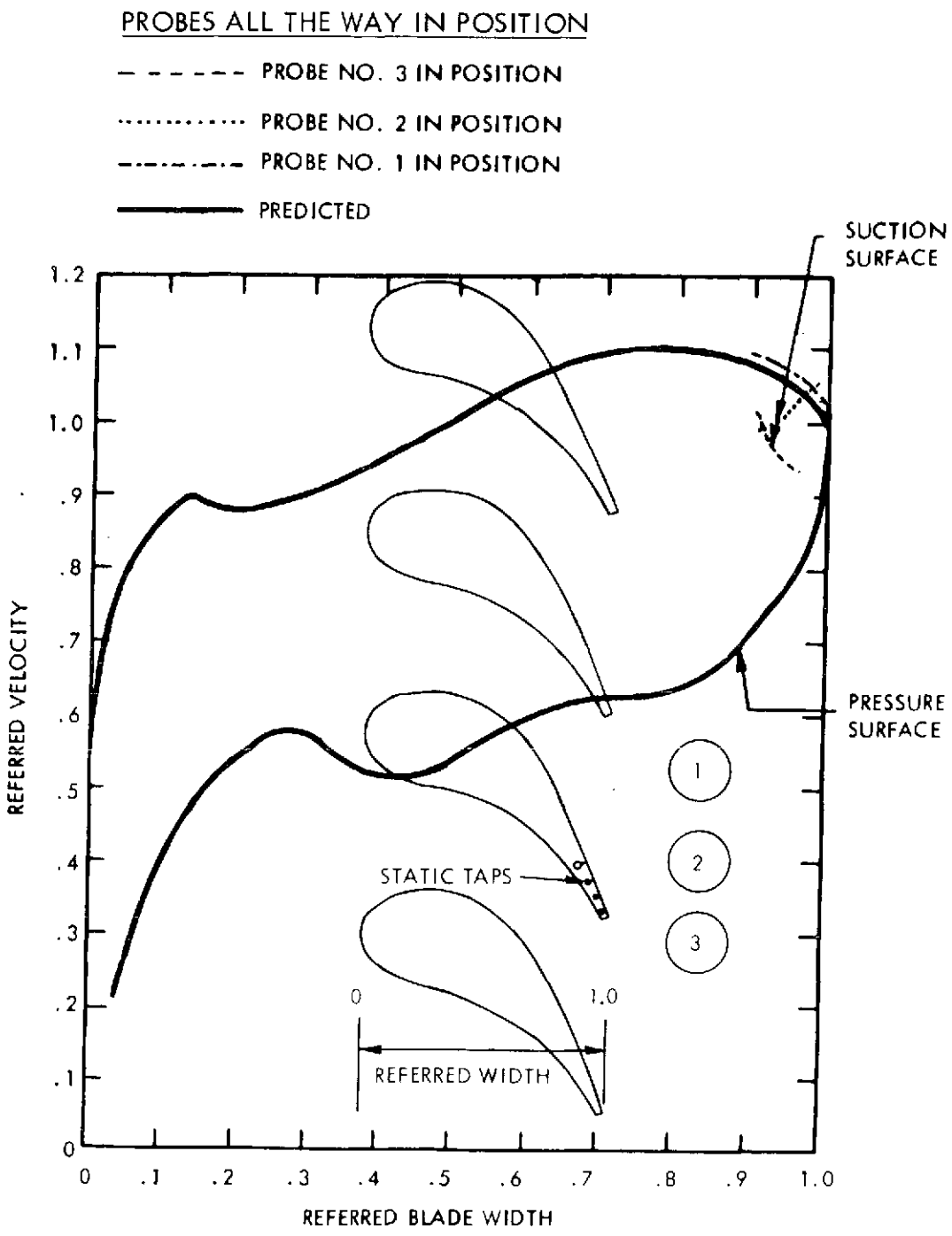

Figure A1-7. Cascade Blade Surface Velocities - Downstream Configuration

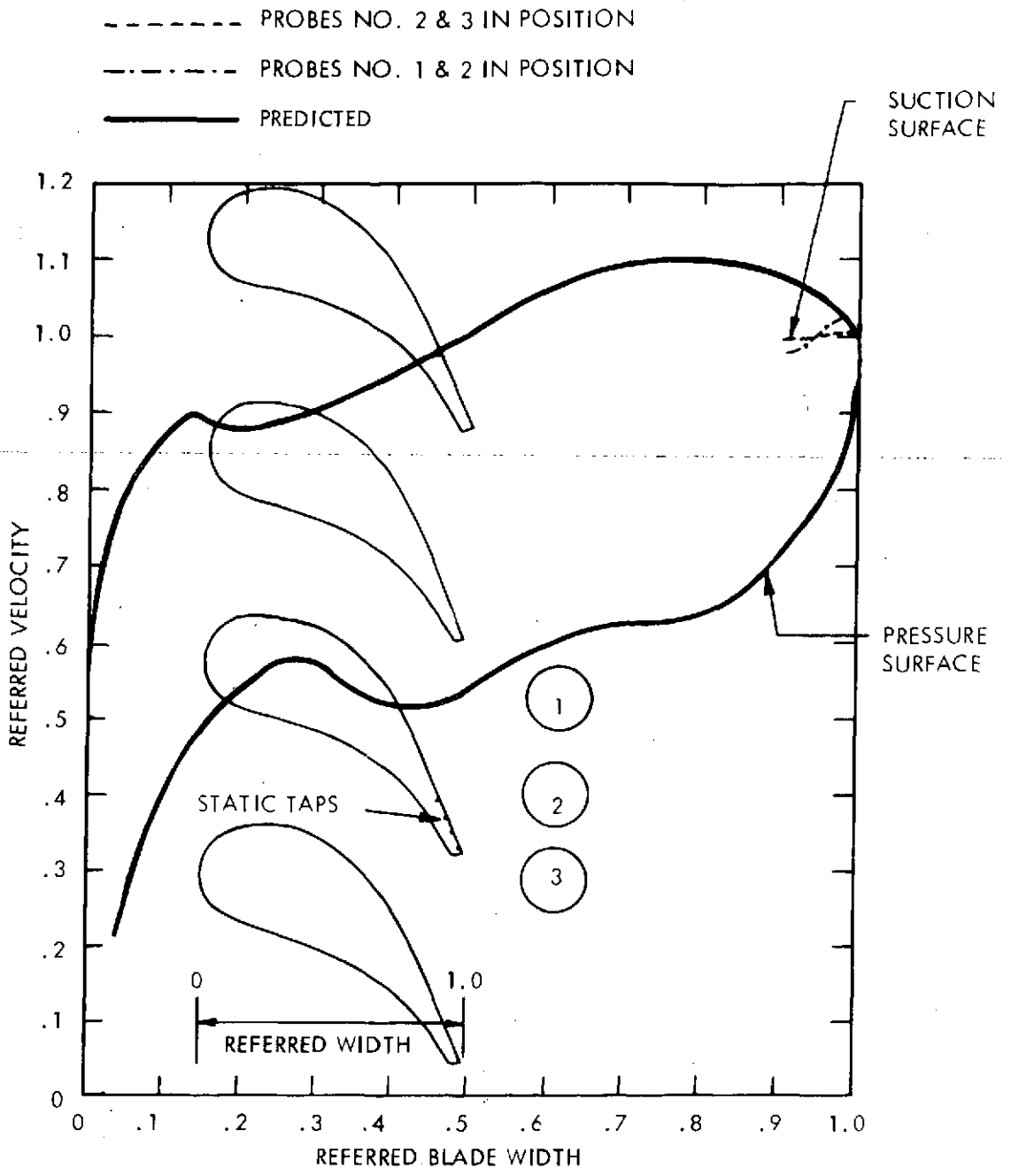

Figure A1-8. Cascade Blade Surface Velocities - Downstream Configuration

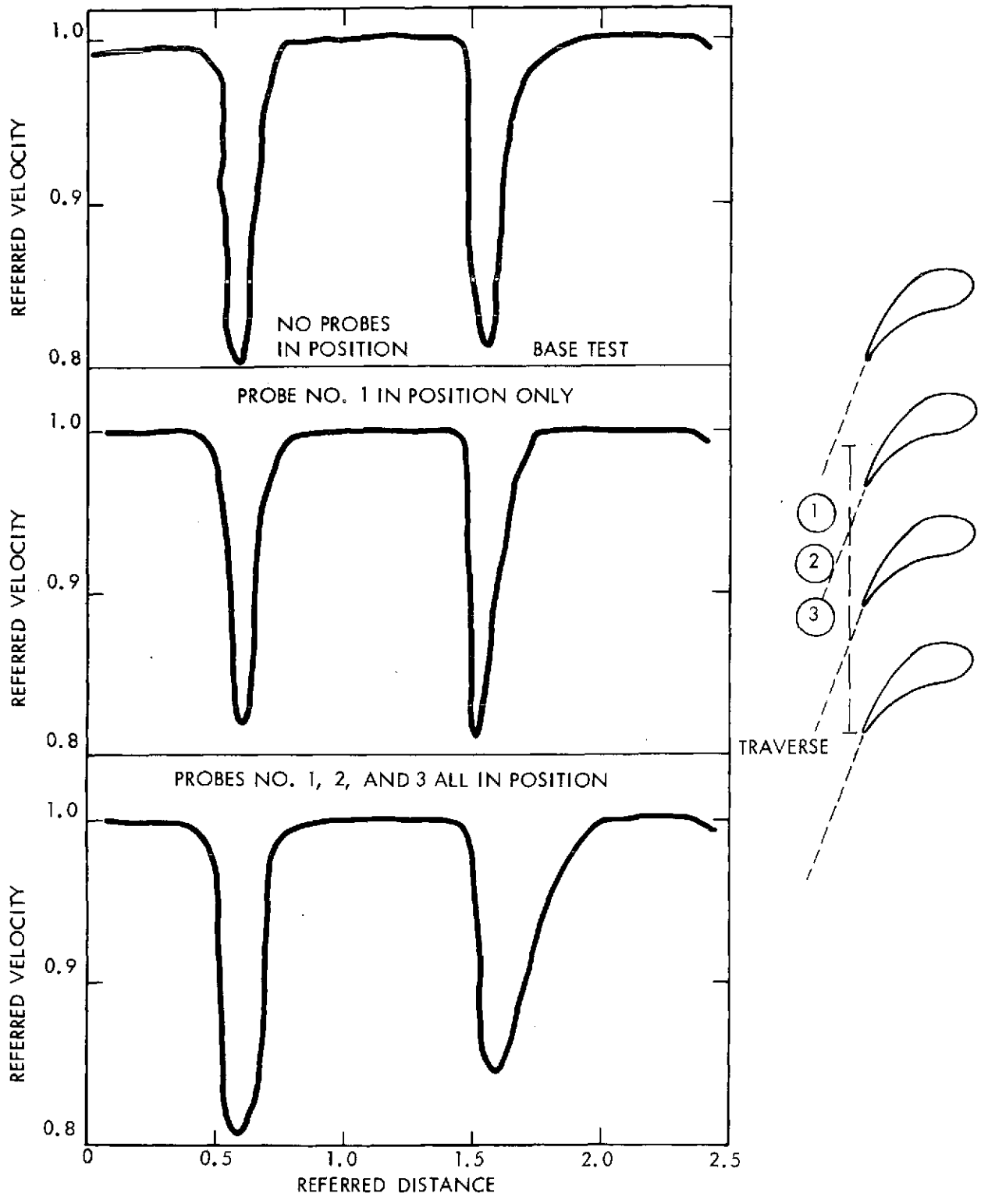

Figure A1-9. Optical Probes - Wake Observations - Downstream Configuration

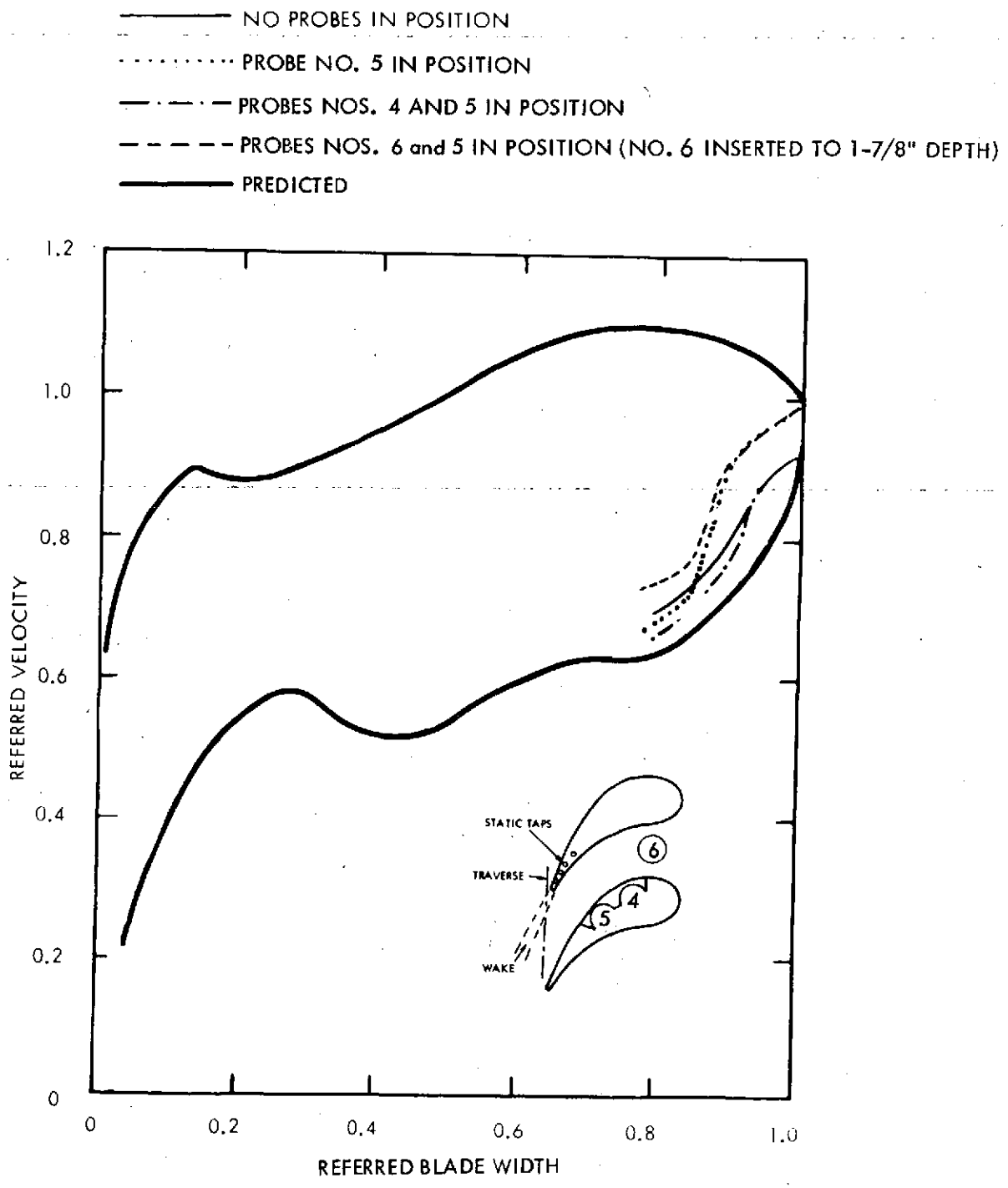

Figure A1-10. Cascade Blade Surface Velocities - Cut-out Blade Configuration

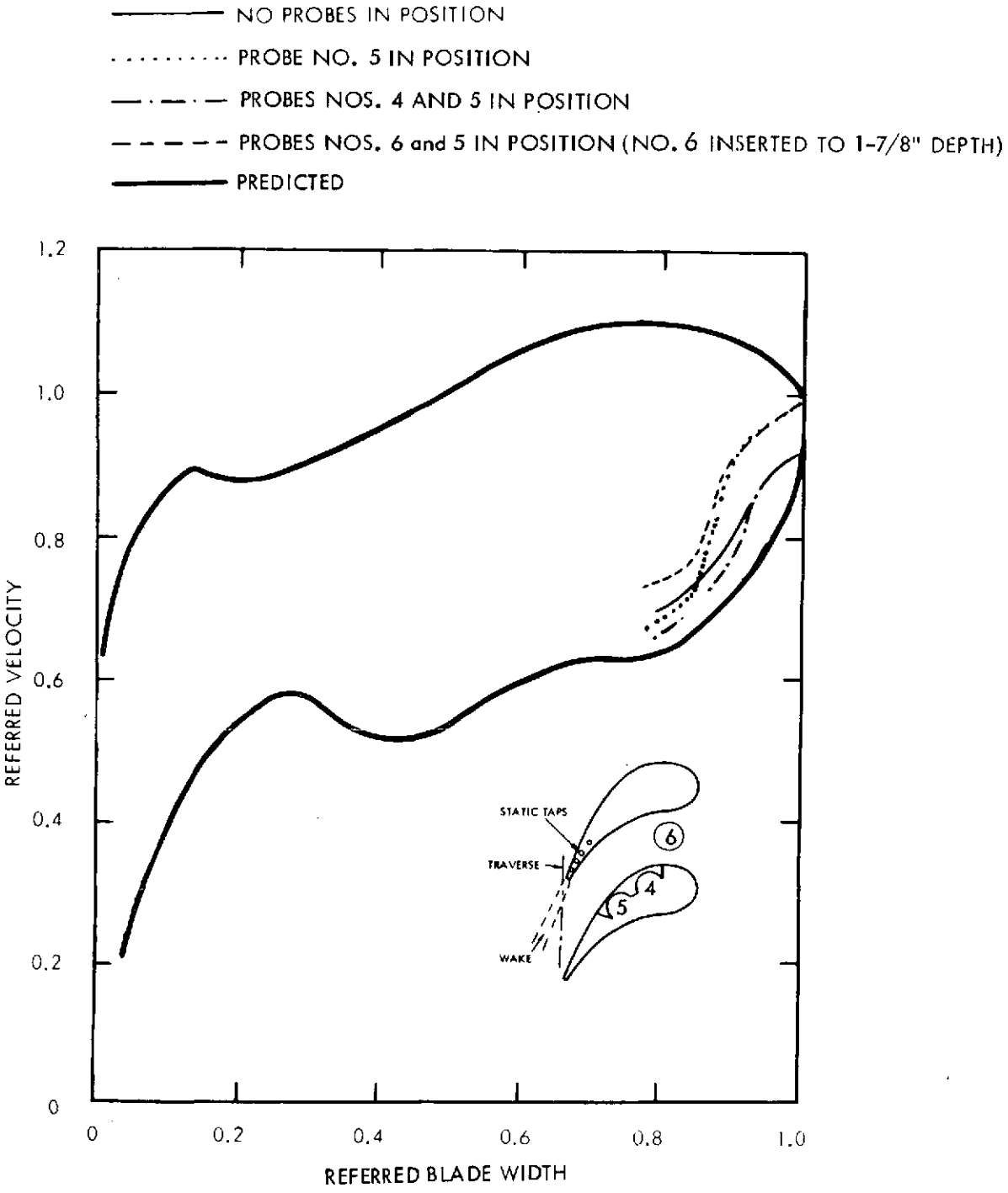

Figure A1-11. Cascade Blade Surface Velocities - Cut-out Blade Configuration

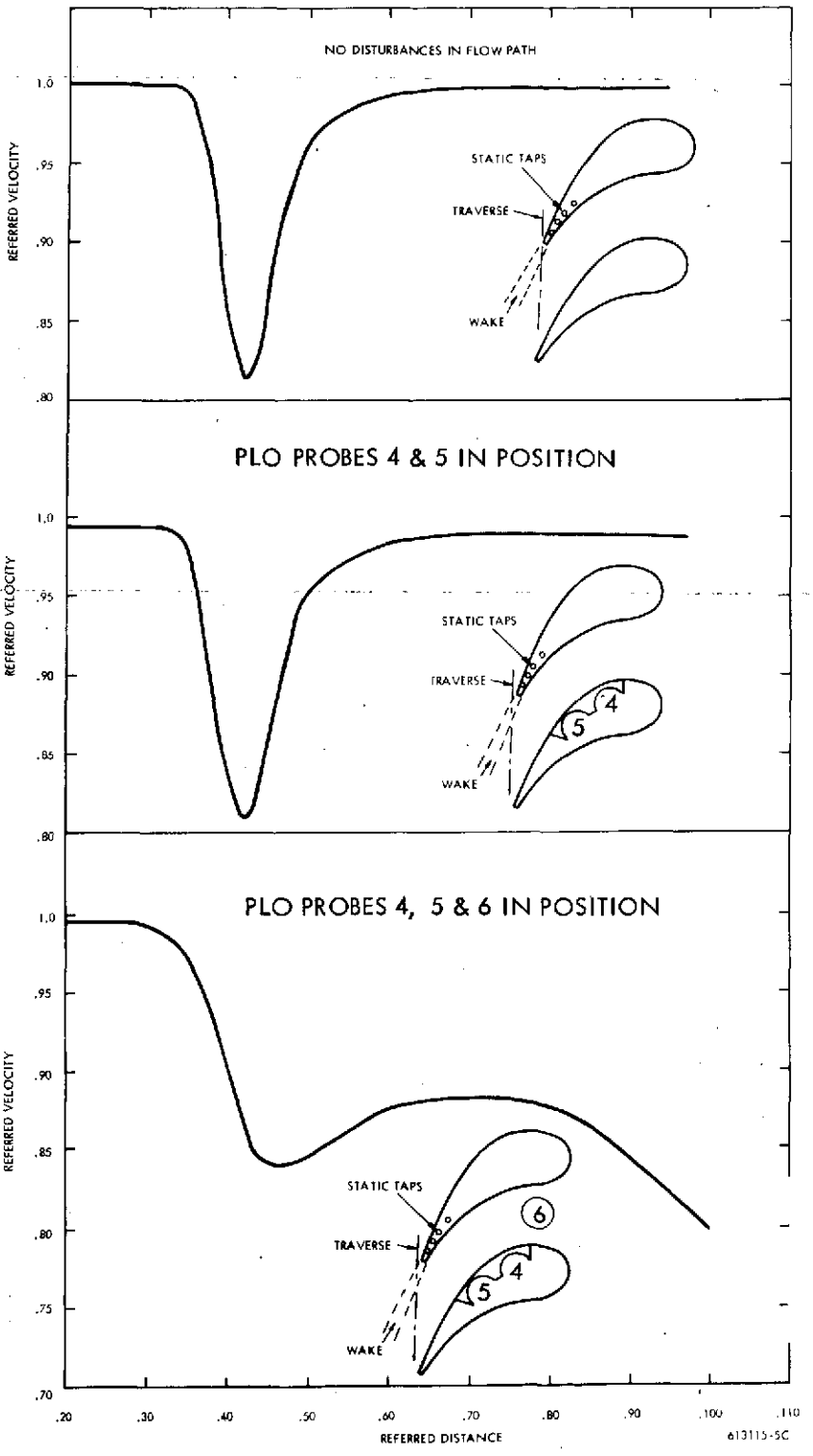

Figure A1-12. Optical Probes - Wake Observations - Cut-out Blade Confuguration

A1.3 CONCLUSIONS

For suction surface liquid flow observation, no more than one optical probe should be used in the downstream position. It should be located at least one pitch distance (tangentially) from the suction surface close to the trailing edge, the region of observation.

For the observation of the pressure surface liquid flow toward the blade trailing edge, upstream location of an optical system probe would not be desirable from the standpoint of minimum flow disturbance. However, optical system probes at locations 4 and 5 in the blade cut-out could be used for the intended photography, causing relatively little disturbance of the flow to be observed.

APPENDIX A2

A2.0 TURBINE BLADE DESIGN

A2.1 FLUID DYNAMIC DESIGN

Row by row data for the slave turbine is given in Table A2-1. These data give the stage loading data for the various stages and blade rows.

As shown, the axial velocity and blade gauging uniformly increase from the inlet to exit of the turbine; the axial velocity increases from 60 m/sec (197 ft/sec) to 100 m/sec (328 ft/sec). Factors in the schedule of axial velocity are the blade heights and annulus flare. Generally, the row by row enthalpy drops are uniformly distributed between the stator and rotor blades; i.e., the stage reaction is approximately 50%. Also, the stage work is approximately the same for each stage. Row exit Mach numbers are in the order of 0.70 to 0.77 and the blade Reynolds numbers, based on the projected blade chord and exit fluid conditions, are in the order of 5. to 10. * 10^5. The stage loading coefficients, $gJ\Delta h/U^2$ is approximately 1.7 in all three stages of the slave turbine. This compares with an approximate value of 1.1 for conventional Westinghouse turbines equipped with these blades. The increase in load coefficients over the optimum value of 1.1 is a consequence of achieving the high moisture levels in a three stage design.

Figure A2-1 gives the airfoil cross-section sketch for the standard blade used throughout the slave turbine. Figure A2-2 gives the surface velocity plot for design operation. The velocity plot applies to all blade rows and blade height positions in the slave turbine. The rather low, 5 degree flare in the test stage is a consequence of the large axial spacing between the fourth stage blade rows. Details of the mean diameter calculations are in line with the following:

1. Loss coefficients: 2 - dimensional energy loss coefficient, based on the blade turning angle, corrected for blade aspect ratio, leakage, and moisture. Leakage correction assumes 1.16% loss per percent leakage

TABLE A2-1

SLAVE TURBINE CONDITIONS (LOW DENSITY)

Speed = 117.7 Hz
Flow = 1.46 kg/sec
Mean Diameter = 64.0 cm
Radial Clearance = 0.025 cm
Total Efficiency = 80.2%

	Inlet Total	1s	1r	2s	2r	3s	3r
		Static					
h - cal/g	651.0	641.0	630.0	620.0	608.0	597.0	586.0
P - $N/m^2 \times 10^{-5}$	2.19	1.57	1.13	0.810	0.566	0.465	0.271
T - Degrees K	402.6	385.3	376.1	367.0	357.6	348.8	340.1
v - m^3/kg		1.10	1.48	1.99	2.75	3.80	5.35
y - moisture - %		0.009	0.002	0.035	0.048	0.060	0.073
γ - specific heat ratio		1.139	1.136	1.133	1.129	1.126	1.123
a - acoustic velocity - m/sec		444.0	435.0	428.0	420.0	410.0	403.0
$gJ\Delta h/U^2$ - stage load coefficient			1.570		1.608		1.550
Δh - stage work - cal/g			21.1		21.6		20.8
Exit blade height - cm		1.058	1.41	1.92	2.49	3.15	3.89
λ - gauging		0.224	0.222	0.224	0.236	0.265	0.299

TABLE A2-1
(Continued)

SLAVE TURBINE CONDITIONS (LOW DENSITY)

Speed	=	7060 rpm
Flow	=	3.21 lb/sec
Mean Diameter	=	25.23 inch
Radial Clearance	=	0.010 inch
Total Efficiency	=	80.2%

	Inlet Total	1s	1r	2s	2r	3s	3r
		----------	----------	Static	----------	----------	----------
h - Btu/lb	1171.2	1150.7	1131.2	1112.1	1092.1	1073.2	1053.9
p - psia	31.76	22.81	16.33	11.74	8.20	6.74	3.93
T - Degrees F	265.1	235.0	217.4	200.9	184.0	168.1	152.2
v - ft^3/lb	--	17.61	23.76	31.90	44.02	60.74	85.52
y - moisture - %		0.009	0.022	0.035	0.048	0.060	0.073
γ - specific heat ratio		1.139	1.136	1.133	1.129	1.126	1.123
a - acoustic velocity		1455.1	1428.7	1402.2	1374.5	1348.2	1321.6
Q^2 - row energy coefficient		0.8179	0.8154	0.8382	0.8319	0.8253	0.8221
$gJ\Delta h/u^2$ - stage load coefficient			1.570		1.608		1.550
Δh - stage work - Btu/lb			38.0		38.8		37.5
Exit Blade height - inches		0.416	0.554	0.756	0.980	1.240	1.530
λ - gauging		0.2240	0.2220	0.2240	0.2360	0.2650	0.2990

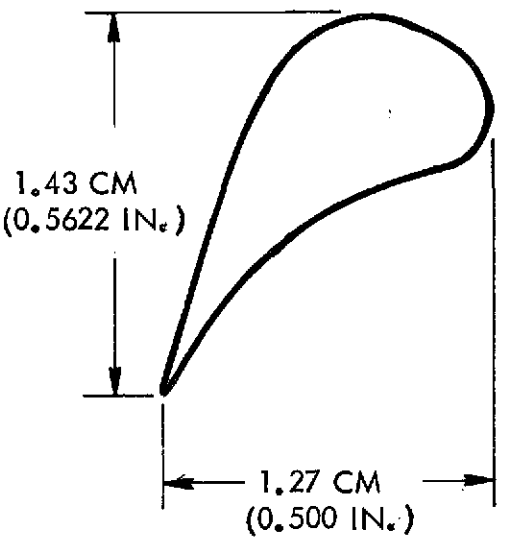

A2-1. Slave Turbine Blade Section

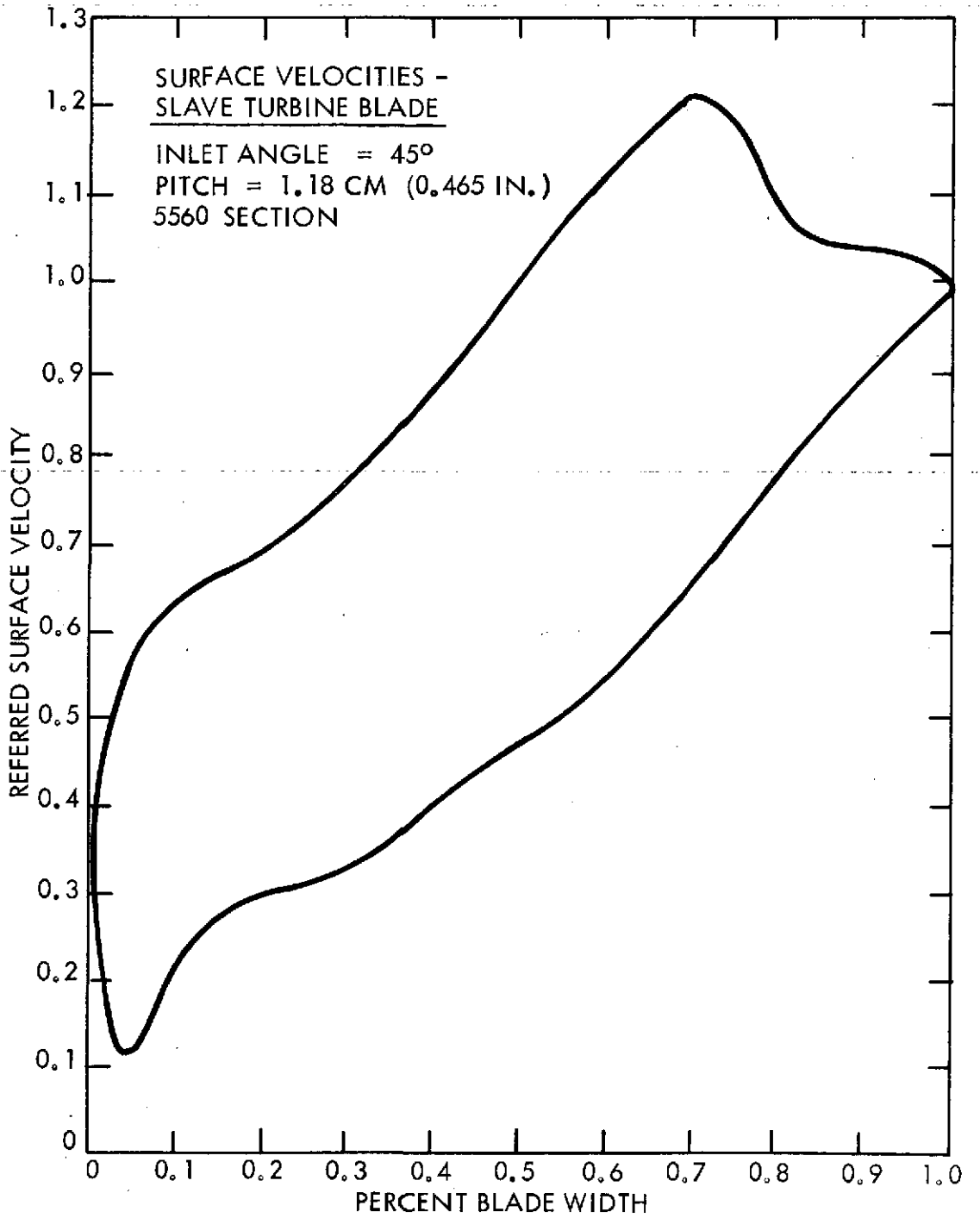

Figure A2-2. Slave Turbine Blade Surface Velocities

area based on the annular area. Moisture correction assumes 1% loss per percent equilibrium moisture content, based on the average moisture in row.

2. Blade heights: Established by continuity calculation, based on the (mean diameter) velocity at exit of row, uncorrected for leakage loss, and the exit flow angle. (This calculation was later confirmed by a more detailed calculation along the height of the blade.)

Row by row data at the mean diameter to establish the fluid conditions at the hub and tip sections are given by Tables A2-1 and A2-2. The solution of the radial equilibrium is in line with the following:

P static pressure

r radial distance

V_z vapor velocity in axial direction

V_θ vapor velocity in circumferential direction

ρ vapor density

constant

$$\rho V_z$$

with radius

$$\frac{1}{\rho}\frac{dP}{dr} = \frac{V_\theta^2}{r}$$

i.e., simple radial equilibrium. This assumes that the meridional stream tubes are straight, conical lines consistent with constant ρV_z. This particular solution was chosen to provide for a constant section, constant angle stator blade. (The equilibrium treatment with constant axial velocity gives an approximate $2\text{-}1/2^\circ$ difference in angle from hub to tip.)

TABLE A2-2

TEST STAGE CONDITIONS (LOW DENSITY)

Speed = 117.7 Hz
Flow = 1.46 kg/sec
Mean Diameter = 64.0 cm
Radial Clearance = 0.025 cm
Total Efficiency = 80.2%

	4s	4r
	------ Static ----------	
h - cal/g	574.0	563.0
p - $N/m^2 \times 10^{-5}$	0.168	0.111
T - Degrees K	329.4	320.9
v - m^3/kg	8.24	12.05
y - moisture - %	0.087	0.099
γ - specific heat ratio	1.118	1.115
a - acoustic velocity - m/sec	393.0	392.0
$gJ\Delta h/u^2$ - stage load coefficient		1.71
Δh - stage work - cal/g		23.2
λ - gauging	0.2904	0.3690

Speed = 7060 rpm
Flow = 3.21 lb/sec
Mean Diameter = 25.23 inches
Radial Clearance = 0.010 inch
Total Efficiency = 80.2%

	4s	4r
	------ Static ----------	
h - Btu/lb	1030.0	1011.0
p - psia	2.44	1.61
T - Degrees F	133.0	118.0
v - ft^3/lb	131.8	193.0
y - moisture - %	0.087	0.099
γ - specific heat ratio	1.118	1.115
a - acoustic velocity - ft/sec	1290.0	1290.0
$gJ\Delta h/u^2$ - stage load coefficient		1.71
Δh - stage work - Btu/lb		41.7
λ - gauging	0.2904	0.3690

Theoretically, the constant ρV_z solution gives a slight variation in $V_\theta r$ and energy with radius, but here the amount of the change is small. There is an approximate 4% change in $V_\theta r$, at stator exit, from hub to tip, and an approximate 6.3×10^2 joules (0.6 Btu) change in stage work from hub to tip.

Blade section sketches are shown by Figures A2-3, A2-4 and A2-5 for the fourth stage blades. Factors in the design of the stator blade are the spacing in the pitchwise direction and the cross-sectional thickness, to allow for the installation of the optical probes. The stator is a constant cross-section blade. The rotor blade sections are based on a linear interpolation with respect to the hub and tip sections. As shown by the surface velocity plots, Figures A2-6 and A2-7, the suction surface diffusion is less than V_{max}/V_{exit} of 1.2 for all sections. The "spike" in the stator velocity curve, in the region of the trailing edge, is associated with a numerical problem in the computer program.

A2.2 BLADE STRESS ANALYSIS

The mechanical design calculations made for the slave turbine rotating blading follow standard commercial procedures for short reaction blading. The various cross-sectional planes of blade analysis are shown in Figure A2-8.

Steady stresses in the blade root tee (Section E of Figure A2-8) are calculated on the assumption of a plastic redistribution of strain. The effective stress based on the Mises yield criterion is then compared to the allowable stress. In the shroud (Section A of Figure A2-8), tenon (Section B), blade section (Section C), and root shank (Section D), elastic stresses are calculated for centrifugal and steady steam loading. The direct centrifugal and steady steam bending stresses are added to give a total steady stress. From a Goodman diagram for the blade material, the vibratory stress that would cause failure if superimposed on the steady stress is found. To determine if the blade is satisfactory, the factor "a" is calculated and

$$\text{"a"} = \frac{\text{Vibratory stress to cause failure}}{\text{Stress Concentration x steady bending stress}}$$

BLADE SECTION - 4th STATOR BLADE

		HUB		MEAN		TIP	
DIAMETER-CM (IN.)		58.6	(23.08)	64.3	(25.32)	70.0	(27.56)
β	- INLET FLOW ANGLE-DEG.	47.90		49.45		51.90	
α	- EXIT FLOW ANGLE-DEG.	17.05		17.23		17.52	
SIN α	-	0.2932		0.2961		0.3010	
O/S	- GAUGING	0.2848		0.2922		0.3003	
O	- THROAT OPENING-CM (IN.)	1.01	(0.397)	1.14	(0.447)	1.27	(0.500)
S	- PITCH-CM (IN.)	3.54	(1.394)	3.89	(1.530)	4.23	(1.665)
C	- PROJECTED CHORD-CM (IN.)	6.16	(2.425)	6.16	(2.425)	6.16	(2.425)
W	- WIDTH-CM (IN.)	3.95	(1.556)	3.95	(1.556)	3.95	(1.556)
S/C	-	0.575		0.631		0.687	
TRAILING EDGE THICKNESS-CM (IN.)		1.17	(0.046)	1.17	(0.046)	1.17	(0.046)

52 BLADES

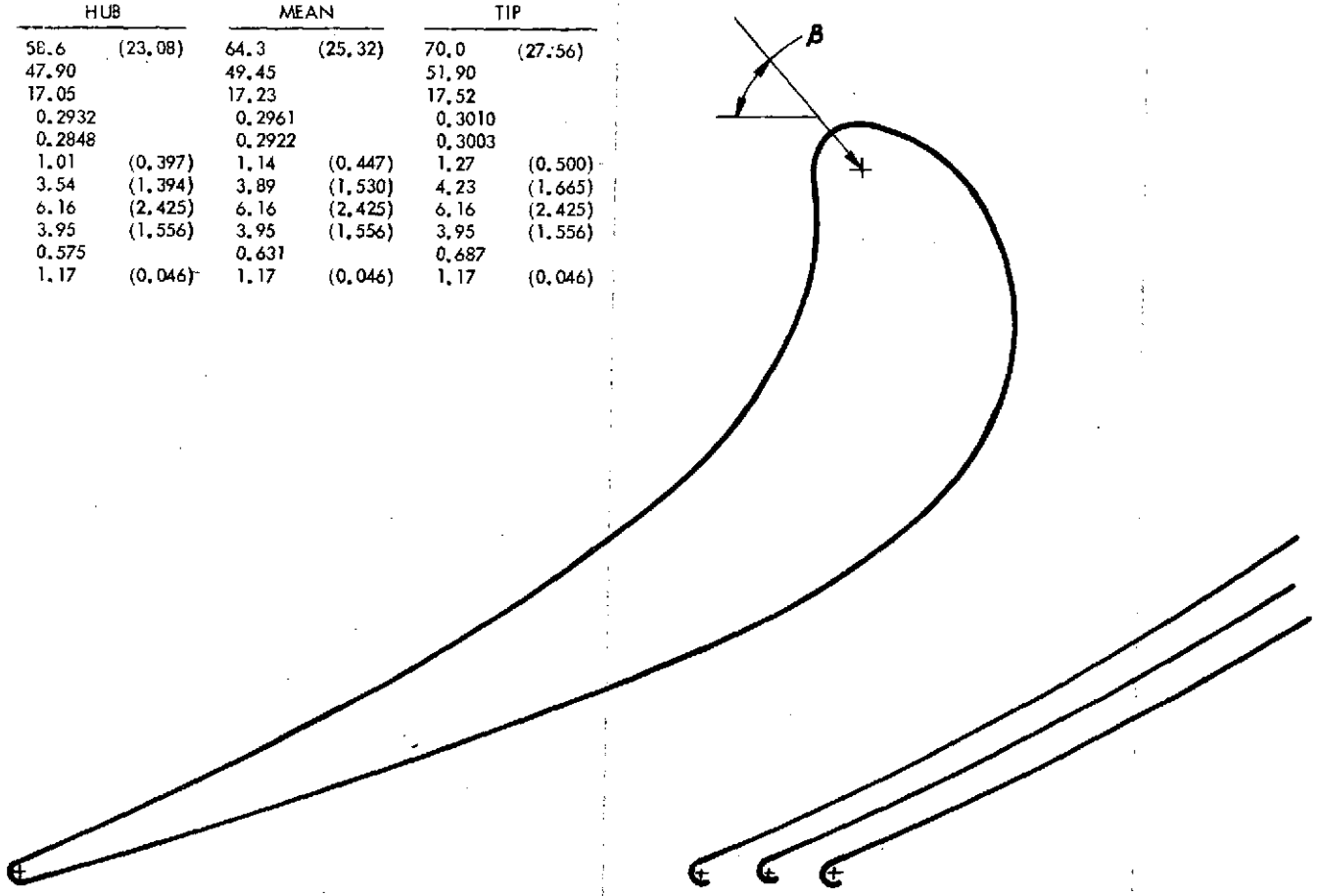

Figure A2-3. Blade Section - 4th Stator Blade

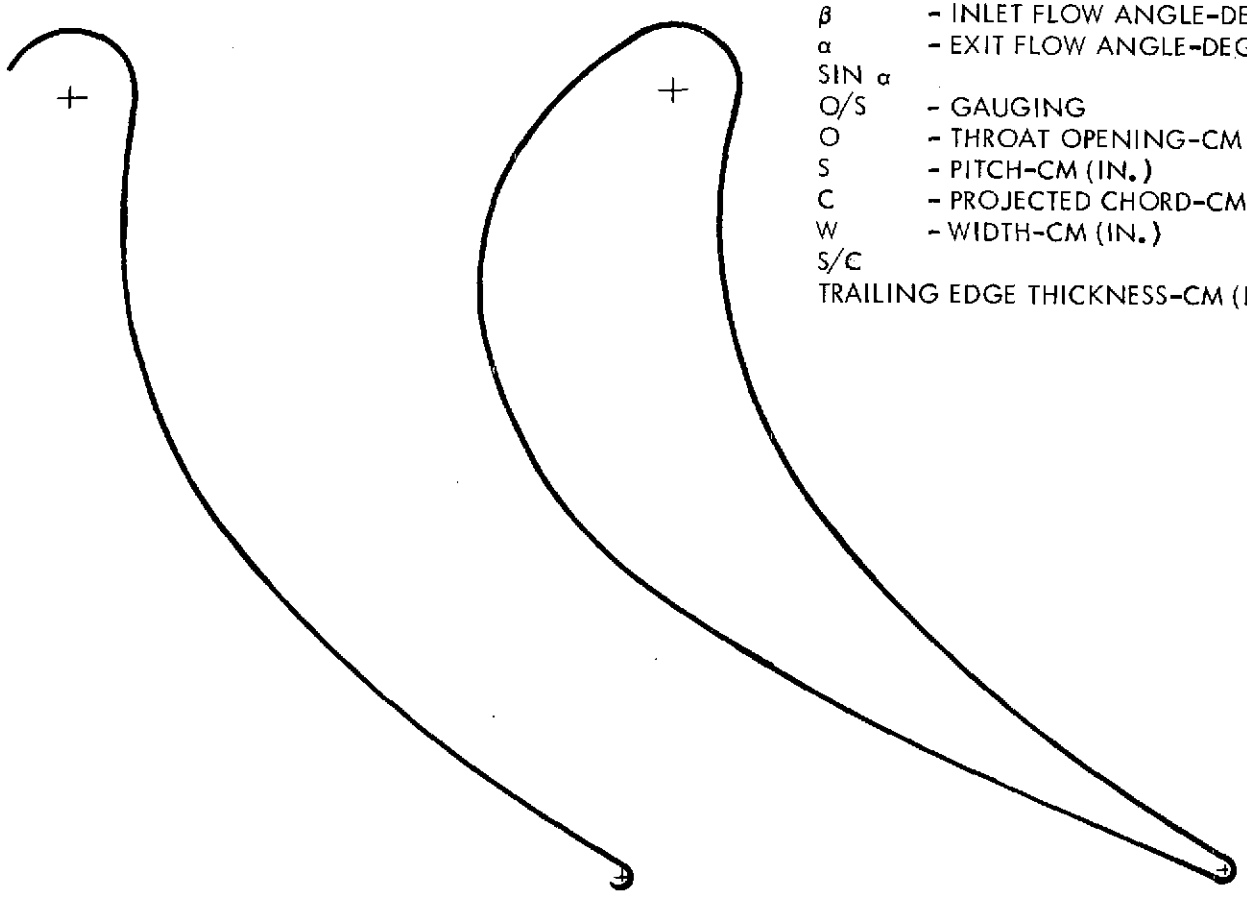

UNITS

BLADE SECTION - 4th ROTOR BLADE - HUB SECTION

DIAMETER-CM (IN.)		57.5	(22.60)
β	- INLET FLOW ANGLE-DEG.	33.80	
α	- EXIT FLOW ANGLE-DEG.	24.01	
SIN α		0.4069	
O/S	- GAUGING	0.4092	
O	- THROAT OPENING-CM (IN.)	1.08	(0.4246)
S	- PITCH-CM (IN.)	2.64	(1.0378)
C	- PROJECTED CHORD-CM (IN.)	4.50	(1.7694)
W	- WIDTH-CM (IN.)	3.78	(1.4875)
S/C		0.5865	
TRAILING EDGE THICKNESS-CM (IN.)		0.0783	(0.0308)

Figure A2-4. Blade Section - 4th Rotor Blade - Hub Section

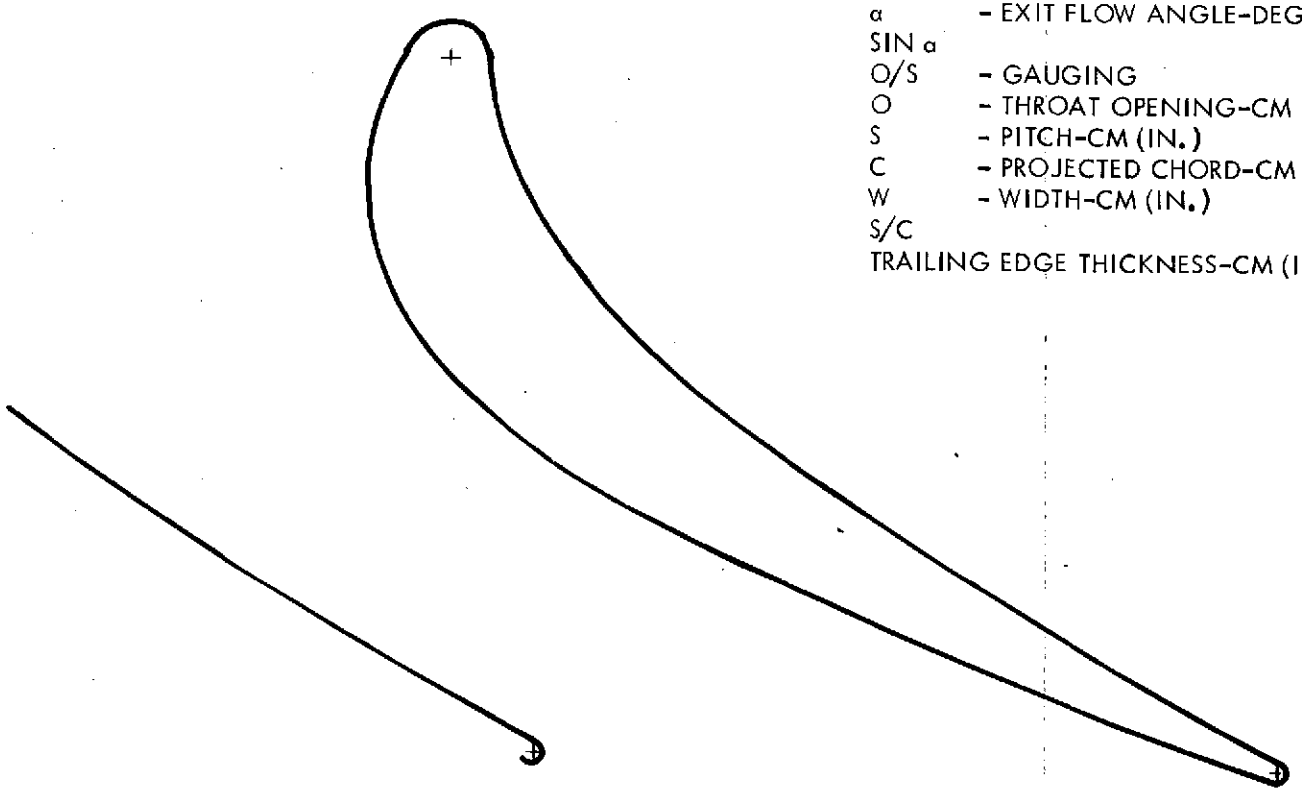

UNITS

BLADE SECTION - 4th ROTOR BLADE - TIP SECTION

DIAMETER-CM (IN.)		71.3	(28.04)
β	- INLET FLOW ANGLE-DEG.	78.8	
α	- EXIT FLOW ANGLE-DEG.	20.52	
SIN α		0.3505	
O/S	- GAUGING	0.3401	
O	- THROAT OPENING-CM (IN.)	1.11	(0.4379)
S	- PITCH-CM (IN.)	3.27	(1.2875)
C	- PROJECTED CHORD-CM (IN.)	5.00	(1.9665)
W	- WIDTH-CM (IN.)	3.21	(1.2626)
S/C		0.655	
TRAILING EDGE THICKNESS-CM (IN.)		0.0885	(0.0348)

Figure A2-5. Blade Section - 4th Rotor Blade - Tip Section

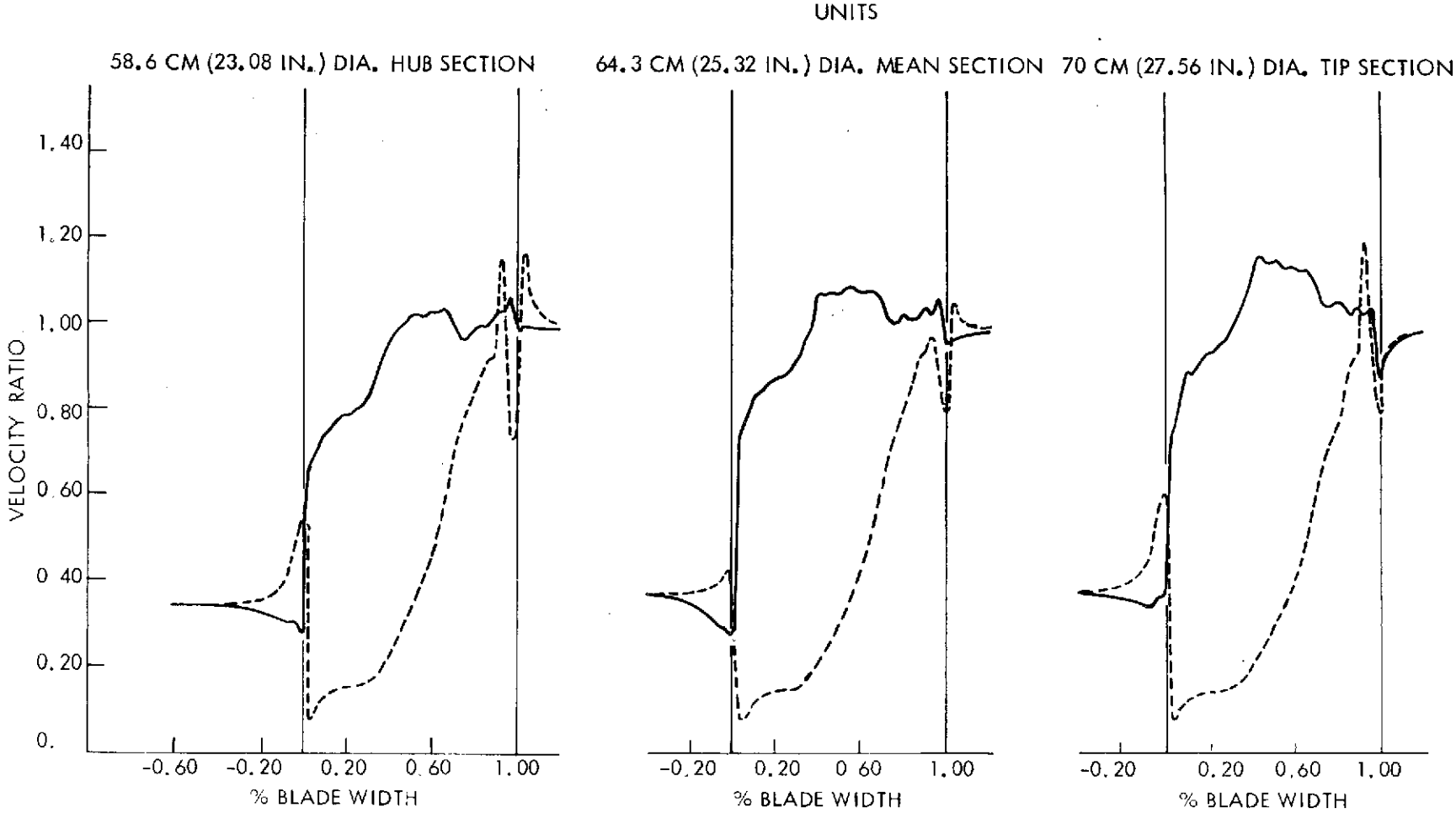

Figure A2-6. Surface Velocities - 4th Stator Blade

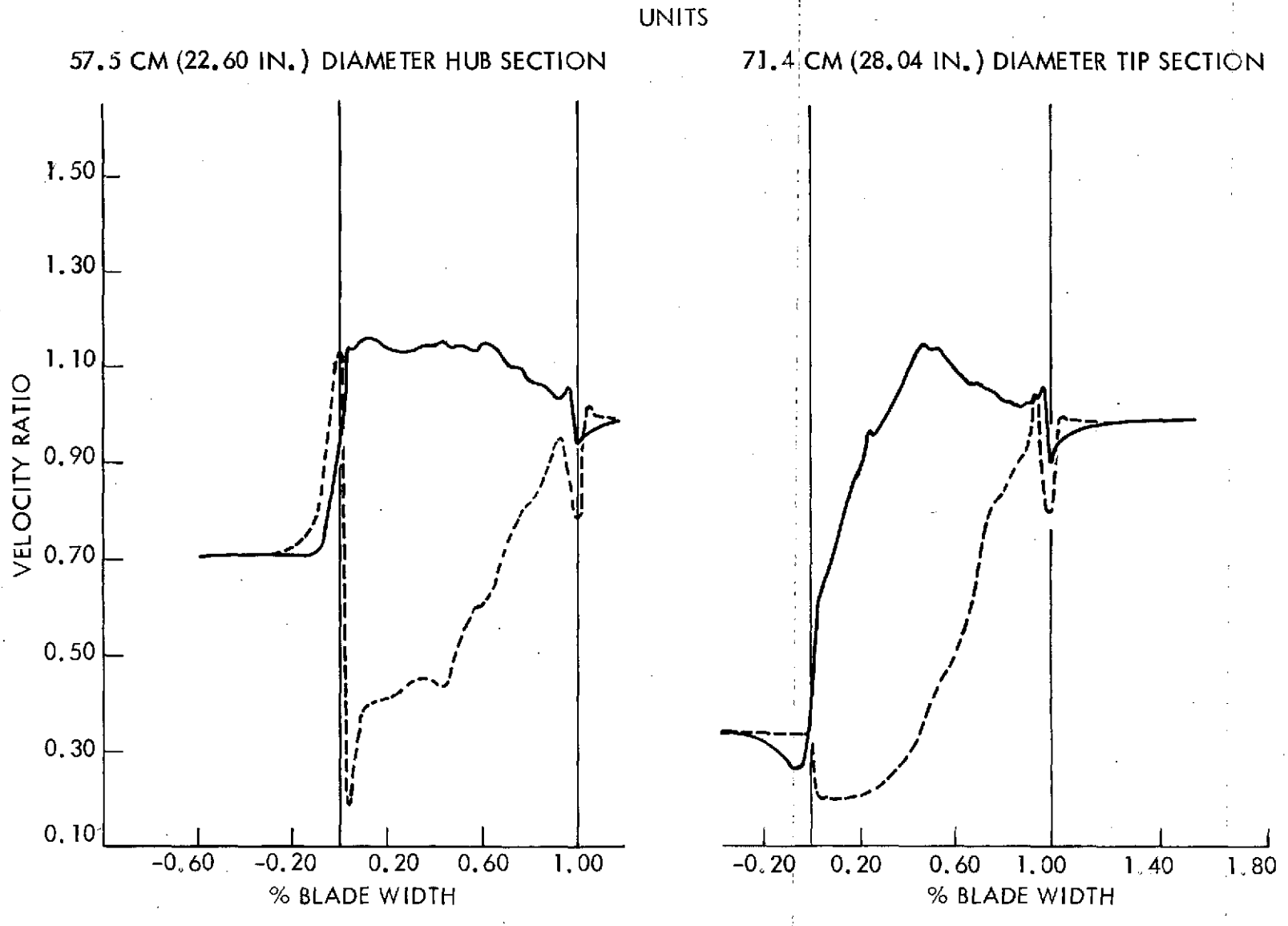

Figure A2-7. Surface Velocities - 4th Rotor Blade

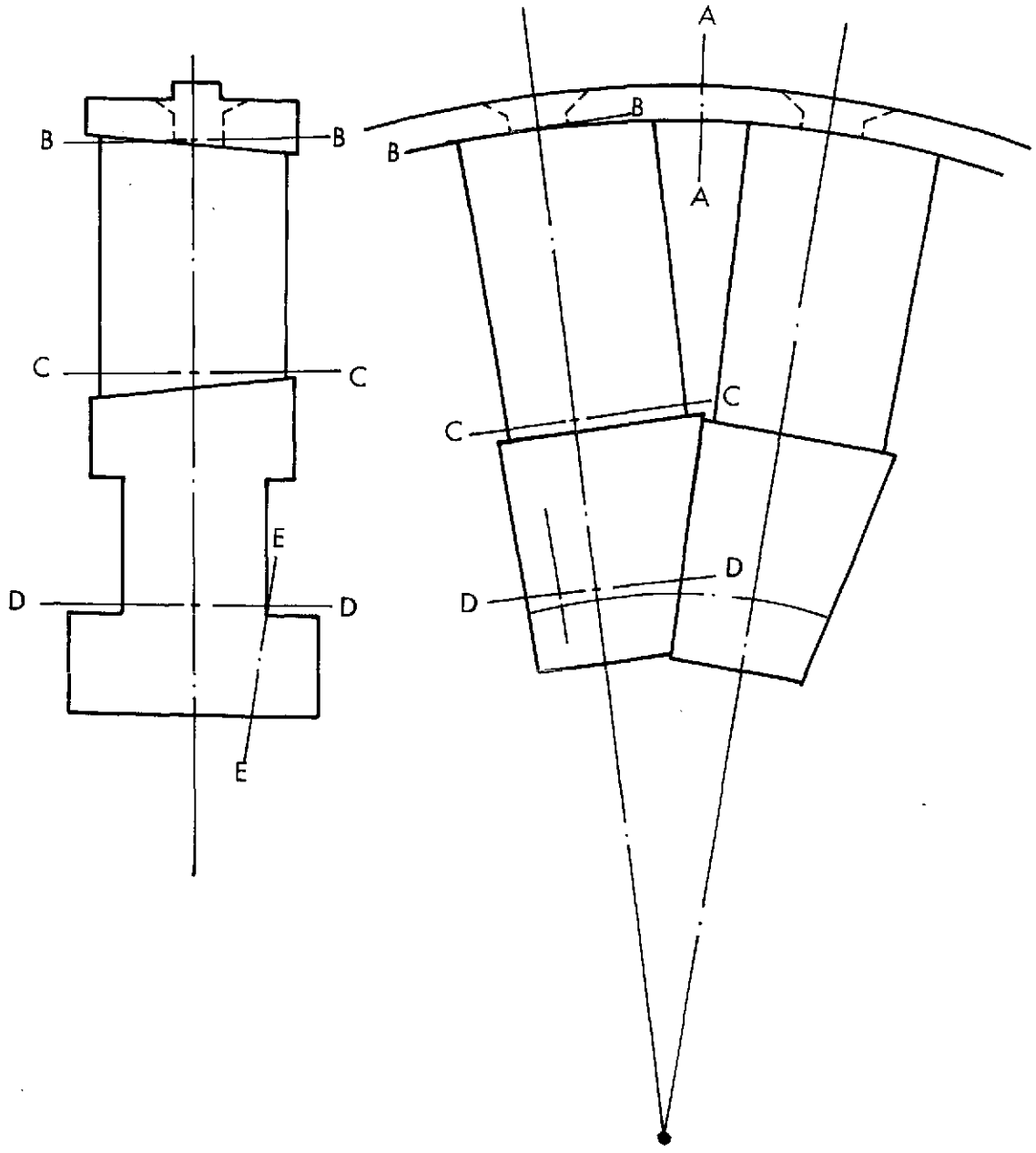

Figure A2-8. Blade Stress Planes

compared to an established minimum allowable value. The minimum allowable value is an experience factor developed over many years and is a function of the blade material, fundamental blade frequency, turbine speed and blade type. The higher the calculated value of "a" compared to the experience established minimum allowable value of "a", the more conservative the mechanical design.

The last row, the third rotor row, of the slave turbine has the highest centrifugal stresses. The steady steam loads on all rows are quite small. Therefore, as is Westinghouse practice, only the stresses in the blades of the third rotor row are calculated and examined. The blade centrifugal rotor groove stress and blade root centrifugal stress are calculated by use of a standard computer program, applicable to these blades. The steady blade bending stresses are calculated from factors determined from generalized design curves for this blade and the pressure and torque forces on the blade. For the third rotor blades computed, representative stresses are:

Location	Section (See Fig. A2-8)	Steady CF ($N/m^2 \times 10^{-8}$)	Steady Bending ($N/m^2 \times 10^{-8}$)	Allowable Vib. Bending ($N/m^2 \times 10^{-8}$)	"a"
Shroud	A-A	0.21	0.04	3.64	90.5
Tenon	B-B	0.51	0.159	3.32	15.2
Blade Base	C-C	0.72	0.104	3.22	25.0
Root Shank	D-D	1.04	0.100	3.04	16.1
Root T	E-E	1.68	--	--	--

Location	Section (See Fig. A2-8)	Steady CF psi	Steady Bending psi	Allowable Vib. Bending psi	"a"
Shroud	A-A	3060	590	52800	90.5
Tenon	B-B	7400	2300	48200	15.2
Blade Base	C-C	10460	1500	46700	25.0
Root Shank	D-D	15050	1440	44000	16.1
Root T	E-E	24300	--	--	--

Fundamental Resonant Frequency = 1750 Hz

Blade Frequency harmonic of running speed = 14.9

Minimum allowable "a" = 1.2

As can be seen, the computed values of "a" for the third rotor blades are many times higher than the experience established minimum allowable value of "a" = 1.2 for these same blades.

The material for the first six rows of blading (rotating and stationary) is a standard blade material, a 12% Cr alloy with a minimum $4.83 \times 10^8 N/m^2$ (70,000 psi) yield strength. The allowable steady stress in the absence of vibration stresses is $2.42 \times 10^8 N/m^2$ (35,000 psi). As mentioned previously, to find the allowable values for combined steady and vibration stresses, a Goodman diagram is used.

The slave turbine stages were manufactured in the same manner as commercial production steam turbines. For production steam turbines, it has been found from experience that exciting forces are a very small fraction of the steady forces if blade frequencies are high harmonics of the running speed frequency. Therefore, as the fundamental blade frequency (1750 Hz) is already many times the running speed frequency (118 Hz), no analysis of higher blade harmonics was carried out.

The only other exciting forces usually present are due to coincidence of rotating blade frequency and stator vane passing frequency. Commercial design criteria indicate possible trouble if the fundamental blade vibration frequency is within $\pm$ 50% of the passing frequency. For the present design, the fundamental blade frequency (1750 Hz) is less than 11% of the passing frequency (16,250 Hz). Therefore, nozzle resonance was not a problem.

The mechanical design calculation made for the test stage blading follows standard procedure for short reaction blading. The design technique described for the standard blading applied also to the test blading. Representative stresses in the test rotating blade are:

Location	Section (See Fig. A2-8)	Steady CF ($N/m^2 \times 10^{-8}$)	Steady Bending ($N/m^2 \times 10^{-8}$)	Allowable Vib. Bending ($N/m^2 \times 10^{-8}$)	Units "a"
Shroud	A-A	0.88	0.0435	3.20	73.4
Tenon	B-B	1.12	0.0635	3.00	34.5
Blade Base	C-C	0.97	0.0240	3.14	105.0
Root Shank	D-D	1.60	0.0300	2.70	47.7
Root T	E-E	2.11	--	--	--

Location	Section (See Fig. A2-8)	Steady CF Psi	Steady Bending Psi	Allowable Vib. Bending Psi	Units "a"
Shroud	A-A	12750	630	46200	73.4
Tenon	B-B	16300	920	43800	34.5
Blade Base	C-C	14100	347	45500	105.0
Root Shank	D-D	23100	432	39100	47.7
Root T	E-E	30600	--	--	--

Fundamental Resonant Frequency = 1350 Hz

Blade Frequency harmonic of running speed = 11.5

Minimum allowable "a" = 3.0

As can be seen, the computed values of "a" for the test stage blade is many times higher than the experience established minimum allowable value of "a" = 3.0 for similar blades.

The material for the test stage blading is also a standard commercial blade material. The allowable steady stress in the absence of vibration stresses is 24,000 N/cm^2 (34,800 psi). As mentioned previously, to find the allowable values in the presence of steady and vibratory

stress, a Goodman diagram is used in conjunction with the minimum allowable "a" and the local stress concentration factor. For the test stage blading, the rotor blade fundamental frequency is 22% of the stator blade passing frequency (6100 Hz) and, therefore, nozzle resonance was not a problem.

APPENDIX A3

A3.0 - MOISTURE CALCULATIONS

A3.1 LIGHT ATTENUATION BY FOG

According to Durbin[14], the light attenuation by a fog is given by the equation:

$$I = I_0 e_{xp}^{-k\pi r^2 n l}$$

where

- I intensity of beam of light after it passes through a length of fog particles
- I_0 incident intensity of beam of light
- k scattering-area coefficient
- l distance light travels through fog particles
- n number of fog particles per unit volume
- r fog particle radius

The scattering area coefficient k is a function of particle size, wavelength of light and index of refraction of the particle and was taken from Durbin. For this purpose, the wavelength of light was assumed to be 0.5 micrometers (19.7 micro-inches) and the index of refraction taken as 1.3. The particle size varies with the pressure level and steam quality. The radii of the particles present were estimated using the data of Gyarmathy and Meyer[8]. The number of particles per unit volume may then be calculated directly on the basis of estimated steam quality. Calculated results of light attenuation as a function of distance (l) at the fourth stator for 6.9×10^4 N/m^2 (10 psia) turbine exhaust pressure are plotted in Figure A3-1 for various moisture levels. Fog particle attenuation at lower pressures is much reduced. In order of magnitude terms, 10% moisture at 0.69×10^4 N/m^2 (1 psia) is equivalent to 1% moisture at 6.9×10^4 N/m^2 (10 psia).

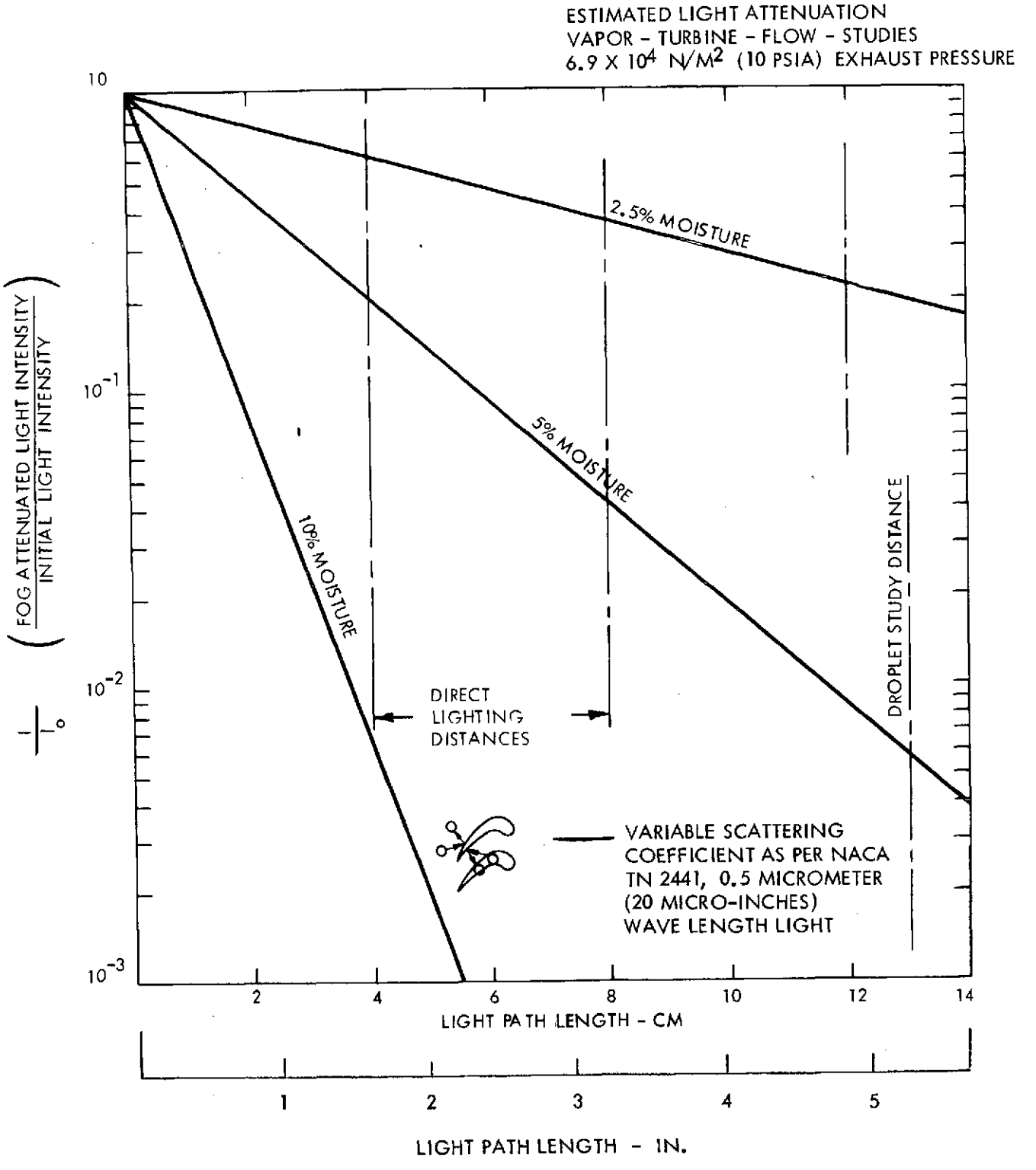

Figure A3-1. Estimated Fog Particle Light Attenuation

A3.2 ATOMIZATION AND TRAJECTORIES OF DROPS FROM FOURTH STATOR BLADES

The calculations were carried out using two computer programs. The first of these is a NASA computer code[10] for calculating blade surface velocities. This code is a network relaxation solution of two-dimensional potential flow within the blade passage. The results of the Katsanis code after some modification are then used as part of the input in an atomized drop code (ADROP)[10] to complete the calculations of drop breakup and acceleration. The modification of Katsanis code as input to the ADROP code is illustrated in Figure A3-2. The surface velocity modification near the trailing edge is intuitive but is based on the premise that the Katsanis calculation is for potential flow and the real situation near the aft stagnation points is not well approximated by a reversible irrotational flow. The modification of the forward stagnation point is done for numerical convenience. There is, on a calculated basis at least, a local region of flow separation just aft of the leading edge on the blade pressure surface. This region of separation (if real) is quite local and does not much affect the flow over the balance of the blade. However, if the ADROP code encounters a region of indicated separation, it must stop since the code is not capable of handling separated flow. Therefore, to get a complete set of atomization and trajectory calculations, the pressure surface conditions near the inlet were modified to eliminate a separated flow indication at this location. This modification was not entirely successful as can be seen by a glance at Table A3-1, where Case D gave an indication of flow separation. The turbine state conditions for the various cases examined is given in Table A3-2. It will be seen that Case D is the lowest pressure among the cases. The pressure range of Case A to Case D was the expected facility test range for the fourth stator of this turbine. Additional turbine input parameters are given in Table A3-3.

The results of some of these atomization and trajectory calculations are given in Figure A3-3 through Figure A3-6. Maximum anticipated secondary drops from the fourth stators vary from 250 micrometers (0.01 inch) at the lowest pressure (Case D) to 40 micrometers (0.0016 inch) at the highest pressure (Case A). Most of the drops observed can be expected to be in the range of 10 to 100 micrometers (0.0004 to 0.004 inch). The distance downstream of the fourth stator at which secondary atomization is completed can be expected to be about 0.5 cm (0.2 inch).

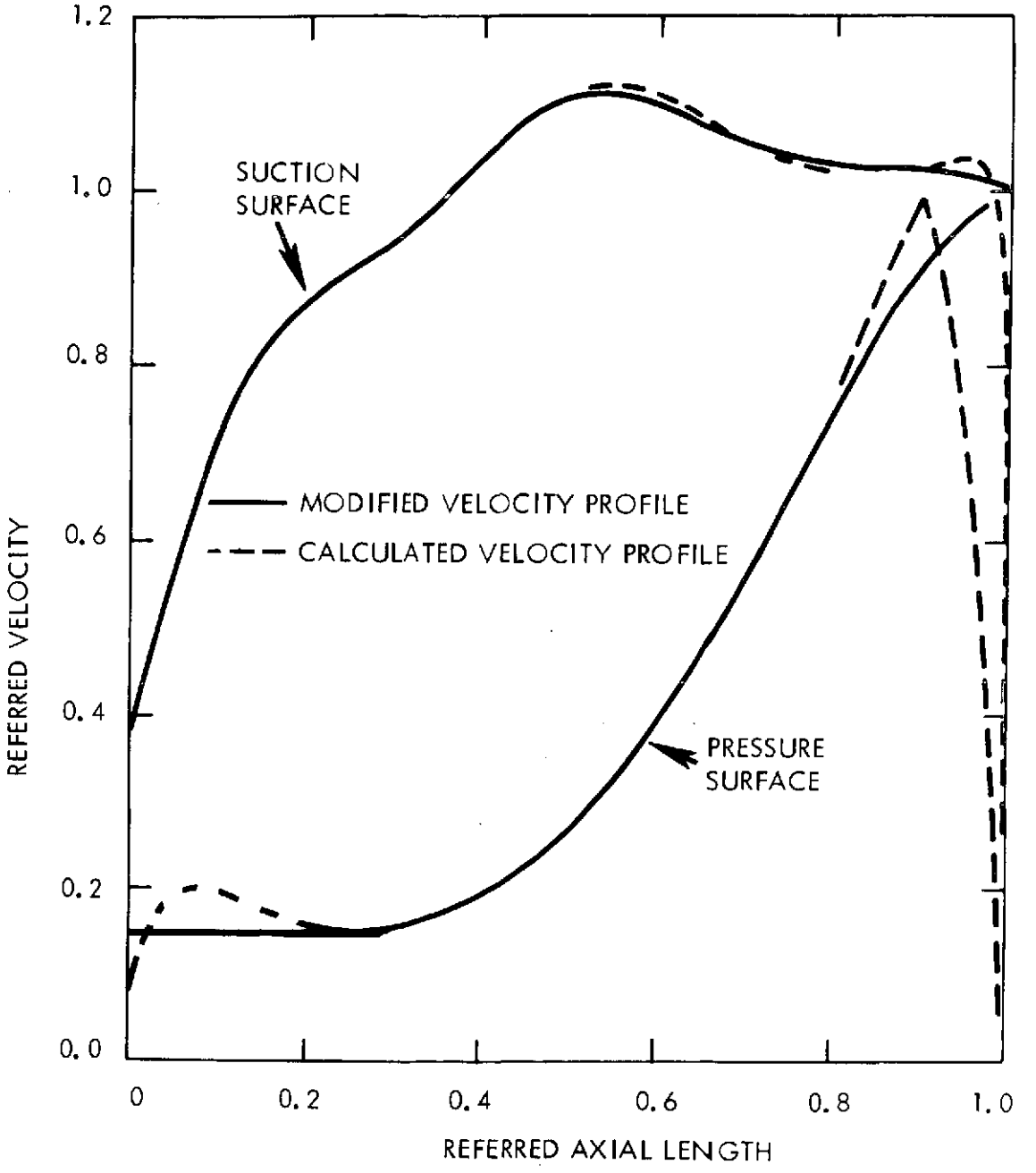

Figure A3-2. Fourth Stator Blade Surface Velocity Profile at 3/4 Height Position

TABLE A3-1

TRAILING EDGE BOUNDARY LAYER SUMMARY

	Case Number				
	A	B	C	D	E
PRESSURE SIDE					
Momentum Thickness (cm)	.00355	.00401	.00449	*	.00399
Displacement Thickness (cm)	.00504	.00580	.00663		.00577
Full Thickness (cm)	.02894	.03171	.03455		.03160
SUCTION SIDE					
Momentum Thickness (cm)	.01688	.01907	.02139	.02532	.01898
Displacement Thickness (cm)	.02471	.02849	.03263	.04020	.02834
Full Thickness (cm)	.13128	.14382	.15686	.17701	.14332
PRESSURE SIDE					
Momentum Thickness (in.)	.00140	.00157	.00177	*	.00157
Displacement Thickness (in.)	.00198	.00228	.00261		.00227
Full Thickness (in.)	.01140	.01250	.01360		.01242
SUCTION SIDE					
Momentum Thickness (in.)	.00665	.00750	.00841	.00996	.00747
Displacement Thickness (in.)	.00972	.01120	.01282	.01582	.01114
Full Thickness (in.)	.05160	.05650	.06160	.06960	.05650

*Flow separation occurs at the leading edge. Problem was run using Case C boundary layer values for the pressure side.

TABLE A3-2

INPUT CONDITIONS AT THE 3/4 BLADE HEIGHT POSITION
FOR STATOR DISCHARGED DROP CALCULATIONS

Fourth Stator Exit

Case Number	Jet Velocity (m/sec)	Bulk Vapor Temperature (°K)	Pressure $N/m^2 \times 10^{-5}$	Turbine Exhaust Pressure $N/m^2 \times 10^{-5}$	Rotor Inlet Flow Angle Degrees
A*	317	368.6	0.872	0.681	60.85
B	310	350.8	0.433	0.338	63.70
C	302	336.0	0.221	0.172	66.50
D	293	316.5	0.089	0.068	70.75
E**	317	368.6	0.432	0.338	60.85

Case Number	Jet Velocity (ft/sec)	Bulk Vapor Temperature (°F)	Pressure PSIA	Turbine Exhaust Pressure PSIA	Rotor Inlet Flow Angle Degrees
A*	1040	204	12.64	9.87	60.85
B	1016	172	6.27	4.90	63.70
C	992	145	3.20	2.50	66.50
D	961	110	1.28	1.00	70.75
E**	1040	172	6.27	4.90	60.85

*Design Point Conditions
**Preliminary Run

TABLE A3-3

INPUT DATA FOR THE FOURTH STAGE OF THE TURBINE AT THE 3/4 BLADE HEIGHT POSITION FOR STATOR DISCHARGED DROPS CALCULATIONS

STATOR	
Number of Blades	52
Section Exit Diameter	67.1 cm
Trailing Edge Thickness (diameter)	0.1029 cm
Chord Length	5.46 cm
Blade Length along Pressure Surface	6.42 cm
Blade Length along Suction Surface	7.59 cm
Exit Flow Angle with Respect to Transverse Plane	17.88°
Exit Jet Velocity	(See Table A3-2)
Exit Bulk Vapor Temperature	(See Table A3-2)
Exit Bulk Vapor Quality	0.9075
MISCELLANEOUS	
Working Fluid	Water
Assumed Critical Weber Number for Secondary Atomization	13.0
Trailing-Edge Multiplier used to Define the Dead-Space	4.0
Axial Space (along Tubine Axis) between the Stator Exit Plane and the Rotor Inlet Plane	2.54 cm

---

STATOR	
Number of Blades	52
Section Exit Diameter	26.44 inches
Trailing Edge Thickness (diameter)	0.0404 inch
Chord Length	2.15 inches
Blade Length along Pressure Surface	2.5281 inches
Blade Length along Suction Surface	2.9821 inches
Exit Flow Angle with Respect to Transverse Plane	17.88°
Exit Jet Velocity	(See Table A3-2)
Exit Bulk Vapor Temperature	(See Table A3-2)
Exit Bulk Vapor Quality	0.9075
MISCELLANEOUS	
Working Fluid	Water
Assumed Critical Weber Number for Secondary Atomization	13.0
Trailing-Edge Multiplier used to Define the Dead-Space	4.0
Axial Space (along Turbine Axis) between the Stator Exit Plane and the Rotor Inlet Plane	1.0 inch

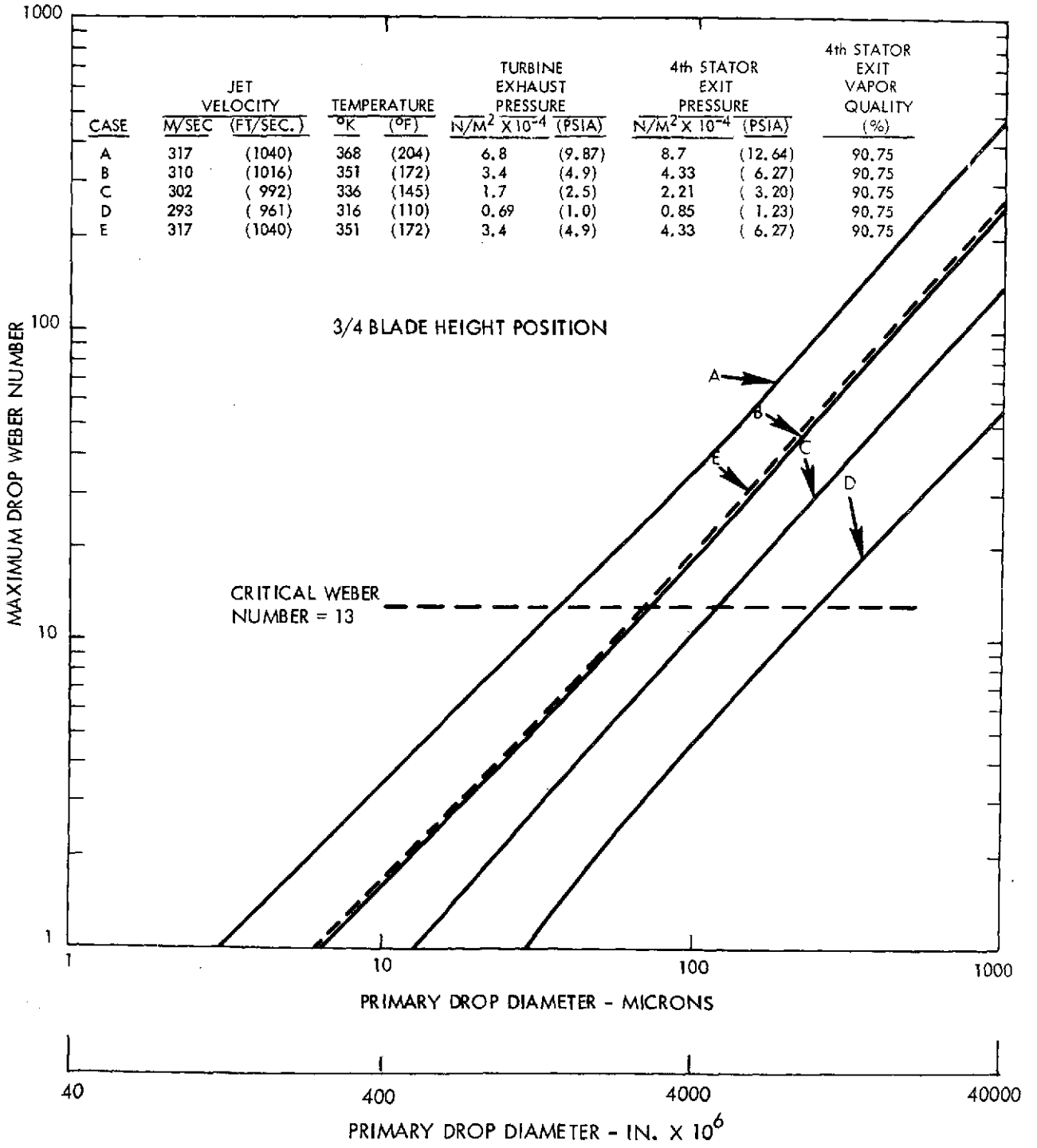

Figure A3-3. Fourth Stator Discharged Drops, Maximum Drop Diameters - Wake Axis Drop

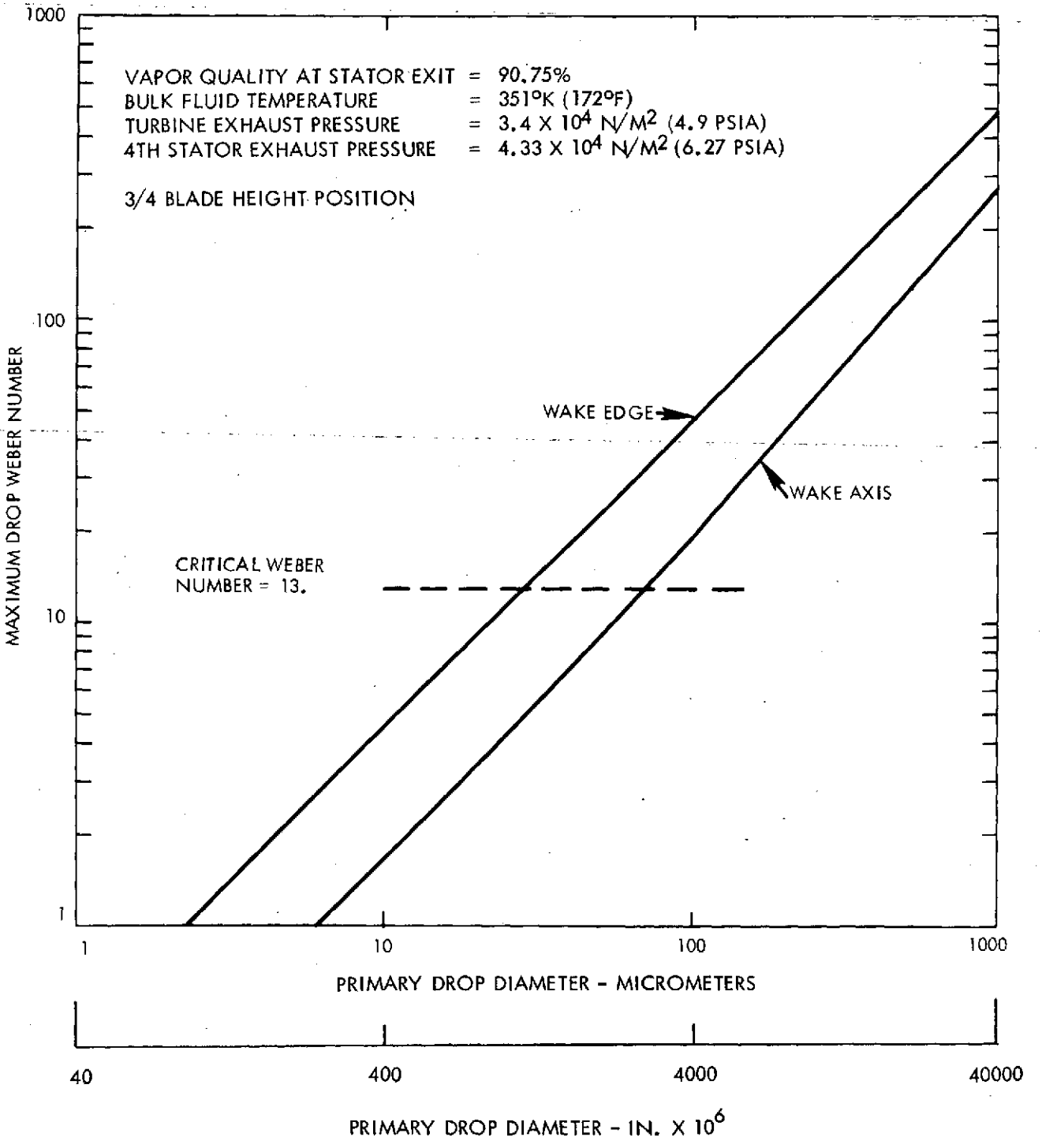

Figure A3-4. Fourth Stator Discharged Drops, Maximum Diameters Wake Edge, Wake Axis Comparison

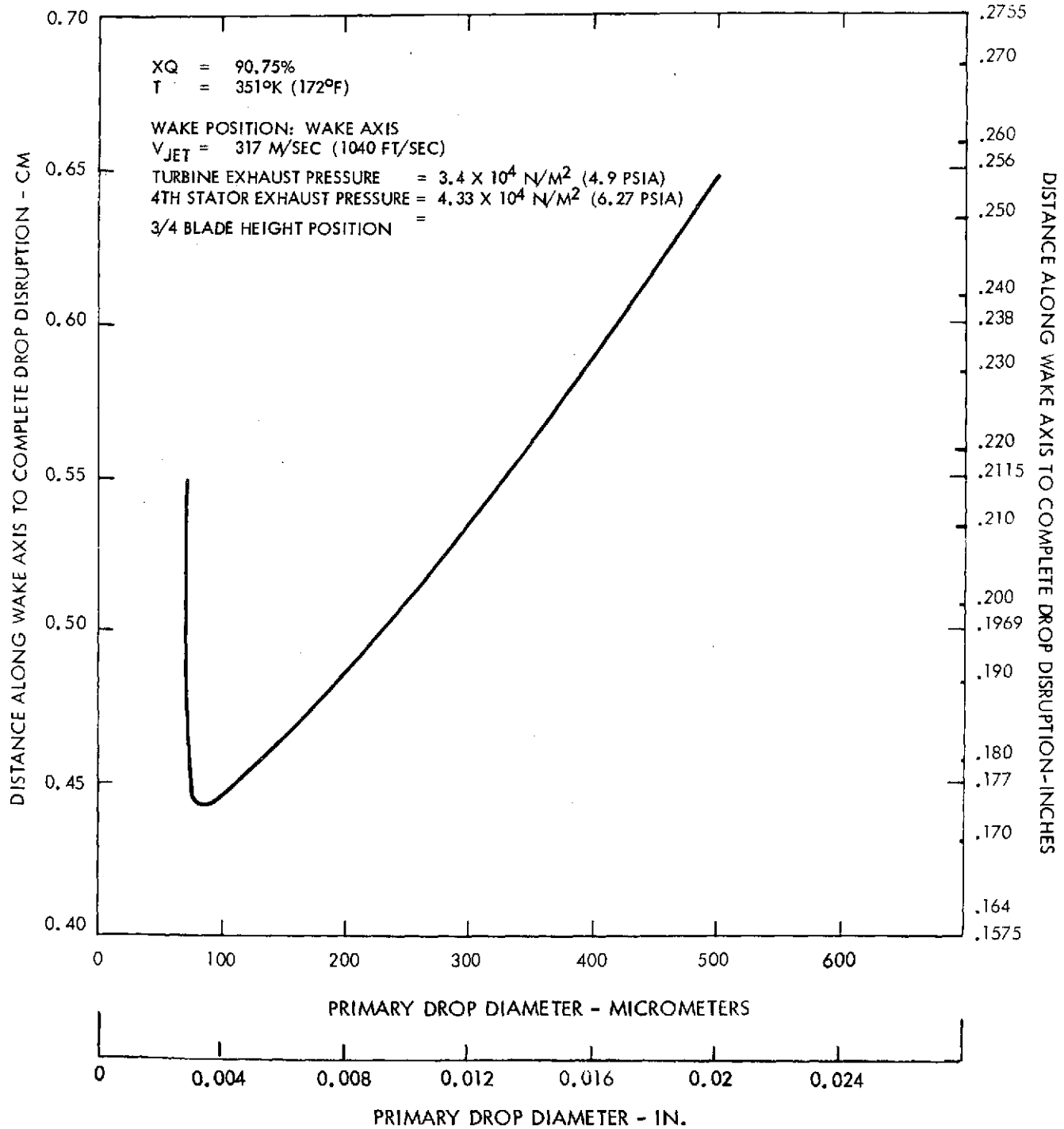

Figure A3-5. Fourth Stator Discharged Drops Secondary Atomization Locations

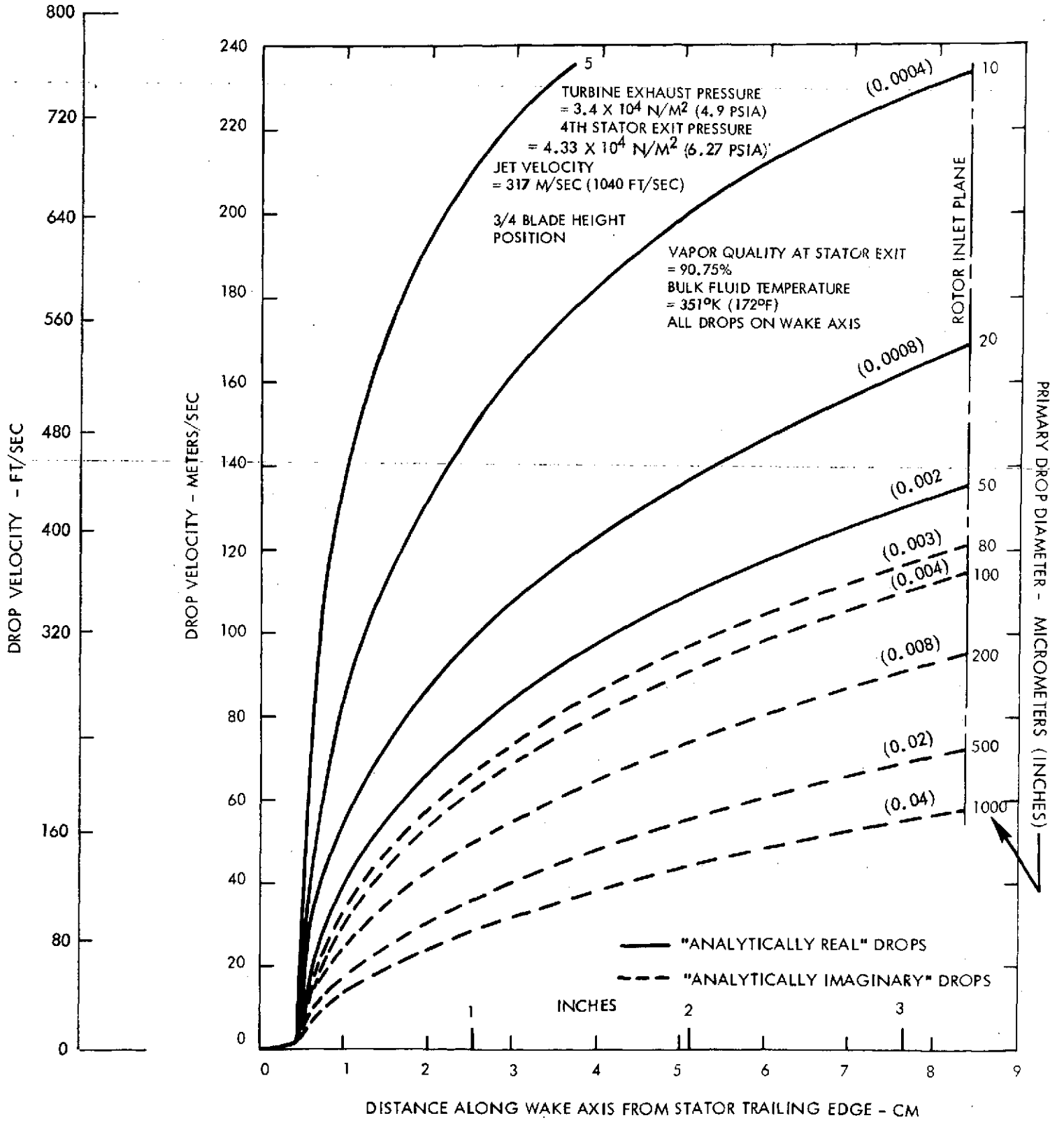

Figure A3-6. Fourth Stator Discharged Drops

A3.3 AMOUNTS OF MOISTURE COLLECTED

Calculations were carried out of moisture collection at a high and a low test pressure. Because review of other calculations[12] indicated that only the concave surfaces of the blades will collect any substantial fraction of the fog particles present, calculation was limited to concave surface collection.

The calculation procedure uses the empirical information on fog particle sizes as observed and reported by Gyarmathy and Meyer[8] for flow of wet steam in nozzles to estimate the average radius particle at the Wilson condensation point. The fog particle radii at downstream locations are then estimated by assuming uniform condensation takes place on each assumed uniform fog particle, allowing for the fog particles lost by collection. The radii thus established are then used in a concave surface collection equation, due to Fentress[13], to estimate the fraction of moisture collected by each turbine row. Iteration is required to allow for fog particles collected.

Turbine geometric variables used for rows 2R through 4R are given in the following. Values are not given for rows upstream of 2R because the flow remains supersaturated until at or near the exit of row 2C.

Turbine Row	Mean Dia. m	No. Blades	Blade Pitch cm	$ Wr
2R	0.643	158	1.28	1.0
3C	0.643	138	1.46	1.0
3R	0.643	144	1.40	1.0
4C	0.643	52	3.90	1.87
4R	0.643	68	2.99	1.52

Turbine Row	Mean Dia. ft.	No. Blades	Blade Pitch ft.	R Wr
2R	2.11	158	0.042	1.0
3C	2.11	138	0.048	1.0
3R	2.11	144	0.046	1.0
4C	2.11	52	0.128	1.87
4R	2.11	68	0.098	1.52

Assumed turbine conditions at the mean diameter are given for nominal high pressure and low pressure test points in the next two tables, respectively.

Turbine Row Exit	Static Temperature (^{o}K)	Static Pressure $N/m^2 \times 10^{-5}$	Axial Velocity (m/sec)	Vapor Density (kg/m^3)	Steam Quality (%)
2C	414	3.66	74.7	2.08	96.0
2R	401	2.54	80.5	1.49	94.5
3C	390	1.78	88.5	1.09	93.2
3R	379	1.23	100.0	0.78	91.9
4C	368	0.84	97.5	0.56	90.8
4R	352	0.68	98.9	0.45	90.1
2C	360	0.74	70.0	0.465	96.6
2R	352	0.52	75.6	0.336	95.4
3C	347	0.36	83.5	0.240	94.0
3R	338	0.25	94.0	0.176	92.6
4C	330	0.17	92.4	0.123	91.6
4R	324	0.13	97.3	0.096	90.0

Turbine Row Exit	Static Temperature (°R)	Static Pressure (psia)	Axial Velocity (ft/sec)	Vapor Density (lb/ft^3)	Steam Quality (%)
2C	745	53.15	245	0.13	96.0
2R	722	36.84	264	0.093	94.5
3C	702	25.85	290	0.068	93.2
3R	682	17.87	327	0.049	91.9
4C	663	12.23	320	0.035	90.8
4R	653	9.87	324	0.028	90.1
2C	647	10.8	230	0.029	96.6
2R	634	7.5	248	0.021	95.4
3C	624	5.2	274	0.015	94.0
3R	608	3.6	308	0.011	92.6
4C	594	2.5	303	0.0077	91.6
4R	583	1.9	319	0.0060	90.0

The results of the collection calculations for two conditions are given in the following tables assuming no turbine moisture is removed.

(INTERNATIONAL SYSTEM OF UNITS)

Row Exit	Total Flow kg/sec	Total Moisture g/sec	Row Moisture Collection g/sec	Cumulative Collected Moisture g/sec	Cumulative Collected Moisture Fraction (%)	Cumulative Collected Fog Particle Fraction (%)	Avera Fog Particle Radius (microns)
2C	6.25	250	--	--	--	--	0.24
2R	6.25	344	5.0	4.54	1.3	1.7	0.27
3C	6.25	425	8.15	13.60	3.2	3.8	0.29
3R	6.25	508	1.31	27.20	5.4	6.6	0.31
4C	6.25	570	1.22	40.70	7.1	8.8	0.32
4R	6.25	620	1.50	54.40	8.8	11.4	0.33
2C	1.26	43	--	--	--	--	0.15
2R	1.26	58	0.54	0.56	0.97	1.10	0.17
3C	1.26	76	1.36	1.91	2.51	2.58	0.18
3R	1.26	93	1.95	3.81	4.10	4.82	0.19
4C	1.26	106	2.22	6.04	5.70	7.01	0.20
4R	1.26	115	3.13	9.20	8.00	10.03	0.21

ENGLISH UNITS

Row Exit	Total Flow lb/sec	Total Moisture lb/sec	Row Moisture Collection lb/sec	Cumulative Collected Moisture lb/sec	Cumulative Collected Moisture Fraction (%)	Cumulative Collected Fog Particle Fraction (%)	Average Fog Particle Radius (microns)
2C	13.8	0.55	--	--	--	--	0.24
2R	13.8	0.76	0.011	0.01	1.3	1.7	0.27
3C	13.8	0.94	0.018	0.03	3.2	3.8	0.29
3R	13.8	1.12	0.029	0.06	5.4	6.6	0.31
4C	13.8	1.26	0.027	0.09	7.1	8.8	0.32
4R	13.8	1.37	0.033	0.12	8.8	11.4	0.33
2C	2.78	0.095	--	--	--	--	0.15
2R	2.78	0.128	0.0012	0.0012	0.97	1.10	0.17
3C	2.78	0.167	0.0030	0.0042	2.51	2.58	0.18
3R	2.78	0.206	0.0043	0.0084	4.10	4.82	0.19
4C	2.78	0.234	0.0049	0.0133	5.70	7.01	0.20
4R	2.78	0.253	0.0069	0.0202	8.00	10.03	0.21

APPENDIX A4 - INSTRUMENTATION

Turbine thermodynamic instrumentation included the turbine monitoring group, utilized by the turbine operator to set test conditions and insure safe turbine operation, and the performance evaluation group consisting of higher precision instruments for measuring turbine performance. Table A4-1 shows the turbine monitoring instrumentation which consists of conventional laboratory instruments. Table A4-2 shows the sensors upon which turbine performance calculations were based. These data were automatically recorded on magnetic tape. Upon concluding a day of testing, these data were then entered into a high speed digital computer for data reduction.

TABLE A4-1

TURBINE PERFORMANCE INSTRUMENTATION

Description	Quantity	Range	Accuracy
Date	-	-	-
Time	-	-	-
Run Number	-	-	-
Turbine Speed	1	0 - 125 Hz	$\pm$ 0.1 Hz
Inlet Pressure	2	0 - 10.3 x 10^5 N/m^2	$\pm$ 1/4% FS
Exhaust Pressure	2	0 - 1.4 x 10^5 N/m^2	$\pm$ 1/4% FS
Inlet Temperature	5	0 - 350°C (273 - 623°K)	$\pm$ 1°C (°K)
Exhaust Temperature	3	0 - 150°C (273 - 423°K)	$\pm$ 1°C (°K)
Bearing Inlet Oil Temp.	1	0 - 150°C (273 - 423°K)	$\pm$ 2°C (°K)
Bearing Drain Oil Temp.	1	0 - 150°C (273 - 423°K)	$\pm$ 2°C (°K)
Steam Condensate Flow	1	0 - 23000 kg/hr	$\pm$ 1/4% FS
Brake Torque	1	0 - 3399 N-m	$\pm$ 1/2% FS
Moisture Removal Press. (3R)	1	0 - 1.4 x 10^4 N/m^2	$\pm$ 1/4% FS
Moisture Removal Press. (4R)	1	0 - 1.4 x 10^4 N/m^2	$\pm$ 1/4% FS
Moisture Removal Press. (4C)	1	0 - 1.4 x 10^4 N/m^2	$\pm$ 1/4% FS

TABLE A4-1
(Continued)

TURBINE PERFORMANCE INSTRUMENTATION

Description	Quantity	Range	Accuracy
Date	-	-	-
Time	-	-	-
Run	-	-	-
Turbine Speed	1	0 - 7500 rpm	$\pm$ 5 rpm
Inlet Pressure	2	0 - 150 psia	$\pm$ 1/4% FS
Exhaust Pressure	2	0 - 20 psia	$\pm$ 1/4% FS
Inlet Temperature	5	0 - 662°F	$\pm$ 2°F
Exhaust Temperature	3	0 - 300°F	$\pm$ 2°F
Bearing Inlet Oil Temp.	1	0 - 300°F	$\pm$ 4° F
Bearing Drain Oil Temp.	1	0 - 300°F	$\pm$ 4°F
Steam Condensate Flow	1	0 - 50000 lb/hr	$\pm$ 1/4% FS
Brake Torque	1	0 - 2500 ft-lb	$\pm$ 1/2% FS
Moisture Removal Press. (3R)	1	0 - 20 psia	$\pm$ 1/4% FS
Moisture Removal Press. (4R)	1	0 - 20 psia	$\pm$ 1/4% FS
Moisture Removal Press. (4C)	1	0 - 20 psia	$\pm$ 1/4% FS

TABLE A4-2

FACILITY MONITORING INSTRUMENTATION

Speed Indicator - Hewlett Packard 521E	
Temp. Indicator 48 point Leeds & Northrup Speedomax	0 - 540°C (273 - 813°K)
Bourdon Tubes Pressure Gages:	
Gland	$0 - 4.1 \times 10^5$ N/m^2 inlet $0 - 4.1 \times 10^5$ N/m^2 exhaust
Const. Head Tank, brake water	$0 - 2 \times 10^5$ N/m^2
Brake Trunion Pressure, 2 gauges	$0 - 6.9 \times 10^5$ N/m^2 and $0 - 20.7 \times 10^5$ N/m^2
Brake Bearing Pressure, Gauge	$0 - 2 \times 10^5$ N/m^2
Exhaust Pressure	$0 - 1 \times 10^5$ N/m^2 and 4.1×10^5 N/m^2
Turbine Bearing Oil	$0 - 2 \times 10^5$ N/m^2
Steam Line Pressure	$0 - 55.1 \times 10^5$ N/m^2
Turbine Inlet Pressure	$0 - 1 \times 10^5$ N/m^2 and $0 - 10.3 \times 10^5$ N/m^2
Brake Water Pressure	$0 - 4.1 \times 10^5$ N/m^2
Brake Torque Gauge	0 - 2600 cal
Screening Gas Pressure	$0 - 6.9 \times 10^5$ N/m^2

TABLE A4-2
(Continued)

FACILITY MONITORING INSTRUMENTATION

Speed Indicator - Hewlett Packard 521E	
Temp. Indicator 48 point Leeds & Northrup Speedomax	0 - 1000°F
Bourdon Tubes Pressure Gages:	
Gland	0 - 60 psig inlet 0 - 60 psig exhaust
Const. Head Tank, brake water	0 - 30 psig
Brake Trunion Pressure, 2 gauges	0 - 100 and 0 - 300 psig
Brake Bearing Pressure, Gauge	0 - 30 psig
Exhaust Pressure	0 - 30 Hg and 0 - 60 psig
Turbine Bearing Oil	0 - 30 psig
Steam Line Pressure	0 - 800 psig
Turbine Inlet Pressure	0 - 30 Hg and 0 - 150 psig
Brake Water Pressure	0 - 60 psig
Brake Torque Gauge	0 - 8000 ft-lb
Screening Gas Pressure	0 - 100 psig

TABLE A4-3

MOISTURE REMOVAL INSTRUMENTATION

Orifice Inlet Pressure	(Manometer)
Orifice ΔP	(Manometer)
Moisture Flow	(Tank Height)
Time	

TABLE A4-4

PHOTOGRAPHIC EQUIPMENT

Equipment List

BORESCOPE APPARATUS

Items

1. 0.2X Borescope with Bayonet and "C" Mount Fittings
2. 0.4X Borescope with Bayonet and "C" Mount Fittings
3. 1.5X Borescope with "C" Mount Fitting and Extension Piece
4. 10X Visual Eyepiece "C" Mount Fitting

LIGHT SOURCES

5. EG&G 2307 Double-Flash Light Source and Spark-Lite
6. EG&G 501 High Speed Strobe with FX-11 Flash Lamp and Holder
7. Large Tungsten-Iodine Incadescent Lamp Holder
8. Small Tungsten-Iodine Incadescent Lamp Holder
9. Mounted Projector Lamp

LIGHT TUBES

10. 9/16" Fiber Optic Light Pipe with Right Angle Mirror Single Exit End and Quadruple Inlet End
11. Ditto Item 10, Except has Shorter Right Angle Mirror End
12. 9/16" Fiber Optic Light Pipe with Single Exit End and Quadruple Inlet End
13. 9/16" Fiber Optic Light Pipe with Angled Single Exit End and Quadruple Inlet End
14. 3/8" Fiber Optic Light Pipe with Single Exit and Inlet Ends

CAMERAS

15. 16 mm High Speed Movie Camera, WF3 Fastax
16. 16 mm Framing Camera

REFERENCES

1. Gardner, F. W., The Erosion of Steam Turbine Blades, The Engineer (London), February 5, February 12, and February 19, 1932.

2. Gyarmathy, G., The Bases for a Theory of the Wet Steam Turbine, Juris-Verlag, Zurich, 1962. Also published in Bulletin No. 6, Institute for Thermal Turbo-Fuel Machines of Federal Technological University, Zurich, Switzerland.

3. Hayes, L. G., Turbine Erosion Research in Great Britain, NASA, Jet Propulsion Laboratory, California Institute of Technology, Technical Memo No. 33-271.

4. Spies, R. Baughman, J. R., and Blake, J. E. T.: Investigation of Variables in Turbine Erosion, Influence of Aerodynamic and Geometric Parameters. Rocketdyne Final Report on Contract NAS 7-391, R-7650, 1968.

5. Pouchot, W. D., et. al: Basic Investigation of Turbine Erosion Phenomena, Westinghouse Electric Corporation, NASA CR-1830, 1971.

6. Schnetzer, E.: 3000-Hour Test - Two Stage Potassium Turbine, Final Report NASA CR-72273, General Electric Company, 1967.

7. Weshig, G. C.: Three Stage Potassium Turbine Performance Test Summary. General Electric Company, NASA CR-1483, 1969.

8. Gyarmathy, G., and H. Meyer, Spontaneous Condensation Phenomena - Parts I and II. CEGB Information Services, C. E. Trans. 4160, Figure 21, Figure 24.

9. Katsanis, Theodore, A Computer Program for Calculating Velocities and Streamlines for Two-Dimensional, Incompressible Flow in Axial Blade Rows, NASA TND-3762, NASA Lewis Research Center, January 1967.

10. Varljen, T. C., Transport of Atomized Drops between Stators and Rotors, Section 2.6, NASA CR-1830, November 1971.

11. Barna, Gerald J., A High Speed Photographic System for Flow Visualization in a Steam Turbine, NASA TM X-2763, NASA Lewis Research Center, April 1973.

12. Fentress, W. K., Collection of Condensate and Movement of Condensate on Turbine Surfaces, Section 2.5, WANL-TME-1977, Rev. 1, January 1971. Figures 2.52-2 and 3.

13. Fentress, W. K., Collection of Condensate and Movement of Condensate on Turbine Surfaces, Section 2.5, WANL-TME-1977, Rev. 1, January 1971. Page 2-153, Eq. 3.

14. Durbin, Enoch J., Optical Methods Involving Light Scattering for Measuring Size and Concentration of Condensation Particles in Super-Cooled Hypersonic Flow, NASA Langley Aeronautical Laboratory TN 2441, August 1951.